TABLET DISSOLUTION DETERIORATION BY SODIUM LAURYL SULFATE - MECHANISM AND MITIGATION STRATEGIES

A DISSERTATION
SUBMITTED TO THE FACULTY OF THE
UNIVERSITY OF MINNESOTA
BY

Yiwang Guo

IN PARTIAL FULFILLMENT OF THE REQUIERMENTS
FOR THE DEGREE OF
DOCTOR OF PHILOSOPHY

Changquan Calvin Sun, Advisor

July 2021

Acknowledgements

While writing of this dissertation, every detail of the experiments, data analyzing and discussions has brought me back to the time when I was working on them, I appreciate the Ph.D. training here at the University of Minnesota, which is a great gift to me and my future life.

Every stage of my Ph.D. life, my advisor, Dr. Changquan Calvin Sun, was there. Dr. Sun is the first person I want to say “thanks”. As a scientist, he has always been enthusiastic. His dedication to the science has always inspired me during the course of my Ph.D. journey. As a mentor, he has been very patient in guiding students thinking, providing constructive suggestions, and generously offering praise to students. If my Ph.D. life is a battle, Dr. Sun is my comrade whose unwavering support I can always depend on.

My appreciation also goes to my committee members, Drs. Wiedmann, Raj Suryanarayanan, Ronald Siegel, and Chun Wang for reviewing my dissertation, offering insightful comments and suggestions. I have received a lot of support from Dr. Wiedmann in preliminary exams, experiments, fellowship recommendation letters, and manuscript revisions. I appreciate his encouragement every time when I feel discouraged. I thank him for not only providing guidance on my research, but also reminding me of being true and simple by the way he talks and behaves. I appreciate Dr. Sury for giving me insightful suggestions on my proposal during my preliminary oral exam, the short discussion in his office gave me a comprehensive understanding of the basic theories related to dissolution. I thank Dr. Siegel, who is always willing to help whenever I seek for help, especially when I had mathematics issues for the artificial stomach and duodenum dissolution apparatus. I also thank him for granting me access to instruments in his lab. My special thanks to Dr. Chun Wang for the prompt response to serve on my defense committee.

I would like to extend my sincere thanks to my current and past lab member, Dr. Shubhajit Paul, Dr. Chenguang Wang, Dr. Manish Kumar Mishra, Dr. Chamara Gunawardana, Dr. Wei-Jhe Sun, Dr. Shao-Yu Chang, Dr. Jiangnan Dun, Shenye Hu, Dr. Hongbo Chen, Dr. Kunlin Wang, Ling Zhu, Sibo Liu, Zhongyang Shi, Zhengxuan Liang, Gerrit Vreeman, Joan Cheng, Zijiang Wang, Shan Wang, Dr. Hiroyuki Yamashita, Prof. Mingjun Wang, Prof. Wenxi Wang, Dr. Cosima Hirschberg, Ms. Hongliang Wen, Prof. Wei Li and Prof. Jun Wen. I would also like to recognize my funding sources, the David J.W. Grant & Marilyn J. Grant Fellowship in Physical Pharmacy, and Doctoral Dissertation Fellowship, for the financially supporting part of my graduate study.

Last but not least, I would like to express my deepest appreciation to my wonderful and dearest friend who always leads me by the right path, gives me immediate help whenever I need. He has been and will continue to be very precious for me during my Ph.D. life and into my future life.

To my wonderful and dearest friend

Abstract

Dissolution in gastrointestinal tract (GI tract) is critical for oral solid dosage forms, especially for drugs with poor solubility. Among the commonly used approaches, applications of surfactant have become a popular way to address the problem of slow dissolution of poor soluble drugs.

Sodium lauryl sulfate (SLS) is a surfactant commonly used as a wetting agent when concentration is below critical micelle concentration (CMC), or a solublizer when concentration is above CMC, both are expected to enhance drug dissolution. However, this anionic surfactant can also readily interact with the positively charged cations in solution, to form a poorly soluble lauryl sulfate salt. This leads to unexpectedly reduced drug dissolution. Given the frequent application of SLS in drug products, understanding the mechanism is important to avoid surprises.

The study was started by systematically investigating the case of ritonavir (RTV), which forms a poorly soluble amorphous $[RTV^{2+}][LS^{-}]_2$ salt with SLS at a low pH, the ion-ion interaction between drug cation and lauryl sulfate anion (LS^{-}), was further proved from an analysis of the single crystal structure of $[NORH^{+}][LS^{-}]$ salt, in which proton transfer was clearly observed between $NORH^{+}$ and LS^{-}. For such an acid – base reaction, the prevalence of lauryl sulfate salt among other pharmaceutical compounds was investigated, using 18 chemicals with diverse molecular structures.

To investigate the precipitation rules of the poorly soluble lauryl sulfate salts, *p*-aminobenzoic acid (PABA), which forms $[PABAH^{+}][LS^{-}]$ salt with SLS, was chosen as the model compound. The thermodynamic driving force as well as precipitation kinetics are discussed. With that, two formulation strategies were proposed to mitigate the negative effect induced by SLS.

In summary, although usually used as a dissolution enhancer, SLS can surprisingly reduce drug dissolution by forming a poorly soluble lauryl sulfate salt. To understand this phenomenon, we systematically investigated its mechanism, prevalence, and formation rules, and demonstrate formulation strategies to mitigate the precipitation. This work provides a solid foundation for the appropriate use of SLS in pharmaceutical formulations.

Table of Contents

List of Tables

List of Figures

Chapter 1

Introduction

1.1 General introduction

The orally dosed tablet is the most popular dosage form of drugs. Absorption after oral administration mainly takes place in the gastrointestinal tract (GI tract). In order to be absorbed, the active pharmaceutical ingredient (API) needs to be released from the bulk solid into the GI fluids through the process of dissolution. Thus, dissolution process directly affects the bioavailability and therapeutic effectiveness of oral dosage forms.

The dissolution process can be treated as a heterogenous reaction, which occurs at the interface between the dissolving solid phase and the liquid medium in the context of oral tablet. [1-2] It includes several steps: 1) wetting by the dissolution medium, 2) breaking the intermolecular bonds, 3) solvation of the released solute molecule, 4) diffusion into the bulk medium through the thin diffusion layer at the solid surface.[3] Any of these steps could potentially become rate limiting for the overall dissolution if they are slow. Common formulation strategies to overcome slow dissolution include 1) use of a wetting agent, 2) solid phase engineering, 3) particle size reduction, and 4) lipid-based formulations.[4]

Among the dissolution enhancement strategies, the an amphiphilic surface active agent (surfactant) is commonly used to enhance the wettability of the poorly soluble drug. Surfactant can also solubilize hydrophobic compounds through micelle formation, which occurs when its concentration is above the critical micelle concentration (CMC). Sodium lauryl sulfate (SLS) is an anionic surfactant widely used in pharmaceutical formulations or *in vitro* dissolution medium to improve dissolution of hydrophobic drugs.

However, under certain circumstances, SLS can also reduce the dissolution of drugs by forming a poorly soluble lauryl sulfate (LS) salt. [5-12] When an SLS-containing dissolution medium is used, experimentally observed poor dissolution of drug from a tablet due to the formation of such an LS salt is misleading, because this dissolution deterioration mechanism is not applicable in the GI tract where no SLS is present. Thus, a clear

understanding of the phenomenon is important for the appropriate use of SLS in tablet formulation and dissolution testing to avoid surprises.

We have systematically investigated this phenomenon to understand the molecular mechanism of LS salt formation [7-8] as well as its prevalence and formation rules. The goal was to develop adequate understanding of this phenomenon to guide the appropriate use of SLS in drug development to eliminate surprise in the course of drug product development.

1.2 Literature review

1.2.1 Pharmaceutical tablets

1.2.1.1 Tablet dosage form for drug delivery – advantage and classification

The tablet accounts for more than 80% of all dosage forms administered to humans [13] because of several advantages, such as 1) high dose precision and outstanding chemical and physical stability; [13-14] 2) convenient for patients because of the non-invasive route of administration, and 3) the low cost of manufacturing, packing, transportation, and storage. A tablet can be formulated to provide flexible drug release profiles to meet various clinical needs, such as immediate release, sustained release, controlled release, and targeted release. [15] In addition to the swallowable tablets, other common tablet types, including multilayer, chewable, orally disintegrating and effervescent tablets, offer tailored approaches for patient needs. While 90% are ingested orally, tablets can be administered by other routes, such as implantation, [16-17] sublingual and buccal. These advantages justify the dominant role of the tablet dosage form in drug delivery.

1.2.1.2 The critical attributes of tablets

To ensure safety and quality, the critical attributes of tablets a tablet must satisfy the compendial standards, including 1) small tablet weight variation and good content

uniformity; 2) adequate hardness and low friability; 3) appropriate disintegration and dissolution.

The disintegration and dissolution tests of an orally administered tablet are critical because a tablet must disintegrate into small particles before appreciable dissolution into the GI liquid and permeation though the gut wall can take place. In fact, both the dissolution and permeation are critical in determining the bioavailability of a drug, i.e., the fraction of an administered dose that enters the systemic circulation,[18] as well as the therapeutic effect.[19] For an immediate release tablet, a rapid disintegration favors fast dissolution of the API, which is typically achieved by incorporating a disintegrant in the tablet formulation.

The Biopharmaceutical Drug Classification system (BCS) classifies drugs into four categories based their solubility and gastrointestinal permeability.[19-20] For BCS II drugs, which have low solubility and high permeability, the rate of dissolution is usually a limiting factor for adequate bioavailability. Importantly, BSC II compounds account nearly 70% of the drug discovery pipeline.[21] To these compounds, improving their rate and extent of dissolution in the GI tract is a major challenge for their successful development.

1.2.2 Dissolution theories and dissolution enhancement

1.2.2.1 Heterogeneous reaction

Chemical reactions generally involve structural changes of molecules in a single homogenous phase. However, heterogeneous reactions encompass chemical reactions occurring at the interface of different phases. A heterogeneous reaction occurs in the following steps: a) transport of solute molecules to the interface, b) adsorption at the interface, c) reaction at the interface, d) desorption of the products and e) recession of the products from the interface.[1-2] Among these steps, a) and e) are mass transport processes

while b), c) and d) are chemical processes characterized by an interaction between reactants.[1]

The dissolution process may be considered as a type of heterogeneous reaction described by Eq. 1, where chemical structures of the reactants are not changed. The dissolution process in water consists of four steps: a) wetting of the particle's surface with water, b) breakdown of solid state bonds, c) solvation of individual species, and d) diffusion to the bulk fluid. [3] Among which, steps a), b) and c) require interaction between reactants and step d) is simple mass transport.

$$Drug_{(solid)} \rightleftharpoons Drug_{(soln)} \quad (1)$$

The rate of dissolution depends on the interplay between the rate of reaction at the interface and mass transport. When the rate of reaction at the interface is much slower than the transport process, dissolution is reaction controlled. When the reaction at the interface occurs much faster than the rate of mass transport, the latter is the rate-limiting step for dissolution. When reaction rate and mass transfer rate are comparable, the rate of dissolution is a function of both processes. [22]

1.2.2.2 Reaction limited dissolution

In a reaction limited dissolution, where the reaction rate at the interface is much slower than that of mass transport, drug molecules will diffuse rapidly into the bulk solution once released from the solid surface.

There are three steps in a reaction process: wetting, chemical bonds breaking, and solvation. Each step is associated with an activation energy, which must be surpassed for the reaction to proceed, and the step with the highest energy barrier controls the overall rate of the process.

The first step of dissolution, wetting, is characterized by the intimate contact of the solvent molecules with the surface of drug solid as a direct consequence of molecular interactions between the two phases. [23] In an aqueous dissolution medium, a hydrophilic compound exhibits a good wettability and a hydrophobic compound exhibits poor wettability. [24] The high interfacial tension between hydrophobic drugs and the aqueous medium can be reduced by a surfactant, which is an amphiphilic molecule containing both hydrophobic and hydrophilic parts. When the two phases are coming into contact, the surfactant molecules preferentially orient at the interface to lower the interfacial energy and facilitate the adhesion, spreading, and immersion.

The other two processes, chemical bonds breaking and solvation, are related to the lattice energy and solvation/hydration energy, respectively. They affect dissolution because of their determining roles in the intrinsic solubility. [25-27] The chemical bond breaking is a prerequisite for the dissociation of solute molecules from crystal lattice. Hence, strong intermolecular interactions within the crystal hinder the dissociation and, hence, dissolution. Such compounds sometimes are vividly described as 'brick dust'. [27-29] The strength of such intermolecular interactions in a crystalline solid can be qualitatively assessed based its melting point (T_m). The solubility of a crystalline solid is considered lattice energy limited when the T_m is higher than 200°C. [29] In this case, solubility can be improved by weakening the intermolecular interactions through changing the molecular packing in the solid state, which may be achieved through using polymorphs with a higher free energy and amorphous solids. [27, 30]

In the hydration/solvation process, the dissociated solute molecule is enveloped by solvent molecules (water if in an aqueous medium) and delivered out from the solid surface. This process is favored by a strong affinity between the drug and solvent molecules. Since hydrophobic molecules are usually large and having a high degree of

flexibility, [31] they have a limited capacity to interact with the polar water molecules, Drugs with this property have a hydration limited solubility and are sometimes described as “greaseballs”. The propensity to the hydration limited solubility may be quantitatively assessed by the logarithm of the octanol/water partition coefficient (logP) for the neutral form and the logarithm of the distribution coefficient of the ionizable compound between octanol and water (logD). [27, 29, 32] Compounds with a high hydrophobicity do not readily interact with water, and usually exhibit a limited solubility and dissolution rate. [27, 29] Formulation strategies successful for delivery of the hydration-limited solubility compounds are lipid-based formulations that are composed of lipids, surfactants and/or cosolvents to essentially change the properties of the media to facilitate their interactions with the drug molecules. [4]

1.2.2.3 Mass transport limited dissolution- diffusion layer theory

In mass transport limited dissolution, the mass transport rate for a released molecule is much slower than that of interfacial reaction rate. Currently, among the proposed dissolution theories, the diffusion layer model, which was proposed by Noyes, Whitney and modified by Brunner and Nernst, has been a commonly used model considering a mass transport limited dissolution process. [33]

1.2.2.3.1 Evolution of the diffusion layer theory

In 1897, Arthur A. Noyes and Willis R. Whitney published the seminal paper on the dissolution of benzoic acid and lead chloride in distilled water. [34] In that paper, the materials were cast uniformly on a glass core to form a cylindrical stick, the stick was then inserted into water-contained wide-mounted bottles and rotated to enable the dissolution. The dissolution surface area of solutes in this way was approximately constant, and the concentration of benzoic acid or lead chloride at pre-determined time points were determined by titration. In the experiment, dissolution was assumed as a simple diffusion

process of molecules from an indefinitely thin layer of saturated solution formed at the surface of the solid. The proposed Eq. (2) indicates that the rate of dissolution is proportional to the difference between the concentration of a saturated solution (C_s) and the bulk medium (C). [34]

$$\frac{dC}{dt} = k(C_S - C) \tag{2}$$

Brunner and Tolloczsko [35] later confirmed that the constant k in Eq. (2) is proportional to the surface area exposed (S). Accordingly, they proposed Eq. (3), to better explain the physical origin of the dissolution rate. They conjured that the constant k' depends on the rate of stirring (or water velocity across the surface), temperature, structure of the surface, and the arrangement of the apparatus.

$$\frac{dC}{dt} = k'S(C_S - C) \tag{3}$$

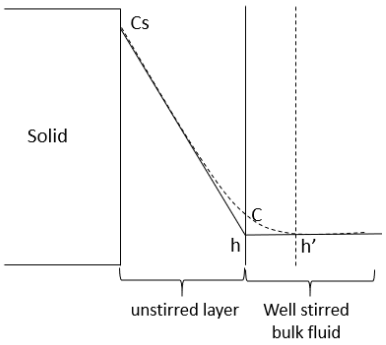

Figure 1. 1. Schematic of film model, solid line represents the concentration distance profile proposed by Nernst-Brunner law, dashed line represents profile proposed by Levich. [36]

Subsequently, Nernst theoretically generalized these views of dissolution to all heterogeneous reactions. He assumed that all the heterogeneous reactions are controlled

by mass transport rate, i.e., the chemical reaction equilibrium in heterogeneous reaction is established much faster at the interface compared to the mass transport of reactants or products. He also introduced the term for thickness of the thin layer of solution adhering to the solid surface, h, through which diffusion occurs (Figure 1.1). The thickness is negatively correlated to the paddle speed through different mathematical functions under different hydrodynamic conditions. [37]

The Fick's first law (Eq. 4) describes the rate at which a dissolved substance diffuses into a solution, i.e., the quantity of solute (dm) diffuses through an area (A) over a time (dt), is proportional to the concentration gradient (dc/dx), in a direction perpendicular to the plane of A.

$$\frac{dm}{dt} = DA\frac{d_c}{d_x} \tag{4}$$

where D is the diffusion coefficient. By converting the mass (m) to concentration (C)

$$\frac{dC}{dt} = \frac{DA}{V}\frac{d_c}{d_x} \tag{5}$$

where V is the volume of the bulk liquid. Nernst assumed that dc/dx can be expressed by $(C_s\text{-}C)/h$. Thus, the Nernst and Brunner equation, Eq. (6), is obtained.

$$\frac{dC}{dt} = \frac{DA}{V}\frac{(C_S - C)}{h} \tag{6}$$

By comparing to Eq. (6), the constant, k, in Eq. (2) can be expressed as:

$$k = \frac{DA}{Vh} \tag{6}$$

When the sink condition is met, the solute concentration, C, in the bulk solution is negligible compared to the concentration in the saturated solution near the solid surface. Thus, Eq. (6) simplified into Eq. (7).

$$\frac{dC}{dt} = \frac{DA}{Vh}C_S \tag{7}$$

With the determining factors known, Eq. (7) points to practical strategies on the improvement of drug dissolution, including a) increasing surface area by reducing particle

size , or increasing the effective surface area for compounds with poor wettability by using a surfactant; b) improving the solubility, which not only enhances the reaction rate as discussed previously, but also enhances the mass transport process in the diffusion layer; c) facilitating diffusion by keeping a low concentration in the bulk fluid to maintain a high concentration gradient; d) increasing the rate of stirring so that the thickness of the adhering layer is decreased; e) decreasing the viscosity of the dissolution media to increase the diffusion coefficient of the drug in the adhering layer.

1.2.2.3.2 Refinement to the diffusion layer theory

Despite being informative and useful in guiding the dissolution rate enhancement, there are also disputes surrounding the Nernst and Brunner's theory.

First, this diffusion layer model assumes that mass transportation is the limited process for dissolution, i.e., the reaction process at the surface proceeds much faster than diffusion. However, for cases of the heterogeneous reactions with a high activation energy, the reaction rate at the interface is slow, which leads to deviation from the theory. [38] A solution to this problem is to use a mathematical model that combines both reaction limited and diffusion limited dissolution process. [39-40]

Second, the model assumes that the aqueous boundary layer adhered to the solid surface is stagnant where diffusion is the only mode of transport. Thus, a linear concentration gradient in the unstirred layer is obtained. The thickness of that layer was estimated to be 20-40 μm, which corresponds to ~ 50,000 molecules. [1] This is too high to be physically probable. [41] In fact, even the existence of such a stagnant layer was disputed. [38, 42] Clearly, abrupt transition from the completely unstirred liquid layer (in which diffusion was the only mode of mass transport) to the well-stirred bulk fluid (in which mass transport occurs mainly via convection) is not realistic. [43] There is likely a zone between the well stirred bulk and the stagnant layer, where convection assumes gradually increasing

importance with increasing distance from the substance's surface. By taking the convective mass transfer into consideration, Levich [36] studied the hydrodynamics of the rotating disk and calculated the concentration at any point. The result showed that the concentration gradient merges asymptotically with the surrounding fields (dashed line in Figure 1.1), and the distance h' is related to h by the expression:

$$h = 0.893\, h' \tag{8}$$

Third, in the model, the change of dissolution surface area was not considered. This approximation is fine at the beginning of particle dissolution, but gross deviations occurs as the particles becomes very small as the dissolution proceeds, which virtually always occurs in pharmaceutical applications. Hixson and Crowell addressed this issue by a "cube-root law" (Eq. 9),

$$M_t{}^{1/3} = M_0{}^{1/3} - kt \tag{9}$$

In the equation, M_0 and M_t represents the mass of the particle at time t = 0 and at time t, respectively, and k is a positive constant. Thus, plotting the cube-root of the remaining particle mass as a function of time gives a straight line, the slope of which is k and the y-axis intercept is the cube-root of the initial mass, M_0. This model was subsequently verified by the dissolution study of $CuSO_4 \cdot 5H_2O$. However, in this model, the following assumptions are made: 1) sink condition is satisfied, 2) particles are spherical (isometric) and the shape does not change with time, 3) particles remain intact and do not disintegrate into smaller fragments during dissolution.

However, in spite of the limitations, the thin layer diffusion model is simple and remains extremely helpful in guiding the use of effective strategies to increase the dissolution rate of a poorly water soluble drugs. The parameters in the equation have been confirmed experimentally to influence dissolution rate, i.e., the dissolution rate is a function of

dissolution surface area, stirring rate, diffusion coefficient of the solute. It was also shown that there is a concentration gradient existed between the solid surface and bulk liquid. Thus, while the quantitative relationships may not be accurate in some situations, the qualitative relationships have been substantiated experimentally.

1.2.3 Deteriorated dissolution performance and mitigation strategies

A theoretical understanding of the dissolution process informs the development of promising formulation strategies to enhance drug dissolution. The commonly used approaches include reducing the particle size; application of a surfactant as wetting agent; preparation of more soluble solid forms of API, such as salts, cocrystals, amorphous solids, and polymorphs; development of lipid-based formulations; and using of complexing agents, such as cyclodextrins. [4, 44] These methods essentially modify either the reaction rate, or the mass transport rate, or both, during dissolution.

However, caution must be exercised when using these approaches, since they may not always result in an improved dissolution. Sometimes, dissolution may deteriorate if these strategies are inappropriately adopted without suitable controls. For example, although particle size reduction is generally an effective way to increase the dissolution surface area and dissolution rate, micronized hydrophobic compounds may form large agglomerates in the aqueous medium because of the high surface energy and poor wettability. Consequently, dissolution rates slower than the unmicronized sample may be obtained. [45-46] It is also possible that precipitation of less soluble solid phase occurs during the dissolution of a soluble solid form, which leads to lower dissolution rate that that expected from the solubility of the soluble solid form. Precipitation during dissolution can take place either at the surface of the solid or in the bulk medium. [47] Surface precipitation leads to dissolution that is comparable to that of the precipitating solid, if it coats the surface of the soluble solid. This is a high probability event since precipitation occurs

more quickly at a higher degree of supersaturation, [48] which is in the solution next to the dissolving solid surface. For example, salts may undergo disproportionation in GI fluids, where the dissociated free API precipitates out instantly on the surface of the solid due to a high degree of supersaturation; [47] amorphous APIs can crystallize at the surface during dissolution; [44, 49] and an anhydrous solid may convert to a less soluble polymorphs or hydrates during dissolution. [50]

To harvest the potential advantage in improving dissolution of soluble solid forms, formulation strategies to prevent, or slow down the precipitation in diffusion layer can be explored. [51-52] An effective formulation strategy is to use polymers in the formulation as a nucleation inhibitor to slowdown the precipitation in the thin diffusion layer. [53-56] Common ion/cofomer effect can also be explored to suppress the solubility of salt or cocrystals. By lowering the solubility of the soluble form in the diffusion layer, precipitation can be retarded or eliminated while the dissolution can still be high. [57-58] A pH modifier can be used to adjust the local environment pH in the diffusion layer based on the pH dependent solubility. [59-60] This approach reduces the degree of supersaturation by elevating the solubility of free base or acid, which also lowers the degree of supersaturation. Precipitation could also take place when a drug and an excipient can form a less soluble complex. Sodium lauryl sulfate (SLS) is a surfactant that is commonly used either in solid dosage forms or the *in vitro* dissolution medium to improve dissolution. However, sometimes drug dissolution may be deteriorated by forming a poorly soluble complex between the LS^- anions and drug cations in solution. This is the focus of this research.

1.2.4 Sodium lauryl sulfate (SLS)

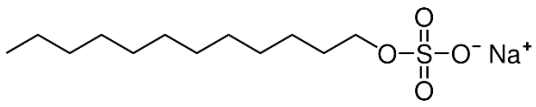

Figure 1. 2. Molecular structure of SLS

Sodium lauryl sulfate (SLS), or sodium dodecyl sulfate, is a synthetic organic compound with the molecular formula, $CH_3(CH_2)_{11}SO_4Na$. The molecule contains a hydrophobic 12-carbon "tail" and a hydrophilic sulfate "head" (Figure 1.2). When dissolved in water at a low concentration, SLS molecules tend to distribute at the surface due to their amphiphilic nature, which reduces surface tension. [61] When the SLS concentration exceeds the CMC, SLS monomers start to self-associate in the bulk medium to form micelles with a hydrophilic shell and hydrophobic core. [62] This micelle formation process is favored as the hydrophobic "tails" are isolated from the aqueous environment by hydrophilic "head", which can readily interact with water molecules. [63] Micelles have the capacity to enhance the apparent aqueous solubility of poorly water-soluble drugs via solubilization in the hydrophobic micelle core or in the head group palisade region. [4]

The CMC of SLS is 8.2 mM in pure water at 25 °C. [64] It is influenced by factors, such as temperature, [64] electrolyte type and concentrations, [65] and pH. [66] Many physicochemical properties of a solution usually are dramatically changed upon the formation of CMC. Therefore, the CMC value can be obtained based on the change of surface tension, conductivity, light transmission, solubility, light scattering, and osmotic pressure. [4]

SLS has been very commonly used in many domestic cleaning products, personal hygiene, and cosmetics products. In pharmaceuticals, SLS is used as an ionic solubilizer

and emulsifier in liquid dispersions, solutions, and emulsions [67-68] as well as a wetting agent and lubricant in solid dosage forms. [20, 69] Some examples of marketed tablet products containing SLS are Brufen ®, Tarceva ®, and Janumet®. Additionally, SLS can also moderately increase the intestinal permeability to facilitate oral absorption of drugs, [70] the mechanism includes affecting the integrity of the tight junctions, [71]concentration-dependent solubilization of cell membranes,[72] etc. SLS is among the list of excipients generally regarded as safe (GRAS) and it is included in the FDA Inactive Ingredients Database (dental preparations; oral capsules, suspensions, and tablets; topical and vaginal preparations). However, due to its degenerative effect on the cell membranes, [73] maximum amounts in topical products, food additives or oral dosage forms should be establish based on carefully conducted experiments. [74]

The negatively charged sulfate group of SLS can readily react with other positively charged ions, such as cationic polymers and APIs. [5-12] This limits the universal application of SLS in pharmaceuticals. For example, in an attempt to investigate the dual functions of SLS as a lubricant and a wetting agent in tablet formulations, the dissolution of ritonavir (RTV) containing SLS was slower than that of the formulation containing magnesium stearate (MgSt), despite the expected faster dissolution due to the improved wetting by SLS. [75-76] Similar observations were made for a few drugs in the literature, [5-6, 9-12] but a mechanistic explanation of such phenomenon remains elusive. Given the frequent application of SLS as a dissolution enhancer for poorly soluble drugs, it is important to understand the underlying mechanism of such phenomena, which helps guide the appropriate use of SLS in solid dosage formulations. In addition, it is useful to understand the prevalence of this phenomenon among pharmaceutical compounds, the rules for the complex to precipitate, and possible formulation strategies to address the problem when it does occur.

1.3 Objectives and hypotheses

1. To systematically investigate the mechanism of the detrimental effect of SLS on drug dissolution.

The investigation was triggered by a peculiar observation during the investigation of the feasibility of SLS as a surrogate for magnesium stearate, MgSt, in tablets. MgSt is an effective lubricant for tablet compaction, but its hydrophobicity usually leads to slower drug dissolution. SLS was used as an excipient with dual functions, i.e., lubrication and dissolution enhancement for poorly soluble drug through improving wetting. However, in the dissolution study using an artificial stomach and duodenum (ASD), the SLS-containing tablets showed unexpectedly retarded dissolution than the MgSt-containing tablet in the stomach chamber, where the dissolution medium is at a low pH. We hypothesized that, 1) such deteriorated dissolution by SLS is due to the formation of a poorly soluble salt between the drug cation and LS^- anion during dissolution.

2. To investigate the prevalence of such negative impact of SLS on drugs and understanding the precipitation thermodynamics and kinetics.

Since the formation of lauryl sulfate salt is an acid - base reaction and the lauryl sulfate acid has a calculated pK_a of -3.29, proton transfer is very likely to occur (> 80% probability) for compounds with a pK_a > 0 according to the ΔpK_a rule. [77] Thus, lauryl sulfate salts with most of drugs containing positive charge(s) or basic groups are expected to form under appropriate conditions.

For precipitation to occur, the degree of supersaturation is the thermodynamic driving force. For the lauryl sulfate salts, we hypothesized that the degree of supersaturation can be quantified as Q/K_{sp}, where Q is the ion product in the solution and

K_{sp} is the solubility product of the salt. Additionally, since SLS is also a surfactant, the concentration of SLS could lead to different precipitation kinetics under the same Q/K_{sp} value.

3.To explore formulation strategies for mitigating the negative impact of SLS on drug dissolution in solid dosage forms.

We hypothesized that reducing the thermodynamic driving force (Q/K_{sp}) by lowering Q in the diffusion layer of a dissolving particle can counter the detrimental effect of LS salt formation on dissolution. As Q is determined by both the concentration of drug cations and the LS^- monomer (equal to CMC of SLS) in the diffusion layer, we explored the strategies of lowering Q value by 1) reducing drug cations concentration by maintaining an elevated local pH in the diffusion layer using a pH modifier, and 2) depressing the CMC of SLS in the diffusion layer using an inorganic salt.

1.4 Research plan and thesis organization

Chapter 2

Chapter 2 describes an unexpected dissolution reduction when SLS was used in a tablet formulation of ritonavir (RTV). Here, SLS was intended to improve wetting, while also functioning as a lubricant. However, tablets containing SLS actually showed slower dissolution rate in simulated gastric fluid than MgSt containing tablets. Systematical investigations revealed that the precipitation of a poorly soluble amorphous salt with LS^-, $[RTV^{2+}][LS^-]_2$, in an acidic environment is the underlying reason.

Chapter 3

In Chapter 3, a crystalline salt of $[NORH^+][LS^-]\cdot 1.5\ H_2O$ between SLS and norfloxacin (NOR) was formed. Based on the solved crystal structure by single crystal X-ray diffraction, we provide direct crystallographic evidence of the ion-ion interaction

between LS^- and $NORH^+$. The available crystal structure also enables the use of the energy framework to gain an understanding of the structural origin of the thermal behavior of $[NORH^+][LS^-]\cdot 1.5\ H_2O$.

Chapter 4

In Chapter 4, we investigated the prevalence of the LS salt among pharmaceutical compounds, formation rules, and its implications on formulation design. We studied 18 compounds with diverse chemical structures, including salts of basic drugs, a quaternary ammonium salt, organic bases, and zwitterionic molecules. A total of 14 compounds formed less soluble LS salts and precipitation occurred when SLS was mixed with respective solutions of these compounds. We further chose *p*-aminobenzoic acid to investigate the precipitation thermodynamic and the kinetics.

Chapter 5

In Chapter 5, we explored possible formulation strategies to mitigate the detrimental effect of LS salt formation on dissolution from a tablet, based on the understanding on the precipitation kinetics in Chapter 4. Here, PABA was used as a model compound. The two strategies we explored are 1) incorporating an inorganic salt to reduce the CMC of SLS, i.e., lower LS concentration in the diffusion layer, and 2) incorporating a pH modifier to maintain an elevated pH in the diffusion layer. Both strategies reduced the ion product (Q) in the diffusion layer, hence, lower driving force for precipitation of the LS salt, but the latter is more effective.

Chapter 2

Mechanism for the reduced dissolution of ritonavir tablets by sodium lauryl sulfate

2.1 Synopsis

Sodium lauryl sulfate (SLS) is an anionic surfactant widely used in pharmaceutical research as a dissolution enhancer for poorly soluble drugs. When SLS was used in ritonavir (RTV) tablet formulation to improve wetting, dissolution of RTV was surprisingly deteriorated in acidic media. To understand this unexpected phenomenon, a systematic investigation, including solubility determination, intrinsic dissolution rate measurement, dissolution in an artificial stomach and duodenum apparatus, and solid-state characterization, revealed the formation of a poorly soluble salt, $[RTV^{2+}][LS^{-}]_2$, in an acidic environment. Solubilization of the poorly soluble RTV salt was observed when the concentration of SLS exceeded the critical micelle concentration. Thus, precipitation of $[RTV^{2+}][LS^{-}]_2$ at a low pH and in presence of a low SLS concentration can lead to deteriorated bioavailability. This unintended negative effect on dissolution should be carefully considered when using SLS in a tablet formulation of a basic drug that can be ionized in gastric fluid.

2.2 Introduction

With the increased number of poorly soluble new chemical entities discovered in pharmaceutical industry, enabling formulation technologies to overcome solubility limited bioavailability have played an increasingly important role in the development of oral solid drug products [4, 19, 78]. To this end, several formulation technologies have been available, such as particle size reduction, cyclodextrins complexation, application of surfactants, polymorph screening, amorphous solid dispersion, and salt or cocrystal preparation.[4, 78-79] Among these, the application of an amphiphilic surfactant to solubilize poorly water-soluble drugs through micellization, and to improve wetting of hydrophobic drugs during dissolution has been widely adopted.[4]

Sodium lauryl sulfate (SLS) is an anionic surfactant commonly used in pharmaceutical formulations and *in vitro* dissolution study.[80-82] It has been used as an emulsifier, solubilizer, tablet lubricant, and wetting agent.[80, 83-86] When applied as a wetting agent, SLS could reduce the surface tension between hydrophobic drugs and aqueous media to prevent the self-aggregation of drug particles, thus increase the effective surface area of dissolution.[83] Above the critical micelle concentration (CMC), SLS monomers aggregate to form micelles that can solubilize hydrophobic drugs.[87-88] In a study to investigate the dual function of SLS as lubricant and wetting agent in a biopharmaceutical classification system II (BSC II) drug, ritonavir (RTV) tablet formulation, using an Artificial Stomach and Duodenum (ASD) apparatus,[50, 89] the use of SLS surprisingly led to slower release of ritonavir than that of the formulation containing a commonly used lubricant, magnesium stearate (MgSt).

A search of the literature led to a handful of reported cases of dissolution slowdown by SLS.[90-95] A possible mechanism was the formation of a poorly soluble complex between drug and SLS during dissolution, where the low diffusivity of the drug-SLS complex could also contribute to the reduced dissolution.[90-95] This phenomenon, although speculated previously, has not been mechanistically proven. The current case of RTV offered a good opportunity to develop mechanistic understanding of this interesting phenomenon. Such understanding is essential to guide the appropriate use of SLS in tablet formulation to avoid surprises.

In this study, we first approached the problem by investigating interactions between RTV and SLS in pH 1.2 and 6.8 media. Then, we isolated and characterized solid-state properties of the insoluble precipitate, followed by examination of the dual process of precipitation and solubilization by SLS and its impact on dissolution behavior.

2.3 Materials and method

2.3.1 Materials

Ritonavir (RTV, Form II, Figure 2.1a) was purchased from Wuhan Beier Biopharm Ltd. (Wuhan, China). Excipients typically used in direct compression tablet formulations, i.e., Microcrystalline cellulose (MCC; Pharmacel 102, DFE Pharma; Goch, Germany), lactose monohydrate (SuperTab 11SD; DFE Pharma; Goch, Germany), Magnesium stearate (MgSt; Covidien, Dublin, Ireland) and croscarmellose sodium (CCS, Ac-Di-Sol, FMC Biopolymer, Philadelphia, PA), and sodium lauryl sulfate (SLS; Ward's Science, Rochester, NY, Figure 1b) were used as received. Other materials were all ACS reagent grade. Hydrochloric acid (36.5-38 %, VWR International, Eagan, MN), sodium phosphate monobasic monohydrate, and sodium phosphate dibasic heptahydrate (Fisher Scientific International, Inc. Fair Lawn, NJ) were used as received to prepare buffer solution.

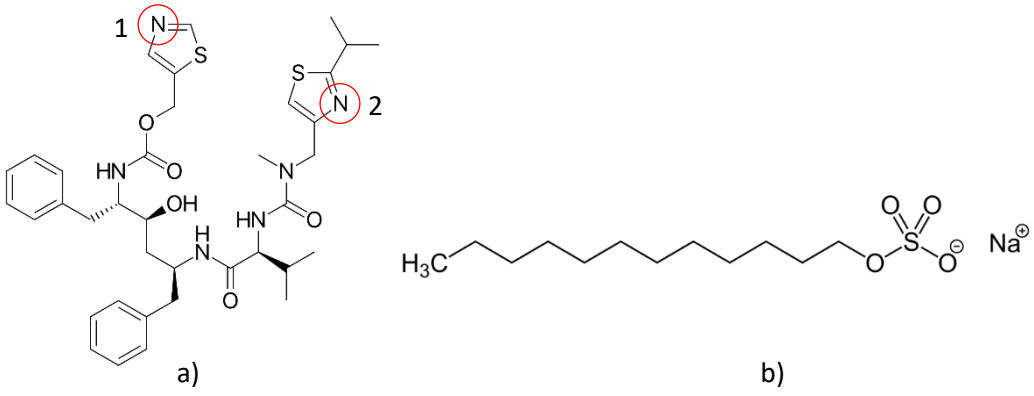

Figure 2.1 Molecular structures of a) ritonavir and b) sodium lauryl sulfate. The calculated pK_a's of RTV are 2.01±0.10 (N_1) and 2.51±0.10 (N_2), and dodecyl hydrogen sulfate is -3.29±0.18.

2.3.2 Methods

2.3.2.1 Calculation pK_a value

The pK_a value was calculated using ACD Lab (V11.01, Advanced Chemistry Development, Inc. Toronto, Canada).

2.3.2.2 Preparation of Tablets

Two formulations (Table 2.1) of ritonavir were prepared by direct compaction. Powder blends were obtained by placing accurately weighed individual components, except the lubricant, in a glass bottle (250 mL), which was then blended on a mixer (Turbula, Glen Mills Inc., Clifton, NJ) at a frequency of 49 rpm for 2 min. Subsequently, a chosen lubricant was added to the bottle and the mixture was blended for another 5 min. Batch size was 40 g in both cases.

Cylindrical tablets (~300 mg) used for ASD study were obtained by compressing the above-mentioned powder blends on a compaction simulator (Presster; Metropolitan Computing Company, East Hanover, NJ) to simulate a 29-station Korsch XL400 tablet press using round flat-faced tooling (10.0 mm diameter). The compaction was conducted at room temperature and approximately 33% RH. The dwell time was set at 30 ms, corresponding to a linear production speed of 0.423 m/s. The compaction pressure was set at approximately 100 MPa without pre-compression.

Table 2.1 Ritonavir tablet formulations (batch size was 40 g).

Material	Amount (*w/w*)	
Ritonavir	5%	5%
60% MCC + 40% Lactose	89%	85%
CCS	5%	5%
MgSt	1%	-
SLS	-	5%
Total	100%	100%

2.3.2.3 Artificial stomach and duodenum dissolution study

The ASD apparatus was similar to that previously described. [50, 96-97] Briefly, it consists of two jacketed beakers with temperature controlled at 37 °C using a water bath to simulate stomach and duodenum, where the fluid flow is regulated by a programmatically controlled peristaltic pump (Masterflex L/S Easy-Load II pump, Cole-Parmer, Vernon Hills, IL).

To simulate human physiological conditions in the fasted state, experiments were conducted with 0.1 N HCl (pH = 1.2) for the stomach and 0.1 M sodium phosphate buffer (pH = 6.8) for the duodenum. The initial fluid volume of the stomach chamber was 250 mL, which was decreased to 50 mL by first-order emptying with a half-life of 15 min. The duodenum volume was maintained at 30 mL throughout the entire study, achieved by setting a vacuum line in the duodenum chamber at a calibrated height. In addition, the

chambers were infused with fresh gastric or duodenal liquid at 2 mL/min to mimic corresponding *in vivo* secretion processes. Drug concentration was monitored by a fiber optic UV/Vis probe. Mixing was achieved by an overhead paddle stirrer in the stomach chamber and a magnetic stirrer in the duodenum chamber. All pumps and spectrometers were calibrated prior to each experiment. All fluids used in the experiment were degassed to avoid the introduction of bubbles that might affect the UV signal transmission.

The drug concentration − time profile in ASD duodenum chamber was analyzed by PKsolver 2.0.[98] The noncompartmental method was used to calculate the peak plasma concentration (C_{max}), time to reach C_{max} (t_{max}), and the area under the concentration − time curve (AUC).

2.3.2.4 Effect of SLS on RTV solution concentration

SLS powder was introduced into a RTV solution (~0.13 mM, 10 mL) at pH 1.2 to arrive at different concentrations of SLS. The systems were stirred for 24 hr using magnetic stirring bars. The suspensions were passed through 0.45 µm filter membrane and RTV concentration in the filtrate was detected by UV spectrometry (DU® 530 UV VIS spectrophotometer, Beckman, Brea, CA).

2.3.2.5 Equilibrium concentration of RTV in SLS solutions

Excess RTV was equilibrated with a series of SLS (0 - 80 mM) solutions at pH 1.2 and pH 6.8 (0.1 M sodium phosphate buffer), respectively. The vials were tightly capped and suspensions were stirred with magnetic stirring bars for 72 hr at room temperature. The samples were filtered and the solutions were diluted appropriately for UV test. The excess solids were collected for powder X-ray diffraction test.

2.3.2.6 Equilibrium concentration of SLS

SLS concentrations were determined using HPLC (Agilent 1290 Infinity), which comprised of the following modules: quaternary pumps, a multi-sampler, multi-column oven, a diode array detector (DAD) and a charged aerosol detector (CAD). The two detectors were connected from outlet of the DAD to the inlet of the CAD by PEEK capillary. Column was a 150 mm × 4.6 mm, 5-µm Thermo Scientific Acclaim Surfactant column. The method details are summarized in Table S2.1. Instrument control and data analysis were carried out with Empower III chromatography data system (Waters Corporation, Milford, MA, USA). The precipitate was dissolved into a mixture of acetonitrile and water (50/50, v/v) to prepare a 1 mg/mL solution, which was injected into the column. The concentration of SLS was determined from the CAD response, which was assumed linear over a narrow range bracketed by two SLS standard solutions. The concentration of RTV was determined by DAD. External standards were used for all the quantifications.

2.3.2.7 Intrinsic dissolution study

Intrinsic dissolution rate (IDR) of RTV was determined by the rotating disc method.[99-100] Dissolution medium was HCl aqueous solution with SLS (0-20 mM) at pH 1.2. Approximately 20 mg of RTV powder was compressed at a force of 2000 lb, using a custom-made stainless steel die, against a flat stainless steel disc for 2 min to prepare pellet (6.39 mm in diameter) with a visually smooth exposed surface that was coplanar with the surface of the die. While rotating at 300 rpm, the die was immersed in 100 mL of the dissolution medium at room temperature, an UV-Vis fiber-optic probe (Ocean Optics, Dunedin, FL) was used to continuously monitor the UV absorbance of the solution at 260 nm. IDR was calculated from the slope of the linear portion of the concentration time profile and the pellet surface area exposed to the dissolution medium.

2.3.2.8 Solid-state characterization

Polarized Light Microscope (PLM)

RTV, SLS, and their complex were observed under a polarized light microscope (Eclipse E200, Nikon, Tokyo, Japan).

Powder X-ray Diffraction (PXRD)

X-ray powder diffractograms were obtained on a wide-angle X-ray diffraction instrument (X'Pert Pro; PANalytical Inc., West Borough, MA) using Cu K_{α} radiation. The voltage and current applied were 45 kV and 40 mA, respectively. Each measurement was performed with a step size of 0.0167° in the two-theta range of 5-35 ° and a dwell time of 1.15 s.

Vibrational Spectroscopy

Fourier transformation infrared (FT-IR) spectra of RTV, SLS and RTV-SLS complex were collected using a FTIR spectrometer (Nicolet iS50; Thermo Scientific, Waltham, MA) with a built-in diamond attenuated total reflection (ATR). The detector was DLaTGS. A total of 32 scans were collected and averaged for each sample. IR spectra in the range of 4000-450 cm^{-1} at a resolution of 2 cm^{-1} were processed using the software OMNIC 9.2. Raman spectroscopy was conducted by spreading approximately 1-3 mg of powder on a glass slide evenly and then flattening using a spatula to facilitate focusing the laser. A point of interest in the powder was focused using the 100× lens of a confocal Raman microscope (Alpha 300R, WITec, Ulm, Germany). The spectra were then acquired using a 532 nm laser source and an integration time of 10 s. The average spectrum of two accumulations was obtained for each sample.

Differential scanning calorimetry

Glass transition temperature (Tg) of the precipitate was determined using differential scanning calorimetry (DSC, Q1000, TA Instruments, New Castle, DE). Before each DSC run, dried and milled precipitate was equilibrated in different RH chambers over saturated aqueous salt solutions (Table S2.2) for at least one week. Equilibrated samples were immediately weighed and packed into aluminum T-zero pans and hermetically sealed with aluminum lids, and cooled to -50 °C from room temperature and then heated to 90 °C at 10 °C/min. The cell was purged with dry nitrogen at 50 mL/min. Tg was determined from the inflection point observed in the heating segment (Figure S2.1), using TA Universal Analysis software.

2.3.2.9 Water sorption isotherm

Water sorption isotherm was obtained using an automated moisture balance (Intrinsic DVS, Surface Measurement Systems Ltd., Allentown, PA, USA) at 25°C. The nitrogen flow rate was 50 mL/min. A sample was first purged with dry nitrogen to a constant weight and then exposed to various relative humidities (RHs) from 0% to 70%. The minimum equilibration time was set as 6 h and equilibration criteria was dm/dt < 0.0005% or maximum equilibration time of 13 h. The RH was changed to the next target value once one of the criteria was met (Figure S2.2). The precipitate became sticky fused mass at the end of the experiment.

2.4 Results and Discussion

2.4.1 Retarded release of RTV in SLS-contained tablet

By more closely mimicking physiological conditions in humans, ASD is a more predictive tool for investigating drug release in GI tract because it considers various processes, such as dissolution, precipitation, and transportation. For drugs with high

permeability, the AUC of the drug concentration – time profile in the duodenum chamber has been shown to be proportional to its *in vivo* bioavailability.[50, 89, 96] Thus, ASD can provide a relative comparison of drug release from formulations or dissolution of different solid forms.

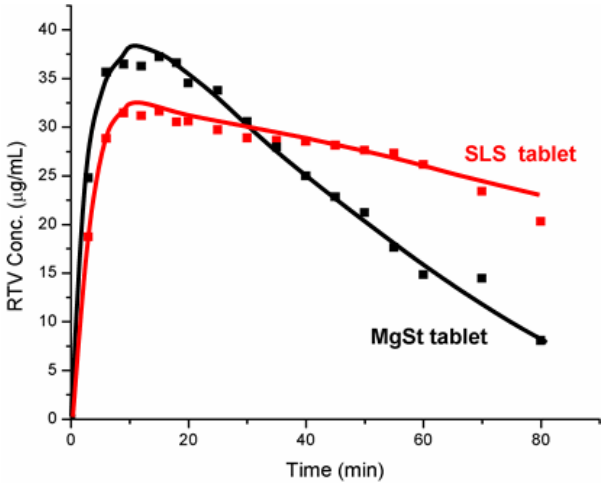

Figure 2. 2. RTV concentration-time profiles of two tablets containing magnesium stearate and SLS in the stomach chamber of ASD.

Due to its hydrophobicity, magnesium stearate (MgSt) might retard drug dissolution.[80, 101-102] SLS has been widely used to either improve wetting or solubilize poorly soluble drugs. Both effects favor faster dissolution. Therefore, replacing MgSt with SLS in an otherwise identical RTV tablet formulation may be expected to improve drug release.[86] However, concentration-time profile in ASD stomach chamber surprisingly exhibited lower C_{max} and longer T_{max} than the MgSt-containing tablet (Figure 2.2). Therefore, an event that leads to slower release of RTV must be at work. An effective solution to this problem requires a mechanistic understanding of the underlying process. We hypothesized that reaction between SLS anions and protonated RTV led to precipitation of a poorly soluble complex, which decreased drug release, as shown in some prior examples.[90-95] This mechanism is possible because the two thiazole nitrogen

atoms to RTV (p$K_{a,1}$ = 1.8 and p$K_{a,2}$ = 2.6 from literature [103] and 2.01±0.10 and 2.51±0.10 by calculation from its molecular structure, Figure 2.1a) undergo protonation at pH 1.2 in the stomach chamber.

2.4.2 Complexation between RTV and SLS

To test the hypothesis, various amounts of SLS powder were introduced to a RTV solution (~0.13 mM, 10 mL) at pH 1.2. The clear RTV solution at pH 1.2 became turbid when SLS was added and RTV concentration continued to decrease until SLS concentration was ~1.1 mM (Figure 2.3). Further increase in SLS concentration above 1.1 mM led to increasing RTV concentration and a clear solution was again obtained. The precipitation upon introduction of SLS and the simultaneous decrease in RTV concentration suggest the precipitate is a complex between SLS and RTV, which is less soluble than pure RTV at pH 1.2.

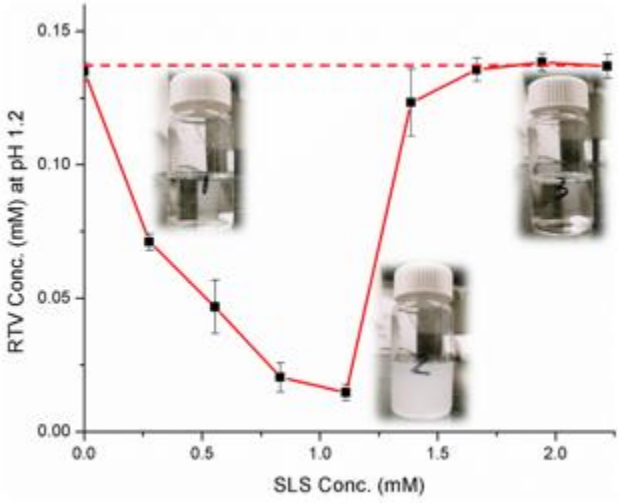

Figure 2.3. Effect of SLS on RTV solution concentration at pH 1.2 (*n*=3)

The precipitate was very fine when they initially formed (Figure 2.4c). However, large particles appeared while fine particles disappeared over time (Figure 2.4d). This may be attributed to the Ostwald ripening where larger particles grow at the expense of smaller ones.[104] The precipitate was recovered through vacuum filtration and characterized using multiple techniques for its chemical composition and solid-state properties. The absence of birefringence under PLM (Figure 2.4c and 2.4d) and mere presence of an amorphous halo in PXRD pattern (Figure 2.5) indicated the amorphous nature of the precipitate. In contrast, both RTV and SLS were crystalline as they exhibited birefringence (Figure 2.4a and 2.4b) and strong X-ray diffraction peaks (Figure 2.5). Furthermore, the glass transition temperature (Tg) of the dried solid was 30.9 °C (Figure 2.6). The fresh precipitate was sticky and gel like when it was in full contact with water. Thus, Tg of fully hydrated precipitate is below room temperature, due to the plasticizing effect of water. This has been proved by the gradual decrease in Tg of the precipitate with water increasing contents when equilibrated at higher RHs (Figures 2.6 and S2.1).

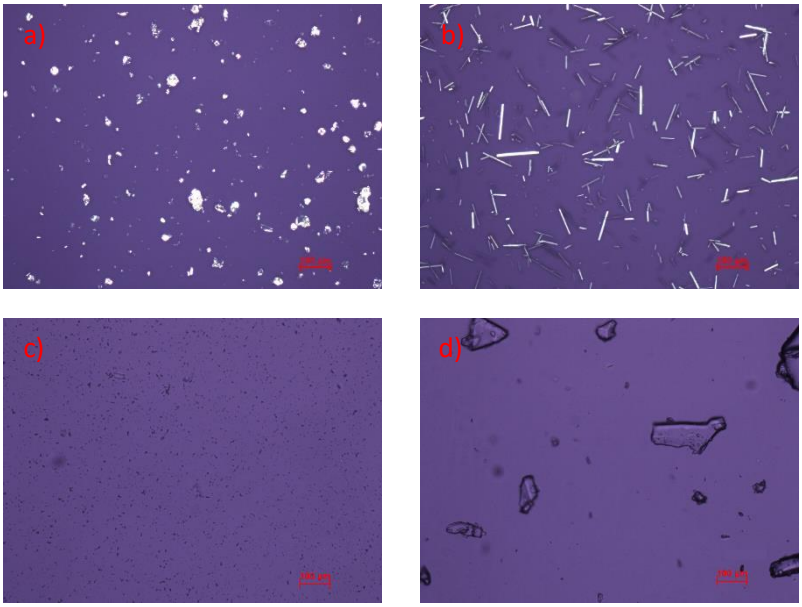

Figure 2.4. PLM of a) SLS, b) RTV, c) fresh precipitate, and d) precipitate aged for 72 hours.

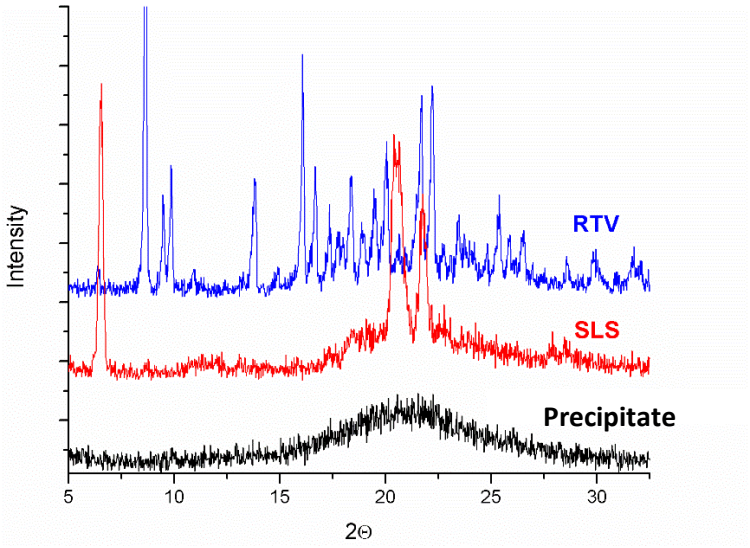

Figure 2.5. PXRD of RTV, SLS, and precipitate.

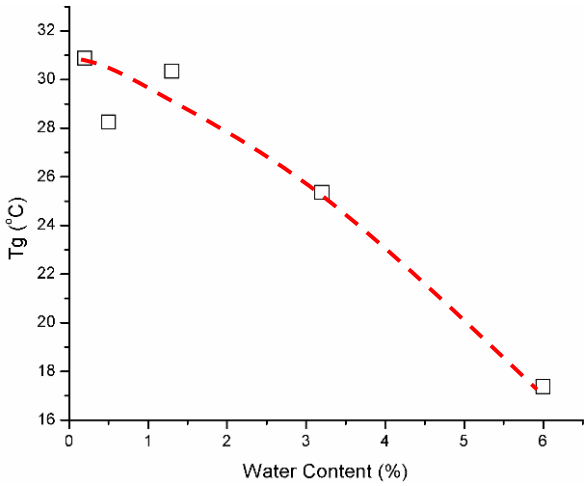

Figure 2.6. Tg of the precipitate as a function of water content**.**

FT-IR and Raman spectra of the RTV, SLS, and the precipitate are shown in Figure 2.7. For both IR (Figure 2.7a) and Raman (Figure 2.7b) spectra, characteristic peaks of RTV and SLS could be observed in the precipitate, confirming it is a complex between RTV and SLS. The single IR peak of 3322 cm^{-1} is attributed to the N-H stretching of amide

groups and the broad peak of 3203 cm^{-1} is assigned to the hydroxyl group to RTV. Several peaks observed in the range of 2800-3000 cm^{-1} correspond to C-H stretching vibrations. The C=O stretching vibrations of amide and ester groups of RTV correspond to peaks at 1702 and 1659 cm^{-1}. The strong absorption peaks in the IR spectrum of SLS at 1248 and 1215 cm^{-1} are assigned to the stretching of S=O. These peaks are red-shifted to 1245 and 1197 cm^{-1}. The IR peak due to the N-H is also red shifted to 3302 cm^{-1}. The peak shifts suggest the presence of an S=O···H-N^{+} hydrogen bond in the precipitate (Figure S2.3). Similar interaction was observed in 9-aminoacridinium dodecyl sulfate, 2-(dodecanoyloxy) ethanaminium dodecyl sulfate, and 1-Octylquinolinium dodecyl sulfate.[105-107]

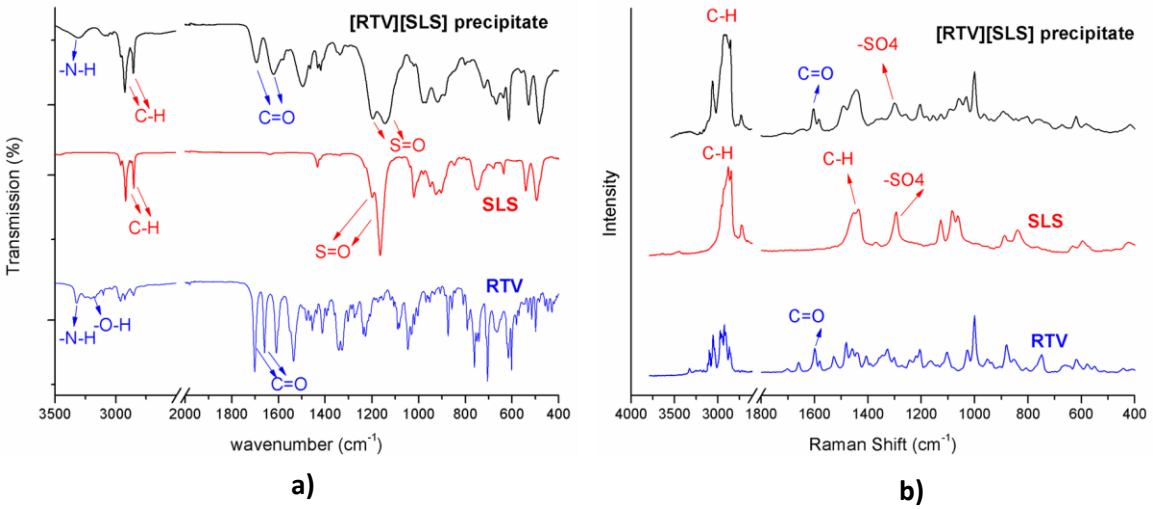

Figure 2.7. Vibrational spectra of RTV, SLS, and precipitate, a) FTIR and b) Raman.

Corresponding to the two thiazole groups of RTV, two types of ionic species of RTV may exist in the solution, RTV^{+} and RTV^{2+}. Based on Henderson-Hasselbalch equation,[4] approximately 80% of RTV ($pK_{a,1}$ = 1.8, $pK_{a,2}$ =2.6) exists as RTV^{+} and 20% are RTV^{2+} at pH 1.2. The pK_a of the conjugate acid of SLS, dodecyl hydrogen sulfate (LS-H), is -0.09 from the literature and -3.29 by calculation.[108] Therefore, essentially all lauryl

sulfate ions, LS^-, remained ionized instead of forming LS-H in 0.1 M HCl, [81] which favors its reaction with the protonated RTV cations to form complexes, either $[RTV^{2+}][LS^-]_2$ or $[RTV^+[LS^-]$. Since the ∆pKa (base – acid) between the calculated pK_a's of LS-H and RTV is larger than 5, proton transfer between RTV and SLS is highly likely.[109]

2.4.3 Effects of SLS and pH on equilibrium concentration of RTV

The solubility of RTV in the pH 1.2 and the pH 6.8 media was 0.2 ± 0.02 mM and 0.008 ± 0.002 mM (Figure 2.8a & 2.8b). The radically higher solubility at pH 1.2 is due to the ionization of RTV, as shown by its pH-solubility profile (Figure S2.4).

At pH 1.2, 10 mL SLS solutions with different concentrations (0-80 mM) were prepared. Approximately 100 mg RTV powder was introduced into each of them (with exception of 150 mg in 80 mM SLS). After stirring for 72 hr, excess solid in each vial was isolated by vacuum filtration. Solution pH increased with increasing SLS concentration, up to 1.6 in the sample containing 80 mM of SLS. Concentration of RTV in solution was determined by UV/VIS spectroscopy with dilution if needed. The RTV concentration decreased with increasing SLS concentration and reached a minimum value at a SLS concentration of approximately 30 mM (Figure 2.8a). However, RTV concentration increased sharply with further increase in SLS concentration (Figure 2.8a). In Figure 2.8a, the total concentration of SLS in the system was used. The actual concentration of SLS in solution was lower because of the precipitation of the SLS-containing salt and possible degradation of SLS at low pH. In the 0-30 mM SLS concentration region, the equilibrating excess solids exhibited decreasing crystallinity with increasing amount of SLS (Figure 2.8c and 2.8d), corresponding to the loss of crystalline RTV due to the increasing extent of complex formation. When total SLS concentration was 30 mM or greater, crystalline RTV disappeared in the equilibrating solid (Figure 2.8d), indicating complete conversion of crystalline RTV to the amorphous salt.

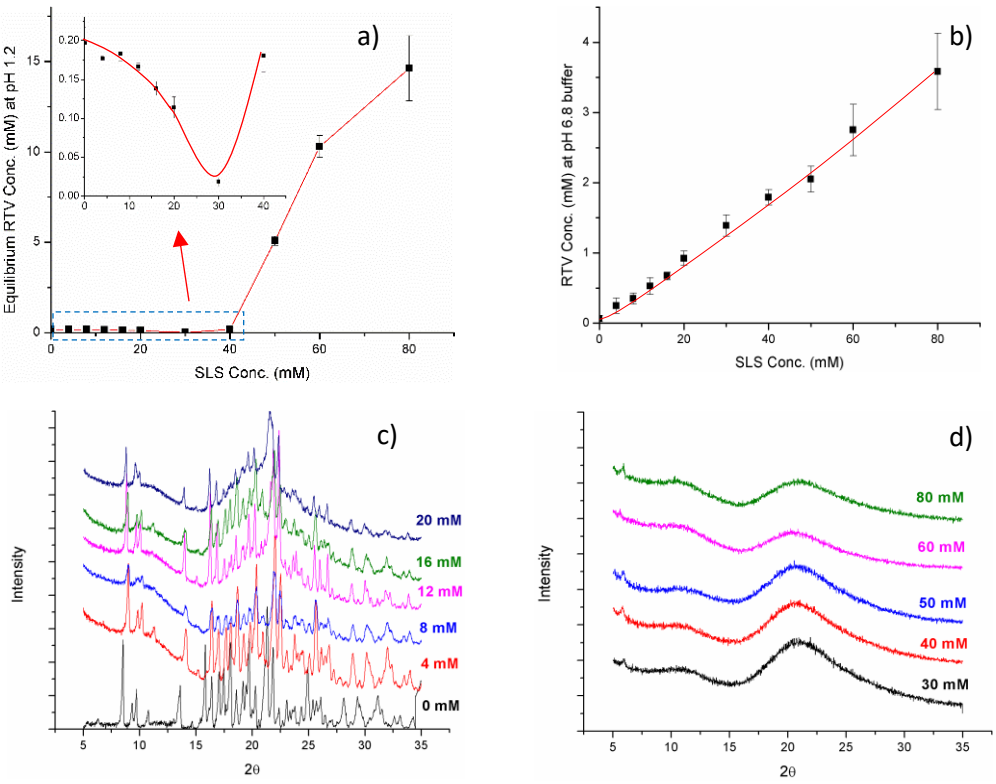

Figure 2.8. Equilibrium concentration of RTV in SLS solutions (0-80 mM, *n*=3) in a) pH 1.2 and b) 0.1 M sodium phosphate pH 6.8 buffer. PXRD analysis of excess solids c) at pH 1.2 with SLS concentration of 0-20 mM and d) 30-80 mM.

Solids at 30 and 80 mM were chosen for determining the stoichiometry of the salt by HPLC-CAD. The CAD detector was employed because the absence of a chromophore in SLS molecule makes it difficult to detect by traditional UV/Vis method.[110] Approximately 1:2 molar ratio of RTV to SLS was determined (Table S2.3) to yield a formula of $[RTV^{2+}][LS^{-}]_2$ for the salt.

At pH 6.8, RTV undergoes minimum ionization (less than 0.01%). Correspondingly, no conversion of the crystalline RTV to the amorphous salt was observed (Figure S2.5). Solution concentration of RTV increased monotonically with increasing SLS concentration while solution pH did not change. CMC value of SLS decreases with increasing electrolyte

concentration and is 1.99 mM in 0.05 M sodium phosphate buffer at pH 7.[111] Therefore, the CMC of SLS in the pH 6.8 phosphate buffer (0.1 M) in this study is expected to be lower than 1.99 mM. Consequently, SLS micelles formed in all SLS solution concentrations in this study because they were all above 1.99 mM. This is in good agreement with the nearly linear rise in RTV solubility with increasing SLS concentration (Figure 2.8b) due to the solubilization of RTV by SLS micelles.

Clearly, solubility of RTV and precipitation of $[RTV^{2+}][LS^-]_2$ depend on both pH and SLS concentration. These complicated effects can be understood from a holistic consideration of possible equilibria in this system (Figure 2.9). For the salt complex to form, RTV cation and SLS anion must be present in the solution at concentrations at which the K_{sp} of the complex is surpassed. From the measured concentrations of SLS and RTV in the solutions containing 0.28 and 0.55 mM total SLS (Figure 2.3), K_{sp} was calculated to be 3.5×10^{-4} and 2.7×10^{-4} $(mg/mL)^3$ (or 5.9×10^{-3}, 4.4×10^{-3} mM^3), respectively. RTV, as a di-basic compound with two ionization sites, can form both monovalent ion and divalent ion. The relative abundance of RTV ions and neutral RTV is affected by the ionization equilibration constants and solution pH. Because the stoichiometry of the complex is 1:2, the mono-salt must be more soluble than the di-salt. Therefore, when a small amount of SLS was added to a RTV solution at pH 1.2, the amorphous di-salt precipitated out. When the SLS concentration is sufficiently high, the precipitate can be re-dissolved by SLS micelles. Various equilibria of this system are summarized in Figure 2.9.

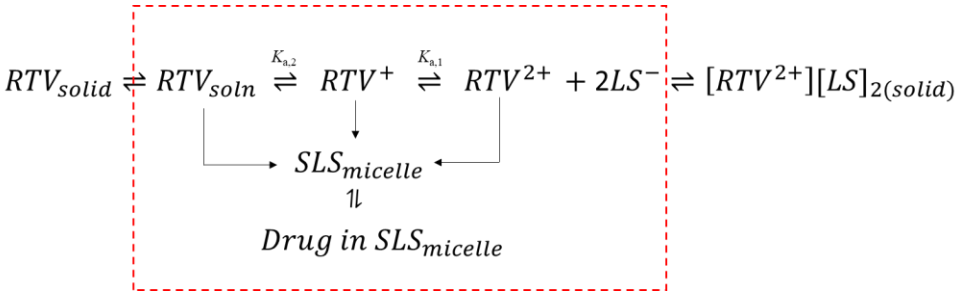

Figure 2.9. Equilibria in the 0.1 M HCl solution containing SLS and RTV.

2.4.4 Impact of SLS-contained media on RTV dissolution

2.4.4.1 Intrinsic dissolution rate (IDR)

So far, the slower release of RTV during dissolution in simulated gastric fluid (Figure 2.2) can be reasonably explained by the formation of a less soluble salt. To confirm this, IDRs of RTV at pH 1.2 in media containing different concentrations of SLS were determined.

The initial portion of some dissolution profiles in IDR study was not strictly linear, which indicates phase change during dissolution (Figure S2.6). We attribute this to the dynamic nature of the precipitation and the time required to establish equilibrium during IDR experiments. Thus, the IDR was calculated using terminal slope to characterize dissolution, assuming this is where the new solid phase would be dominant. IDR initially decreased with increasing SLS concentration in the media up to 2 mM SLS. Further increase in SLS concentration in the dissolution medium led to steady increase in IDR (Figure 2.10). This is consistent with the trend observed in solubility plot (Figure 2.8a). The precipitation reaction and formation of the less soluble salt hinders IDR and this detrimental effect is more obvious in a more concentrated SLS medium, which explains the initial decrease in IDR. When SLS concentration is above CMC, solubilization of RTV by micelles also occurs. The rate of solubilization is higher in a more concentrated SLS medium, which favors higher IDR. With increasing SLS concentration, IDR transitions

from the precipitation dominating phase to the solubilization domain. The transition point roughly agrees with the CMC of SLS, which is likely slightly below 1.99 mM.

The nominal SLS concentration corresponding to the turning point in the IDR plot is 2 mM while 30 mM in the solubility plot (Figure 2.8). This discrepancy may be explained by the different designs of the two experiments. In the equilibrium concentration study, RTV introduced into each vial consumes SLS in the solution. Thus, the actual SLS concentration is far lower. In contrast, the dissolution of a small amount of RTV into the medium did not noticeably lower the SLS concentration in the medium. Hence, solubilization effect is observed at a much lower SLS concentration.

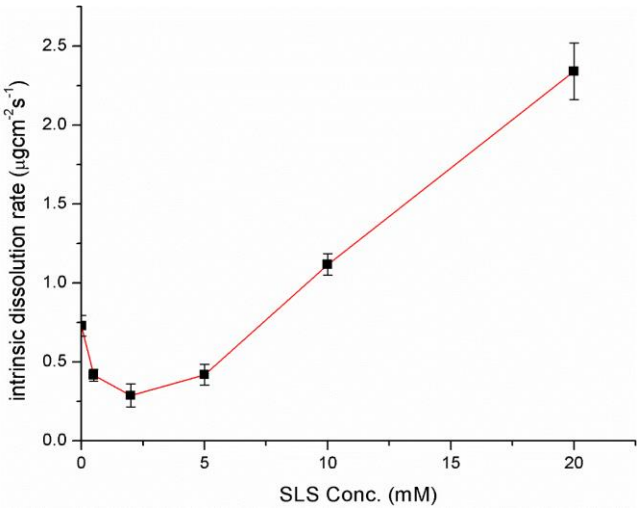

Figure 2.10. Dependence of intrinsic dissolution rate of the di-salt as a function of SLS concentration (*n*=3).

2.4.4.2 Artificial Stomach and Duodenum (ASD) dissolution study

The effect of SLS on drug release was also evaluated in ASD at different concentrations of SLS, which was kept the same in stomach and intestine chambers (Figure S2.7). With increasing SLS concentration, both AUC and C_{max} first decreased and then increased (Figures 2.11a and 2.11b). This is similar to the trend observed in the IDR and solubility experiments, The reduced dissolution is explained by the formation of the less soluble $[RTV^{2+}][LS^{-}]_2$ salt. The subsequent increase with increasing SLS concentration is due to solubilization by SLS micelles. Thus, the impact of SLS on RTV bioavailability depends on SLS amount in the formulation. Since SLS in a tablet formulation is usually not used at a very large amount due to the toxicity concern, the detrimental effect by SLS likely dominates the dissolution performance of tablets. However, such detrimental effect is less likely to occur if protonation of APIs can be avoided or suppressed, such as by avoiding low pH gastric fluid using enterically coated tablets.

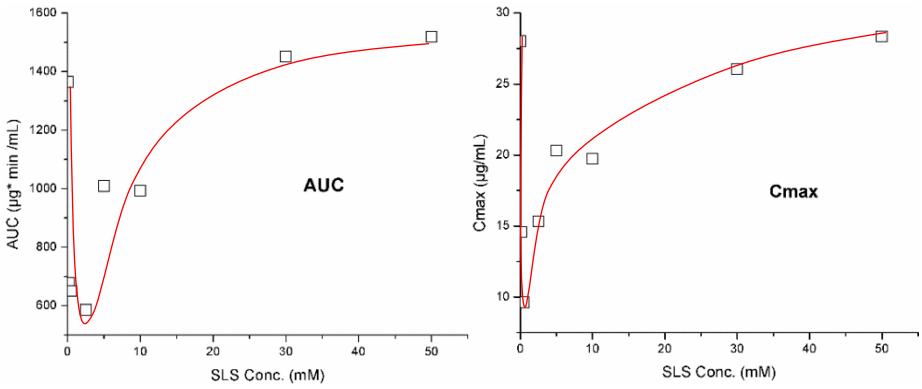

Figure 2.11. Duodenum Concentration-Time Profile parameters for RTV tablet a) AUC, and b) C_{max}

Since SLS is not naturally present in the GI tract, this effect is not a threat to drug dissolution if the drug product does not contain SLS. However, for poorly soluble drugs,

SLS is often used to either improve wetting or create a sink condition during *in vitro* dissolution. In this context, the complicated precipitation and solubilization mechanism detailed above is relevant. If not carefully controlled, the *in vitro* dissolution study may yield misleading results and possible erroneous conclusions on tablet quality and biopharmaceutical performance.

2.5 Conclusion

The use of SLS in the RTV tablet formulation deteriorated RTV dissolution in simulated gastric fluid due to the formation of a poorly soluble salt, $[RTV^{2+}][LS^{-}]_2$. The salt was formed only when pH was sufficiently low to assure a significant concentration of protonated RTV in solution. This leads to detrimental effect on RTV dissolution. Given the frequent use of SLS in pharmaceutical formulations, the results from this study highlight the need to carefully consider potential complexation between SLS and basic drugs during dissolution during tablet formulation development. Potential issue to consider include: 1) the risk of slower release of basic drugs by forming poorly soluble complexes with SLS; 2) SLS containing dissolution media may lead to erroneous conclusion of poor dissolution performance of a formulation that may actually exhibit excellent dissolution in SLS free human GI tract.

2.6 Support information

Differential scanning calorimetry study of RTV-SLS precipitate equilibrated at different RHs

Glass transition temperature was determined from the inflection point observed in the heating cycle.

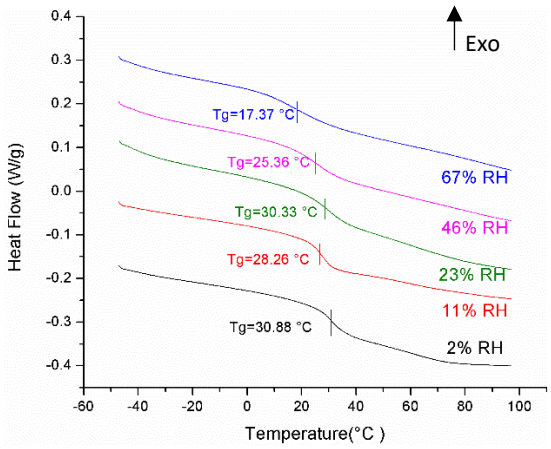

Figure S2.1. Effect of water content on the glass transition temperature. Samples were equilibrated at different RHs for at least 1 week.

Dynamic vaper sorption isotherm

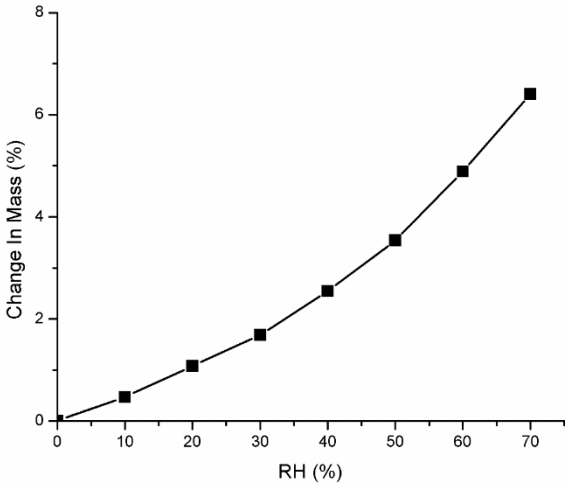

Figure S2. 2. Water sorption isotherm of the precipitate at 25 ^{o}C.

Molecular interaction

The majority of intermolecular interactions involve the sulfate group of LS^-. The charged $-NH^+$ nitrogen is favorable to form S=O…H-N+ interaction with LS^-.

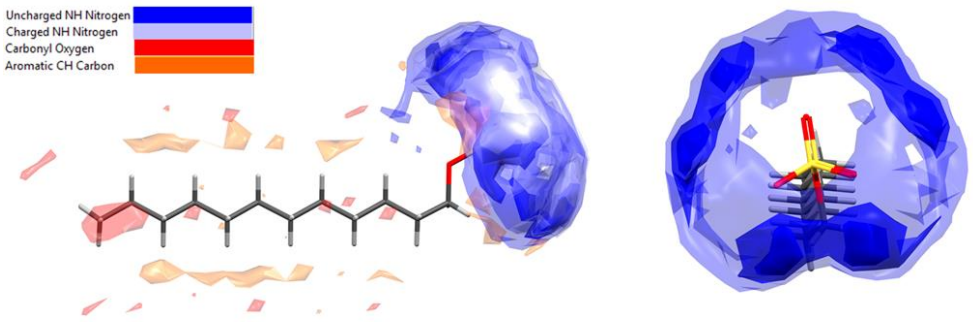

Figure S2.3. Full interaction maps of SLS.

pH dependent solubility of ritonavir

The pH dependent solubility of ritonavir was calculated based on Henderson-Hasselbalch equation with $pK_{a,1}$ = 1.8, $pK_{a,2}$ = 2.6 of RTV, and intrinsic solubility of 1 μg/mL.

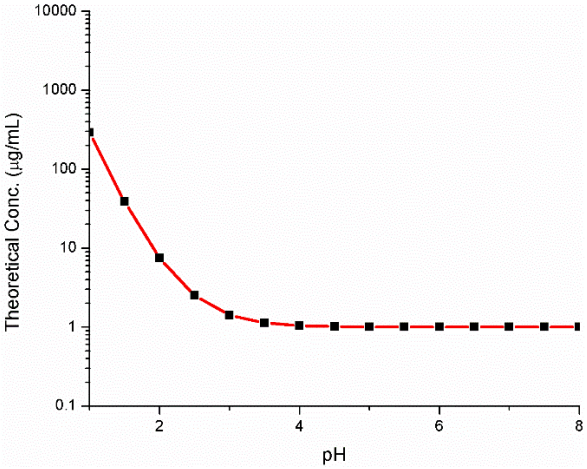

Figure S2.4. pH dependent solubility of ritonavir

Equilibrium concentration of RTV in SLS solutions at pH 6.8

Excess RTV was equilibrated with series concentration of SLS (0-80 mM) solution at pH 6.8 (0.1 M sodium phosphate buffer). Excess solid was collected for powder X-ray Diffraction test study after 72 hours stirring at room temperature. The presence of crystalline peaks through the entire SLS range indicated no conversion of the crystalline RTV to the amorphous salt at in phosphate buffer at pH 6.8.

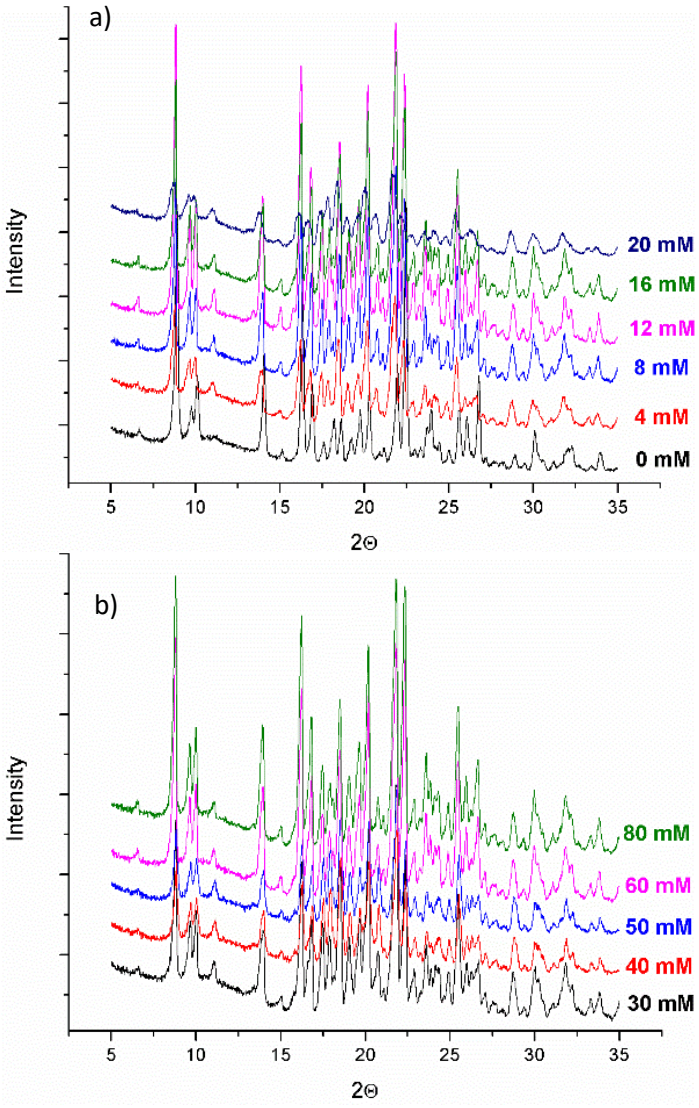

Figure S2. 5. PXRD analysis of excess solid in pH 6.8 phosphate buffer with SLS concentration a) 0-20mM, and b)30-80mM

Intrinsic Dissolution Rate

RTV concentration – time profiles in 0.1 M HCl with different concentrations of SLS are shown in Figure S2.6. The IDR profiles are non-linear in most cases but highly reproducible. We attribute this to the simultaneous occurrence of two competing

processes, precipitation and solubilization of the SLS-RTV complex, in the diffusion layer of different concentrations of SLS.

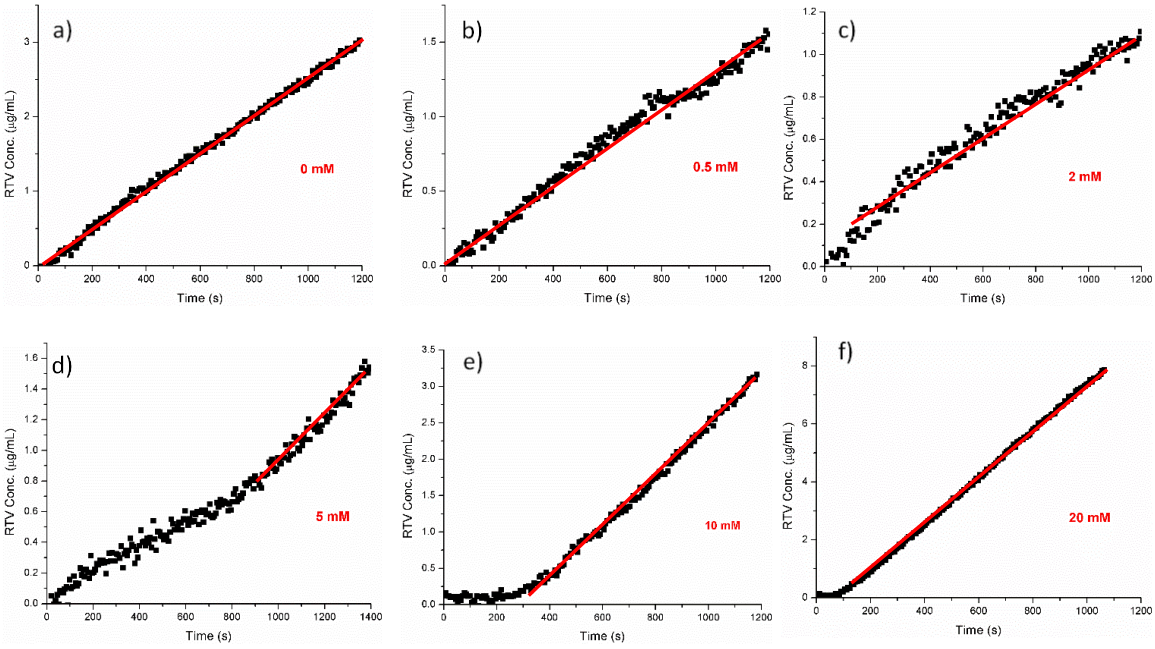

Figure S2. 6. Dissolution profiles of RTV discs in pH 1.2 media containing different concentrations of SLS.

Dissolution studies using an artificial stomach and duodenum (ASD)

Different concentrations (0-80 mM) of SLS were prepared for both simulated gastric and intestinal fluids used in the ASD experiments. The concentration of SLS was kept the same in both chambers in each experiment. Two UV/VIS fiber probes were inserted into both chambers to monitor the drug release. RTV concentration – time profiles in the duodenum chamber are shown in Figure S2.7. These profiles are fitted using a non-compartment pharmacokinetic model.

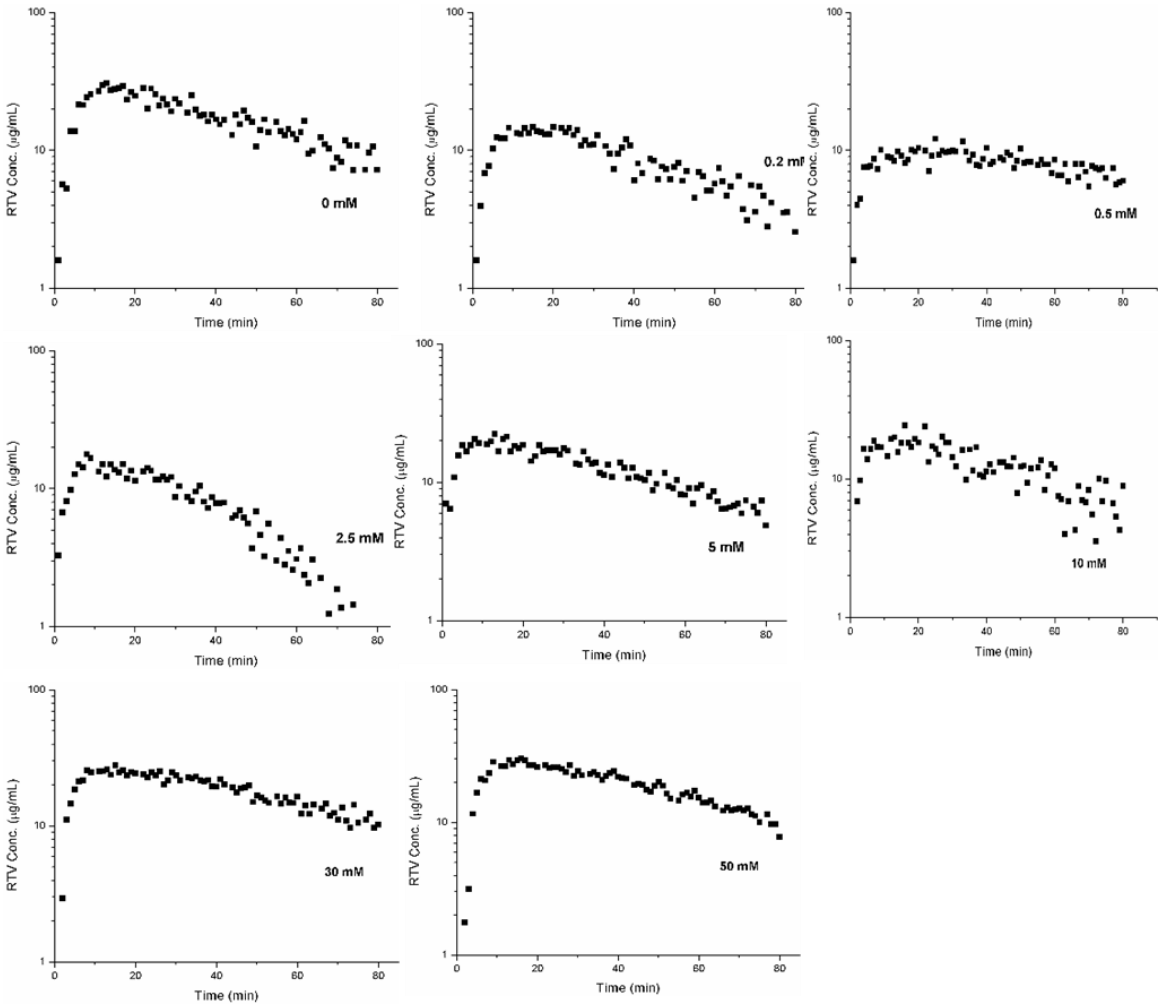

Figure S2. 7. Dissolution profiles in ASD duodenum chamber containing media with different SLS concentrations.

Table S2. 1. SLS Method parameters

Column	Thermo Scientific Acclaim Surfactant column, 150 mm × 4.6 mm, 5-µm
Eluent A	100 mM of Ammonium acetate buffer, pH 5.4
Eluent B	Acetonitrile
Flow rate	1.0 mL/min
Gradient	0-4.5 min: 50%B; 4.5-12.0 min: 50%B-90%B; Hold 90%B for 5 min. Post time: 4 min at 50%B
Column oven	30°C
Sampler temperature	Ambient
DAD Wavelength	240 nm, Reference Wavelength: 500 nm
CAD	data rate: 5 Hz, nebulizer temperature: 35°C
Injection volume	10 µL

Saturated aqueous salts solution with different relative humidity.

Saturated aqueous salts solutions were prepared in a 50 mL plastic wide-mouth container, different amount of salts was dissolved by 10 - 20 mL deionized water. The screw-capped containers were equilibrated under room temperature for 72 hours to meet the targeted humidity. Drierite-contained chamber was used to provide a low RH of 2%.

Table S2. 2. Saturated salt solution with different RH

Salt	Relative humidity (%)
LiCl	11
$KC_2H_3O_2$	23
K_2CO_3	43
$CuCl_2$	67

Stoichiometry determination of RTV and SLS

Table S2. 3. Stoichiometry determination of RTV and SLS

SLS Conc. (mM)	Mol Ratio of SLS to Ritonavir	Ritonavir%	SLS%
30	2.00	51.32*	44.6*
80	2.25	43.79*	42.7*

* The total weight of SLS and RTV do not add up to 100% due to the presence of water and some impurities. SLS is known to undergo degradation in media with pH lower than 2.5.

Chapter 3

Crystallographic and Energetic Insights into Reduced Dissolution and Physical Stability of a Drug-Surfactant Salt – The Case of Norfloxacin Lauryl Sulfate

3.1 Synopsis

A commonly used pharmaceutical surfactant, sodium lauryl sulfate (SLS), has been reported to reduce the dissolution rate of drugs due to the formation of a less soluble drug-lauryl sulfate salt. In this study, we provide direct crystallographic evidence of the formation of salt between SLS and norfloxacin (NOR), $[NORH^+][LS^-]\cdot 1.5\ H_2O$. The available crystal structure also enables the use of the energy framework to gain an understanding of structure – property relationship. Results show that the hydrophobic methyl groups in SLS dominate the surfaces of the $[NORH^+][LS^-]\cdot 1.5\ H_2O$ crystals, resulting in the increased hydrophobicity and reduced wettability by aqueous media. Moreover, an analysis of molecular environments and energy calculation of water molecules provides insight into the stability of $[NORH^+][LS^-]\cdot 1.5\ H_2O$ with variations in relative humidity and temperature. In summary, important pharmaceutical properties, such as solubility, dissolution, and thermal stability, of the drug-surfactant salt $[NORH^+][LS^-]\cdot 1.5\ H_2O$ have been characterized and understood based on crystallographic and energetic analyses of the crystal structure.

3.2 Introduction

Dissolution of a solid drug is critical for successful drug delivery as a prerequisite for absorption.[4] A surfactant is often used to enhance the dissolution of a poorly soluble drug, [112] through either improving wetting of the solid by the aqueous medium[113] or solubilizing drugs when micelles are formed.[114]

The sodium salt of lauryl sulfuric acid (LS-H with a pK_a of -3.29, Figure 3.1b), is one of the most commonly used surfactants in non-parenteral pharmaceutical formulations and cosmetics.[115] However, sodium lauryl sulfate (SLS) was found to reduce the solubility and dissolution rate of some basic drugs in low pH media by forming poorly soluble complexes. [8, 90-93, 116] This phenomenon highlights the need to exercise caution when using SLS in solid dosage formulations to avoid the unexpected decrease in drug dissolution.[8]

The formation of such drug-surfactant complexes has been confirmed by visual observation, PXRD, IR, Raman, and compositional analysis of the complex. The Coulombic interaction between drug cation and lauryl sulfate anion (LS^-) has been proposed based on the ΔpK_a rule. This is supported by the fact that precipitation only occurred at pH values, where drugs are protonated. [8, 92-93] Such charge-charge interaction of LS^- was also reported with amine functional polymer cations via solubility diagram and surface tension measurement. [94]

In this study, we provide a more direct evidence of proton transfer between drug cation and LS^- anion through an analysis of crystal structure, from which molecular insights into the changes in pharmaceutical properties, such as solubility and dissolution rate, could be gained. Crystal structures of a handful of complexes between LS^- and organic molecules have been reported, including berberine,[117] 9-aminoacridine (a cationic dye), *O*-lauroylethanolamine,[107] quinolinium and isoquinolinium (ionic liquid crystals).[105] However, most reported drug-lauryl sulfate complexes are amorphous, except for

trimethoprim and metformin, which precipitated out as crystalline solids.[90-91] Single crystal structures of trimethoprim and metformin complexes with LS^- have not been reported. Consequently, direct crystallographic insights into some important pharmaceutical properties remain elusive.

In a systematic screening for drug lauryl sulfates, we successfully grew single crystals of the complex formed between norfloxacin (NOR, a broad-spectrum antibacterial compound) and SLS and solved its structure. This provides an opportunity for gaining direct molecular insight into the nature of such drug-LS^- complexes and their solid-state properties. [118]

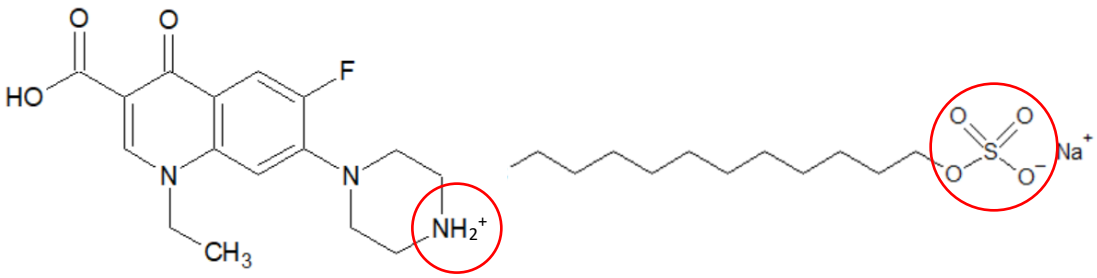

a) b)

Figure 3. 1. Molecular structure of a) norfloxacin cation ($NORH^+$) and b) SLS.

3.3 Materials and methods

3.3.1 Materials

Norfloxacin was purchased from SINCH Pharmaceuticals (Shanghai, China). Sodium lauryl sulfate was purchased from Ward's Science (Rochester, NY). Hydrochloride acid (36.5%-38%, VWR international, Eagan, MN) was ACS reagent grade. Sodium phosphate monobasic and sodium phosphate dibasic heptahydrate were purchased from Fisher Scientific International, Inc (Fair Lawn, NJ). All materials were used as received.

3.3.2 Methods

3.3.2.1 Calculation of pK_a value

The pK_a value of LS-H was calculated using the ACD Lab (V11.01; Advanced Chemistry Development, Inc., Toronto, Canada). The prediction was made based on a statistical model between molecular structures and experimentally measured pK_a values, which was established using a large set of molecules.

3.3.2.2 Precipitation of NOR by adding SLS

An excess amount of NOR powder was suspended in 15 mL of pH 1.2 hydrochloric acid (HCl) aqueous solution. After about 8 hours, the suspension was filtered to obtain a NOR solution, to which ~50 mg of SLS powder was slowly introduced. Precipitation occurred immediately after SLS was dissolved (Video S3.1). The precipitate was recovered by vacuum filtration and air-dried on the bench.

3.3.2.3 Powder X-ray diffraction (PXRD)

X-ray diffractograms of powders were collected by a wide-angle X-ray diffraction instrument (X'Pert Pro; PANalytical Inc., West Borough, MA) using Cu-*K*α radiation. The voltage and amperage were 45 kV and 40 mA, respectively. Each measurement was performed with a step size of 0.0167° in the two-theta range of 5-35° and a dwell time of 1.15 s.

3.3.2.4 Polarized Light Microscopy

The precipitate was observed under a polarized light microscope (Eclipse E200; Nikon, Tokyo, Japan). A small drop of the solution containing solid precipitate was put on a glass slide. A cover glass was then applied, which was gently pressed to further disperse the sample.

3.3.2.5 Karl Fischer titration (KFT)

Water content of the precipitate was determined with a Karl Fischer Titrator (Metrohm 831 KF coulometer equipped with a Metrohm 703 Ti Stand mixer). Titrations were carried out in HYDRANAL®-Coulomat AG (methanol-based anolyte, Sigma Alderich, St. Louis, MO) under constant stirring. An accurately weighed sample (approximately 10 mg) was introduced into the titration vessel, which was immediate capped to minimize interference by moisture from the environment. Water content was recorded at the end of each titration run. Measurements were repeated six times.

3.3.2.6 Moisture sorption isotherm

Water sorption isotherm of the precipitate powder was collected using an automated dynamic vapor sorption analyzer (Intrinsic DVS, Surface Measurement Systems Ltd., Allentown, PA) at 25 °C. The nitrogen flow rate was 50 mL/min. The sample was first purged with nitrogen at 70% relative humidity (RH) until a constant weight was obtained. Then, the sample was exposed to a series of RHs from 70 to 0%, 0 to 95% and 95 to 0%, with a step size of 5% RH. At each specific RH, the equilibration criterion of either dm/dt ≤0.002% with a minimum equilibration time of 0.5 h or a maximum equilibration time of 6 h was applied. The RH moved to the next target value once one of the criteria was met. This experiment was started at 70% RH instead of 0% because the sample, consisting of hydrate crystals, undergoes dehydration on exposure to dry nitrogen purge.

3.3.2.7 Thermal analyses

Thermal properties of the precipitate powder were characterized by differential scanning calorimetry (DSC, TA Instruments, New Castle, DE), thermogravimetric analysis (TGA, Q500, TA Instruments, New Castle, DE) and variable temperature powder X-ray diffractometry (vtPXRD,TK450; Anton Paar, Graz-Straßgang, Austria). In DSC, each

sample was packed into an aluminum T-zero pan and hermetically sealed with an aluminum lid, a pin hole was made to allow the escape of volatiles produced during heating. The heating rate was 10 °C/min unless specified. The DSC cell was purged with nitrogen gas at 50 mL/min. In TGA, the samples were purged with dry nitrogen at 60 mL/min and heated at rate of either 0.5 or 10 °C/min. In vtPXRD, a temperature stage (TTK 450; Anton Paar, Graz-Straÿgang, Austria) was used to control the sample temperature on a powder X-ray diffractometer (D8 CEVANCE; Bruker AXS, Madison, WI) using Cu *K*α radiation (40 kV, 40 mA) and Si strip one-dimensional detector (LynxEye; Bruker AXS, Madison, WI). Under the nitrogen purge (50 mL/min), the sample was heated to the target temperatures from room temperature at a rate of 10 °C/min and then maintained under isothermal conditions during data collection (5-30° 2θ with a step size of 0.02° and a dwell time of 0.5 s). Hot-Stage Microscopy (HSM) was conducted using a polarized light microscope (Eclipse e200; Nikon, Tokyo, Japan) equipped with a hot stage with a temperature controller (Linksys 32; V.2.2.0, Linkam Scientific Instruments, Ltd., Waterfield, UK). A single crystal was immersed in a drop of silicone oil on a glass slide and heated to 300 °C at a rate of 10 °C/min.

3.3.2.8 Thermodynamic solubility

The solubilities of the NOR and the precipitate powders were determined by equilibrating excess amount of each sample in ~10 mL of pH 1.2 HCl (adjust pH when necessary) solution or a pH 6.8 sodium phosphate buffer (0.1 M) at 23 °C under vigorous stirring for 48 h. The suspensions were filtered with 0.45 µm polypropylene membrane filters. The concentration of filtrates was determined using a UV spectrometer (DU® 530 UV-vis spectrophotometer; Beckman, Brea, CA) after appropriate dilution and interpolation from a standard curve. The nature of the equilibrating solid phase was identified by PXRD.

3.3.2.9 Intrinsic dissolution rate (IDR)

IDR was measured using a rotating disk method. Dissolution was performed in both a pH 1.2 HCl solution and a pH 6.8 sodium phosphate buffer (0.1 M). Approximately 20 mg of sample powder was compressed using a custom-made stainless-steel die against a flat stainless steel disc for 2 min to prepare pellets (6.39 mm in diameter). A force of 1000 lb was used to prepare pellets of the precipitate to avoid extensive sticking to the steel disc at high pressures. For NOR, a force of 2000 lb was applied to favor the formation of smoother surfaces since it did not stick. The exposed surface of the pellet was visually smooth and coplanar with the surface of the die. While rotating at 200 rpm, the die was immersed in 300 mL of the dissolution medium in a water jacketed beaker with temperature maintained at 23 °C. UV absorbance of the solution was continuously monitored with an UV-Vis fiber-optic probe (Ocean Optics, Dunedin, FL). Absorbance was converted to concentration based on a separately established calibration curve.

3.3.2.10 Contact angle measurement

Contact angles were determined by the sessile drop method on a goniometer (DM-CE1, Kyowa Interface Science, Saitama, Japan). NOR, the precipitate, and SLS powders were compressed at 300 MPa into thin ribbons. A drop (~2.5 µL) of HCl solution (pH 1.2) or 0.1 M phosphate buffer solution (pH 6.8) was placed on the surface of the ribbon using a fine needle attached to a dispenser. The shape of the water drop was recorded every 1 s for 30 s using a high-speed camera. The angle between the sample surface and the tangent line at the edge of the drop was determined using image analysis software, FAMAS3.72 (Kyowa Interface Science Co. Ltd., Japan). Three measurements were made at different locations on each film, and the mean and standard deviations were calculated.

3.3.2.11 Single crystal X-ray diffraction (SCXRD)

Single crystals of the precipitate were grown by dissolving 10 mg of the precipitate in 6 mL of water and methanol 4:1 (v:v) mixture facilitated with slightly heating. The solution was allowed to slowly evaporate at 4 °C to produce single crystals.

Single crystal X-ray diffraction (SCXRD) was performed on a Bruker D8 Venture diffractometer (Bruker AXS Inc., Madison, Wisconsin), equipped with a Bruker PHOTON-II CMOS detector. Data was collected at 100(2) K with a Mo-Kα radiation source (IμS 3.0 microfocus tube). Data integration was performed with the SAINT program. The SADABS program was used for scaling and absorption correction and XPREP was used for space group determination and data merging. The crystal structure was solved by direct methods and refined using ShelXle program (a graphical user interface for SHELXL1)[119]. The crystal structure was solved using SHELXT (Intrinsic Phasing) methods. Hydrogen atom or proton bonded to $NORH^+$ cation were located from the difference Fourier map. Their coordinates were allowed to refine while their thermal parameters were constrained to ride on the carrier atoms. Hydrogen atoms bonded to other atoms were placed in calculated positions, and their coordinates and thermal parameters were constrained to ride on the carrier atoms in the refinement cycles. All non-hydrogen atoms were refined with anisotropic displacement parameters. The three carbon atoms C17, C21, and C22 in one of the lauryl sulfate anions have positional disorders.

3.3.2.12 Intermolecular interaction energy calculation

The pairwise intermolecular interaction energy was estimated with B3LYP-D2/6-31G(d,p) molecular wave functions using the experimental crystal geometry (CrystalExplorer V.17 and Gaussian09).[120-122] For the disordered carbons of the lauryl sulfate anion, one set of the carbons were used in the calculation. This is not expected to significantly impact the calculated energy framework results because these carbons, as a

part of the long hydrophobic tail of anion, only weakly interact with neighboring molecules. Before each calculation, hydrogen atoms were automatically placed at bond lengths corresponding to standard neutron diffraction values. The intermolecular interaction energy was the sum of electrostatic, polarization, dispersion, and exchange-repulsion terms.[123-124] Each term was properly scaled based on values from a large training set. The total interaction energies of water with all molecules having any atom within 3.8 Å of water molecule were calculated and summed to obtain the total energy. The water-host molecule interaction energies were represented by cylinders, where cylinder thickness was proportional to the total intermolecular interaction energy.

3.4 Results and discussion

3.4.1 Precipitation of a NOR solution by adding SLS

The precipitation of a drug by SLS generally requires the presence of drug cations in the solution. [8, 92-93] Excess NOR powder was used to saturate a pH 1.2 hydrochloride solution (similar to the pH of the physiological gastric liquid, in which the piperazine nitrogen of NOR is protonated since the solution pH is significantly lower than its basic pK_a (8.7) (Figure 3.1a).[125-126] Immediate precipitation from this saturated NOR solution was observed after SLS was added (Figure S3.1, Video S3.1). The precipitate contains lauryl sulfate and NOR in 1:1 ratio as suggested by the solution NMR data (Figure S3.2).

3.4.2 Solid-state properties of the precipitate

The precipitate showed birefringence under PLM (Figure 3.2a) and a PXRD pattern distinct from those of NOR and SLS (Figure 3.2b), suggesting a new crystalline phase was formed. Moreover, the PXRD of the precipitate matched well with the calculated PXRD pattern from the solved single crystal structure, which is a NOR lauryl sulfate mono-salt sesquihydrate, $[NORH^+][LS^-]\cdot 1.5\ H_2O$ (Figure 3.2b). The systematic

shifts of diffraction peaks are attributed to the much lower temperature at which the crystal structure was solved (100 K) than that of the experimental PXRD (298 K). The thermal expansion of crystal lattice from 100 to 298 K leads to larger d-spacing for certain (h k l) planes, which corresponds to lower two theta angles. [127] Water content of the precipitate measured by KFT is 4.55 ± 0.07% (n = 6, Table S3.1), which matches reasonably well with the theoretical value of 4.41% for a sesquihydrate. This further supports that the precipitate and the single crystals are the same phase.

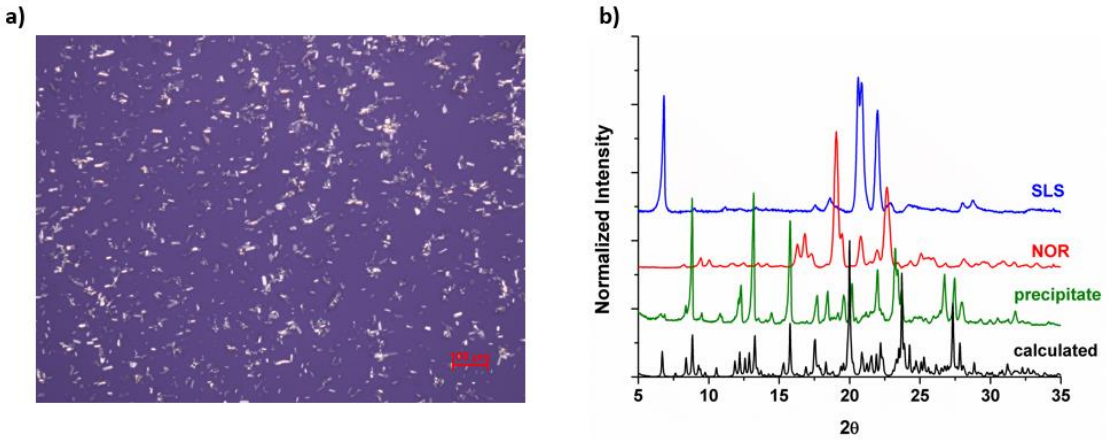

Figure 3. 2. a) Polarized light microscopy of the precipitate; b) PXRD patterns of NOR, SLS, and the precipitate along with the calculated PXRD pattern of $[NORH^+][LS^-]\cdot 1.5\ H_2O$.

3.4.3 Physical stability of the precipitate

The stability of the $[NORH^+][LS^-]\cdot 1.5\ H_2O$ precipitate under different RHs at 25 °C is shown in Figure 3.3a. When RH decreased from 70% to 5%, the mass of the sesquihydrate was only reduced by 0.33%, corresponding to surface moisture. Since the 5% - 70% RH range covers most ambient RHs, the hydrate is stable under typical ambient RHs. When RH reached 0%, the sample started to lose weight, after the criteria of maximum 6 h was reached, the weight loss was <2%, which indicates incomplete dehydration of the 4.41% theoretical amount of water. In an effort of completing water

releasing, sample was purged with dry nitrogen, which led to ~3% total weight loss after 6.3 days. This corresponds to one stoichiometric water in the sesquihydrate (Figure 3.3b). Therefore, the dehydration at 0% RH led to the formation of a hemihydrate (containing 0.5 stoichiometric water). Thus, two different chemical environments of water molecules in $[NORH^+][LS^-]\cdot 1.5\ H_2O$ was indicated, where one stoichiometric water is less strongly bonded than the 0.5 stoichiometric water.

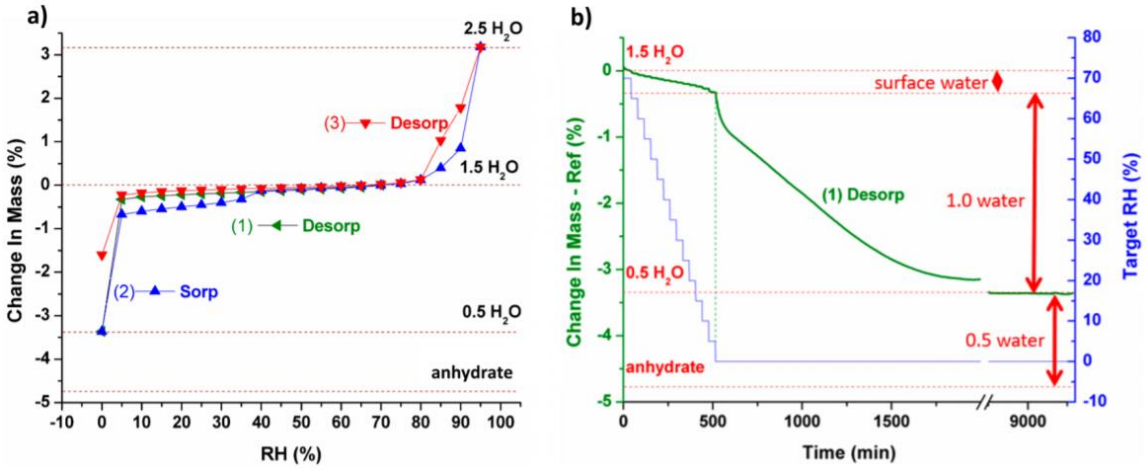

Figure 3. 3. Dynamic vapor sorption of $[NORH^+]\ [LS^-]\cdot 1.5\ H_2O$ at 25 °C, a) sorption-desorption isotherms, b) desorption kinetics from 70% to 0% RH (n = 1).

The phase change from the sesquihydrate to hemihydrate is reversible, as the hemihydrate converted to the sesquihydrate when RH was ≥5% (Figure 3.3a). There is only slight hysteresis between the sorption-desorption curves in the entire RH range. The weight loss at 0% RH during the second desorption cycle is only about 1.6% when the 6 h criterion was reached. Therefore, the shorter exposure time did not allow complete dehydration of the sesquihydrate to form phase pure hemihydrate. The water content in the sample exposed to 95% RH corresponds to that of a 2.5 hydrate (Figure 3.3a). However, additional data are required to establish it as a new hydrate phase.

Although the stability of two types of water was significantly different at 25 °C, no difference was observed at elevated temperature in TGA and DSC open pan, where a single dehydration event was observed at both conditions (Figure 3.4a). When a hermetically sealed DSC pan with a pinhole was used, two endotherms were observed in which the second peak could be attributed to the evaporation of released water, which did not readily escape the pan through the pinhole (Figure S3.2a). This implies the important effect of pan type on the DSC thermogram.[128] TGA also shows significant weight loss at temperature above 150 °C (Figure S3.2b), suggesting dissociation or degradation of the [NORH$^+$] [LS$^-$] salt.

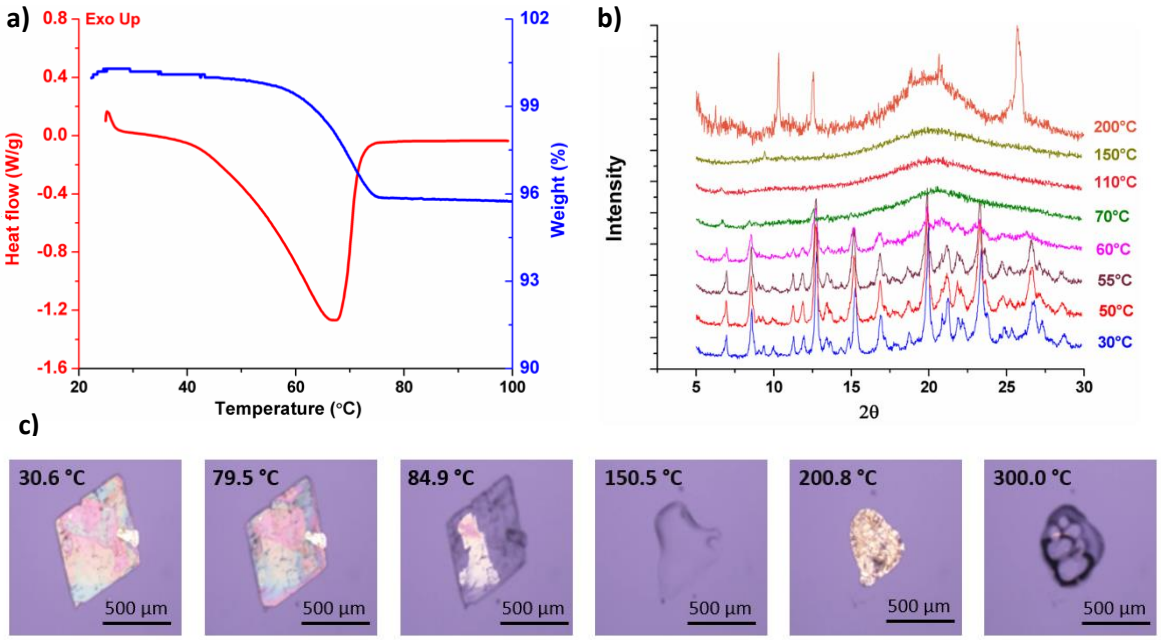

Figure 3. 4. Thermal behavior of [NORH$^+$][LS]$^-$·1.5 H_2O salt, a) DSC and TGA (with open pans), b) vtPXRD, c) hot-stage microscopic images (n = 1).

During the vtPXRD experiment, the PXRD pattern of the sample remained essentially unchanged up to 55 °C. Therefore, dehydration of the sesquihydrate at or

below 55 °C did not lead to a noticeable change in crystal structure. However, partial loss of crystallinity at 60 °C and nearly complete loss of crystallinity at 70 °C (Figure 3.4b) suggest destruction of crystal lattice when dehydration occurred at higher temperatures, resulting in an amorphous [$NORH^+$][LS^-] salt. Mechanistic understanding of the dehydration process would require monitoring dehydration kinetics under controlled RHs and temperatures, which was beyond the scope of this work. [129] The new peaks observed at 200 °C (Figure 3.4b) indicated recrystallization of the products after degradation of the molten [$NORH^+$] [LS^-].

Hot stage microscopy (HSM) provided further insight into the thermal behavior of the [$NORH^+$] [LS^-]·1.5 H_2O (Figure 3.4c, Video S3.2). On heating at the rate of 10 °C/min, a sesquihydrate crystal did not show any observable changes up to ~78 °C. This is consistent with the initially unchanged PXRD in the vtPXRD experiment (Figure 3.4b). Loss of birefringence of the crystal commenced at 80 °C and was completed at 89 °C, corresponding to the dehydration process. The amorphous phase formed a liquid drop at 130 °C. Subsequently, recrystallization occurred during the temperature range of 158-190 °C. This is consistent with the vtPXRD data where the amorphous phase at 150 °C became partially crystalline at 200 °C (Figure 3.4b). The new crystalline phase melted at 250 - 280 °C (Figure 3.4c). Therefore, the HSM and vtPXRD data are in good agreement. However, a glass transition of the amorphous [$NORH^+$] [LS^-] salt was not detected by DSC (Figures 3.4a and S3.2a). It is likely that the glass transition event was hidden by the dehydration endotherm. In addition, the amorphous [$NORH^+$] [LS^-] prepared by drying [$NORH^+$] [LS^-]·1.5 H_2O in a 100 °C oven for ~15 min, gained 6.5% weight when RH rose from 0% to 70% (Figure S3.3). Thus, the amorphous [$NORH^+$] [LS^-] is hygroscopic and water removed from crystal lattice was likely retained in the resulting amorphous phase. Consequently, the Tg of the “wet” amorphous phase is depressed and glass transition

event had already occurred as soon as the amorphous phase was formed. In other words, the dehydration of [$NORH^+$] [LS^-]·1.5 H_2O by heating in DSC led to a rubbery phase. Hence, a glass transition is not detected by DSC.

To test this hypothesis, the sesquihydrate powder was heated in DSC from room temperature to 100 °C in an open pan to ensure complete drying of the amorphous phase (1st cycle). The sample was then cooled to 0 °C (2nd cycle) and reheated to 110 °C (3rd cycle) (Figure 3.5). A Tg of 83.2 °C was observed in the 3rd cycle, confirming the hypothesis of depressed Tg of the resulting amorphous phase by water. When amorphous [$NORH^+$][LS^-], prepared by heating the sesquihydrate in 100 °C oven for ~15 min, was heated in DSC from room temperature to 150 °C, a glass transition was observed at ~50 °C (Figure S3.4). This lower Tg, compared to the dry amorphous [$NORH^+$][LS^-], likely occurred because the amorphous sample absorbed some water (up to 4.5%) from the environment (RH = 50%), despite the short exposure time (~10 min), before DSC experiment was run.

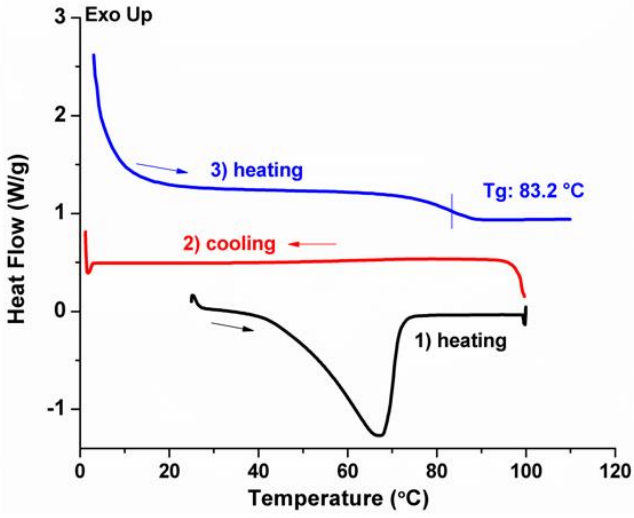

Figure 3. 5. DSC of $[NORH^+][LS^-]\cdot 1.5\ H_2O$ powder with cycles of 1) heating at 10 °C/min from 25 °C to 100 °C; 2) cooling at 20 °C/min to 0 °C; 3) heating at 50 °C/min to 110 °C (n = 1).

3.4.4 Reduced solubility and intrinsic dissolution rate of the precipitate

At 23 °C, measured solubility values of NOR in pH 1.2 (21067 ± 578 µg/mL) and pH 6.8 (581 ±11 µg/mL) media (Table S3.2) are similar to those reported previously.[130] The equilibrating solid phases were different from the initial NOR powder, possibly corresponding to a HCl salt at pH 1.2 and a phosphate salt monohydrate at pH 6.8.[131] $[NORH^+][LS^-]\cdot 1.5\ H_2O$, on the other hand, was phase stable in both conditions and the measured solubility was 179 ± 50 µg/mL at pH 6.8 and 136 ± 20 µg/mL at pH 1.2 (Table S3.2). The comparable solubility values of $[NORH^+][LS^-]\cdot 1.5\ H_2O$ at pH 1.2 and 6.8 is consistent with the expected pH independence of solubility of a salt, provided there is no common ion effect. The solubility of $[NORH^+][LS^-]\cdot 1.5\ H_2O$ was 31% and 0.6% of that of NOR at pH 6.8 and pH1.2, respectively. At the same temperature, the IDR of $[NORH^+][LS^-]\cdot 1.5\ H_2O$ was around 8% and 0.7% of those of NOR at pH 6.8 and 1.2, respectively (Figure 3.6, Table S3.2). The lower IDR of $[NORH^+][LS^-]\cdot 1.5\ H_2O$ is qualitatively consistent with the lower solubility in both media. At pH 1.2, the IDR and solubility of $[NORH^+][LS^-]\cdot 1.5\ H_2O$ were both 0.6-0.7% of those of NOR. This suggests that the significantly reduced IDR of $[NORH^+][LS^-]\cdot 1.5\ H_2O$ was mainly driven by its lower solubility at pH 1.2. However, at pH 6.8, the IDR and solubility of $[NORH^+][LS^-]\cdot 1.5\ H_2O$ were 8% and 31% those of NOR, respectively. The different ratios between solubility and IDR may reflect the more complete phase conversion to a less soluble solid phase during the solubility measurement (48 hr) than that during IDR measurement (~4 min). However, it should be cautioned that the relatively large errors in some of the experimentally determined IDR and solubility values could also affect the calculated ratios (Table S3.2). In any case, the

reduced solubility and IDR of [$NORH^+$] [LS^-]·1.5 H_2O highlight the risk of lower bioavailability when using SLS in the formulation of NOR.

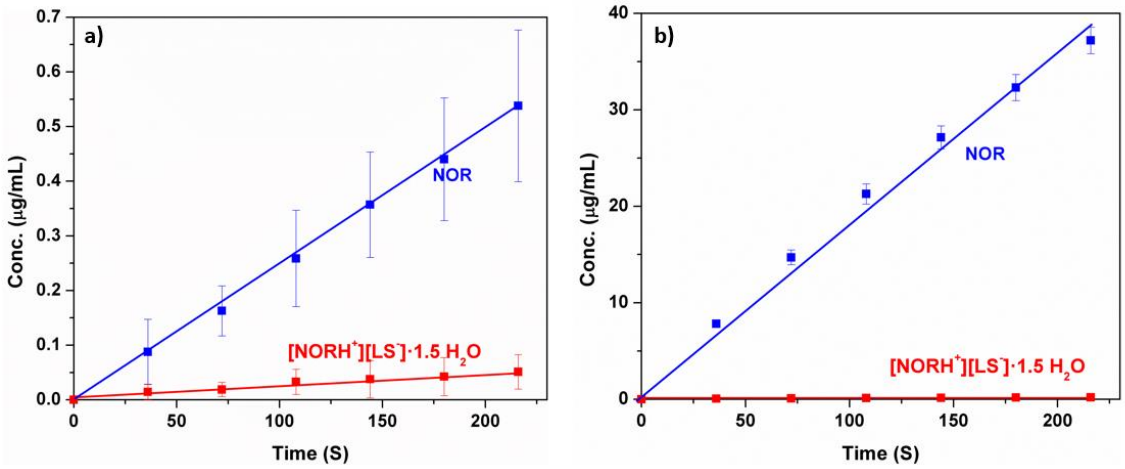

Figure 3. 6. Intrinsic dissolution test of NOR and [$NORH^+$] [LS^-]·1.5 H_2O salt in a) 0.1 M sodium phosphate buffer at pH 6.8 and b) HCl solution at pH 1.2 (n = 3). Compared to NOR, the IDR of [$NORH^+$] [LS^-]·1.5 H_2O was significantly reduced in both media.

In addition to the lower solubility, the reduced dissolution of [$NORH^+$][LS^-]·1.5 H_2O may also have resulted from its higher hydrophobicity relative to NOR. Higher hydrophobicity of particle surfaces often leads to reduced wetting by aqueous media, which slows dissolution since wetting is a prerequisite for dissolution. [3, 132] In fact, despite the presence of the surface active LS^-, [$NORH^+$][LS^-]·1.5 H_2O is more hydrophobic than NOR as suggested by its larger contact angles than those of NOR by both acidic (pH 1.2) and nearly neutral (pH 6.8) media (Figure 3.7). Therefore, the slower dissolution rate of [$NORH^+$][LS^-]·1.5 H_2O compared to NOR is a combined effect of lower solubility and less wetting.

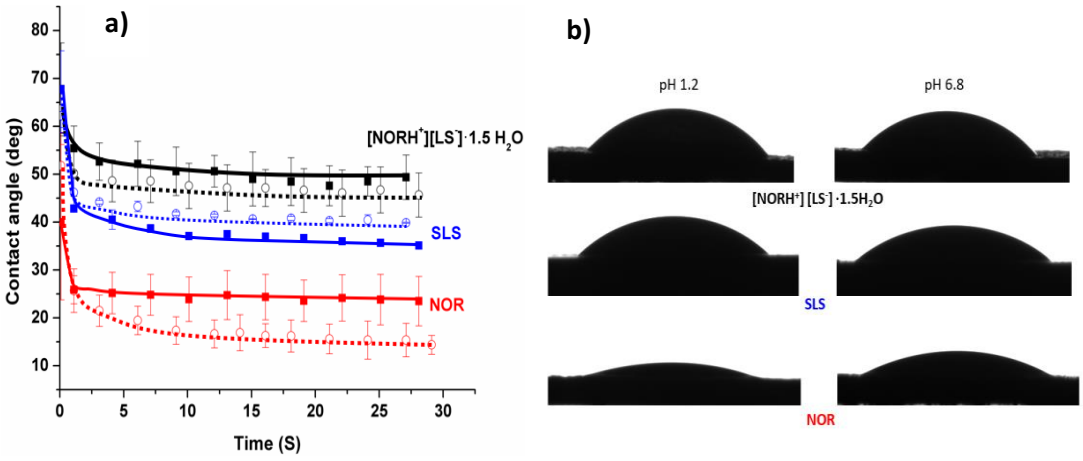

Figure 3. 7. Wettability of NOR, SLS, and [$NORH^+$] [LS^-] ·1.5 H_2O to 0.1M pH 6.8 phosphate buffer (Solid square) and pH 1.2 HCl solution (open circles). a) time course of contact angle (n = 3), b) drop images.

Interestingly, the contact angle of SLS is only slightly lower than that of [$NORH^+$][LS^-]·1.5 H_2O and significantly higher than that of NOR under both acidic and neutral conditions. This result is counterintuitive as low contact angles are expected based on the very high solubility of SLS in water and aqueous media. The PXRD pattern of a compressed pellet clearly suggested preferred orientation of SLS (Figure S3.5), where the dominating peak at around 7º two theta corresponds to the (6 0 0) plane. Therefore, the high hydrophobicity, indicated by the high contact angle, suggests that the hydrocarbon tail of LS^- is enriched at the surfaces of compressed pellet.

3.4.5 Structure – properties relationship of the [$NORH^+$] [LS^-]·1.5 H_2O

The crystal structure of the [$NORH^+$] [LS^-]·1.5 H_2O belongs to the centrosymmetric triclinic $P\bar{1}$ space group (Table S3.3). The asymmetric unit consists of two $NORH^+$, two LS^-, and three H_2O molecules, confirming the 1.5 stoichiometry of water, i.e., [$NORH^+$][LS^-]·1.5 H_2O (Figure 3.8). Though the two $NORH^+$ cations ($NORH^+_{(1)}$ and $NORH^+_{(2)}$) have similar conformation (Figure S3.6a), significantly different conformations

were observed between the two LS^- anions ($LS^-_{(1)}$ and $LS^-_{(2)}$), where the $LS^-_{(2)}$ has a more twisted carbon chain compared to that of the $LS^-_{(1)}$ (Figure S3.6b).

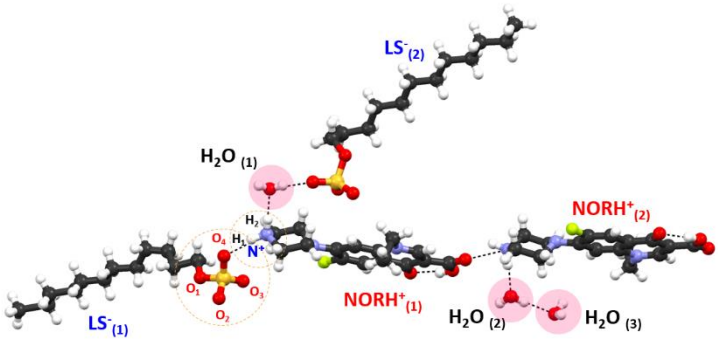

Figure 3. 8. Asymmetric unit of $[NORH^+][LS^-]\cdot 1.5\ H_2O$

IR and Raman spectroscopy, surface tension measurement and solubility determination were used to probe the impact of the drug-SLS complexation on pharmaceutically important physical properties.[8, 91-92, 94] The availability of the crystal structure offers an opportunity to examine the intermolecular interactions between $NORH^+$ and LS^- that underlies such property modifications. In the $[NORH^+][LS^-]\cdot 1.5\ H_2O$ crystal, $LS^-_{(1)}$ interacts with two $NORH^+$ cations via charge assisted hydrogen bonds of N^+-H···O^--S (2.742 Å) and N^+-H···O=S (2.928 Å) (Figure 3.8). The $LS^-_{(2)}$ anion is connected to water molecules ($H_2O_{(1)}$ and $H_2O_{(3)}$) via O-H···O^--S (2.710 Å) and O-H···O=S (2.817 Å) hydrogen bonds. The ionized piperazine nitrogen in $NORH^+_{(1)}$ forms N^+-H···O hydrogen bonds with $LS^-_{(1)}$ and $H_2O_{(1)}$, while that in $NORH^+_{(2)}$ forms N^+-H···O hydrogen bonds with $LS^-_{(1)}$, $NORH^+_{(1)}$ and $H_2O_{(2)}$ (Figure 3.8).

The $[NORH^+][LS^-]\cdot 1.5\ H_2O$ crystal consists of stacked layers running parallel to the *ab* plane (Figure 3.9a). Each layer exhibits a sandwiched structure, where polar functional groups, including ionized piperazine, sulfate, water, and carboxylic acid interacting through a number of hydrogen bonds, are located between two hydrocarbon layers. This

structure explains the poor wettability and very low solubility of [NORH$^+$][LS$^-$]·1.5 H_2O in aqueous media.

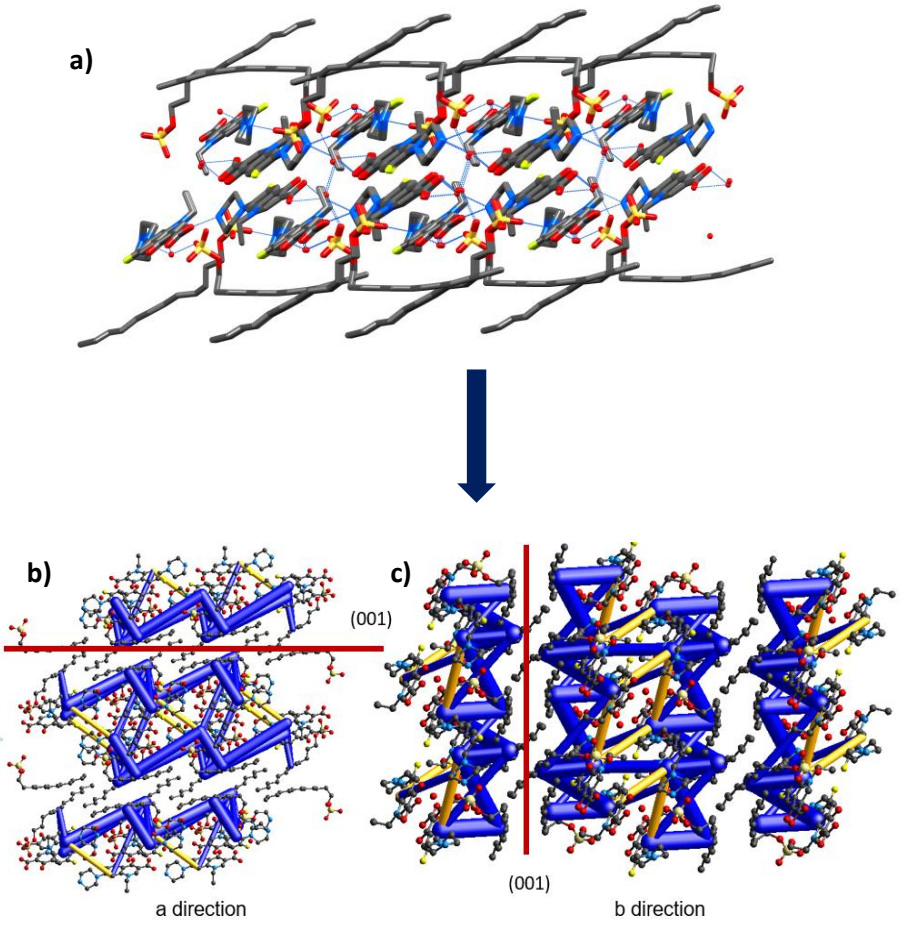

Figure 3. 9. a) Structure of one layer in the [NORH$^+$][LS$^-$]·1.5 H_2O crystal, and the energy framework of [NORH$^+$][LS$^-$]·1.5 H_2O crystal viewed into b) unit cell *a* axis and c) unit cell *b* axis. The radius of cylinder represents the relative strength of intermolecular interaction energy, blue cylinder implied attractive interaction and the orange cylinder indicate repulsive interactions.

3.4.6 Energy framework of the [$NORH^+$] [LS^-]·1.5 H_2O

The energy framework of [$NORH^+$][LS^-]·1.5 H_2O shows that the molecules within the stacking layers interact with each other strongly (Table S3.4, Figures 3.9b, 3.9c). This is consistent with the presence of strong ionic interaction, hydrogen bond, and π-π stacking among molecules in the polar region of the layers. In contrast, interlayer interactions are only weak dispersive forces between hydrocarbon tails of LS^-. Therefore, it is energetically favored to have the (0 0 1) facet of the [$NORH^+$][LS^-]·1.5 H_2O crystal covered with hydrocarbon chains, which makes this crystal hydrophobic. This is in agreement with the (0 0 1) being the major facet of the predicted crystal morphology (Figure S3.9).[133] It also explains the poor wetting behavior of [$NORH^+$][LS^-]·1.5 H_2O by aqueous media (Figure 3.7).

The strong interactions in the stacking layers potentially leads to a higher lattice energy than NOR. Such higher lattice energy disfavors the solubility of [$NORH^+$][LS^-]·1.5 H_2O. However, the different solvation energy and molecular hydrophobicity (indicated by LogD) due to the lauryl sulfate in [$NORH^+$][LS^-]·1.5 H_2O also plays a role. [25, 134-135] A detailed discussion of these effects is outside the scope of this work.

The physical stability of the sesquihydrate salt can also be explained by considering the interaction energy of each water molecule in the crystal. Among the three water molecules in the asymmetric unit (Figure 3.8), the $H_2O_{(1)}$ connects with two $NORH^+$ cations and one LS^- anion via classical N-H^+···O and O-H···O hydrogen bonds (Figure 3.10a). However, $H_2O_{(2)}$ and $H_2O_{(3)}$ form a tetranuclear planner structure through O-H···O hydrogen bonds (Figure 3.10b). The tetranuclear structure of water molecules is surrounded by $NORH^+$ cations and LS^- anions via N-H^+···O and O-H···O^- hydrogen bonds. The removal of water molecules from the crystal lattice requires -128.3 kJ/mol, -87.8 kJ/mol and -101.1 kJ/mol energy for $H_2O_{(1)}$, $H_2O_{(2)}$ and $H_2O_{(3)}$, respectively (Figure S3.8).

Thus, the relative stability of three water molecules follows the order: $H_2O_{(1)}$ > $H_2O_{(3)}$ > $H_2O_{(2)}$. The total water-host interaction energy of $H_2O_{(1)}$ (-128.3 kJ/mol) is even higher than that of the stable lactose monohydrate (-114.5 kJ/mol). This explains the good stability of the hemihydrate even at 0% RH during DVS experiment at 25 °C (Figure 3.3). To put things in perspective, the total water bonding energy is -76.3 kJ/mol and -83.4 kJ/mol in unstable theophylline monohydrate and p-hydroxybenzoic acid monohydrate.[136] Since the bonding energy (-87.8 kJ/mol) of $H_2O_{(2)}$ with surrounding molecules is close to those of unstable hydrates, its removal from crystal lattice at 0% RH was possible at 25 °C . Because of the cooperative nature of the tetra water ring formed by $H_2O_{(2)}$ and $H_2O_{(3)}$, $H_2O_{(3)}$ can also be easily removed after the removal of $H_2O_{(2)}$. Therefore, both water molecules are removed in a single step (Figure 4a), despite the higher bonding energy for $H_2O_{(3)}$.

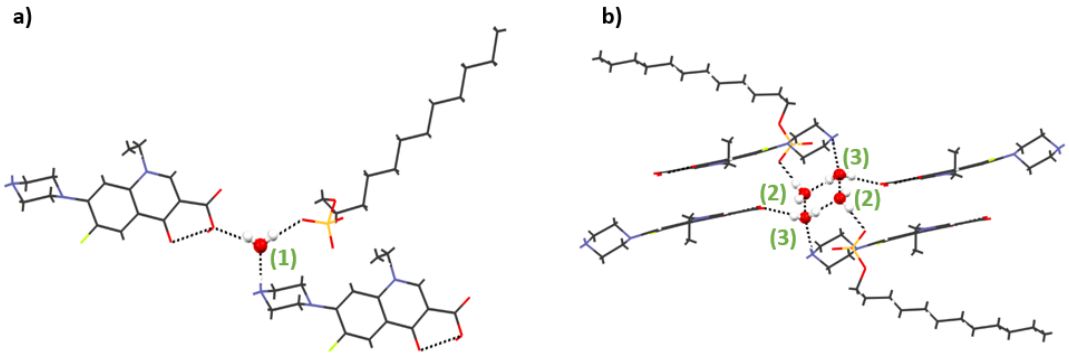

Figure 3. 10. Different molecular environments of water in the [NORH$^+$] [LS$^-$]·1.5 H_2O

3.5 Conclusion

The elucidation of the drug-surfactant salt crystal structure of $[NORH^+][LS^-]\cdot 1.5\ H_2O$ provided useful insight into the low solubility and dehydration behaviors. The sandwiched molecular layer structure of hydrophobic surfaces and polar core explains the poor wetting and low solubility of $[NORH^+][LS^-]\cdot 1.5\ H_2O$. The crystal energy framework offers mechanistic insight into the physical stability of $[NORH^+][LS^-]\cdot 1.5\ H_2O$ with respect to RH.

3.6 Accession Code

CCDC 1949137 contains the supplementary crystallographic data for [NOR][LS]1.5 H2O.These data can be obtained free of charge via www.ccdc.cam.ac.uk/data_request/cif, or by emailing data_request@ccdc.cam.ac.uk, or by contacting The Cambridge Crystallographic Data Centre, 12 Union Road, Cambridge CB2 1EZ, UK; fax: +44 1223 336033.

3.7 Support information

Table S3. 1. Water content determination by Karl Fischer Titration (KFT) method

No.	Water Content (%)
1	4.64
2	4.61
3	4.59
4	4.53
5	4.47
6	4.49
Average	4.55

Table S3. 2. Solubility and intrinsic dissolution rate (IDR) of NOR and $[NORH^+][LS^-]\cdot 1.5\ H_2O$ at 23 °C (n=3).

	IDR ($\mu g\cdot mL^{-2}\cdot S^{-1}$)		**Solubility (μg/mL)**	
	pH 1.2	pH 6.8	pH 1.2	pH 6.8
$[NORH^+][LS^-]\cdot 1.5\ H_2O$	0.7 ± 0.3	0.2 ± 0.1	136 ± 20	179 ± 50
NOR	98 ± 10	2.4 ± 0.5	21067 ± 578	581 ±11

Table S3. 3. Crystallographic information table for $[NORH^{+}][LS^{-}]\cdot 1.5\ H_2O$

Formula	$C_{28}H_{47}FN_3O_{8.5}S$
Molecular weight	612.749
Crystal system	Triclinic
Space group	P-1
a (Å)	11.6164 (11)
b (Å)	14.2842 (13)
c (°)	20.0986 (18)
α (°)	84.266 (3)
β (°)	89.012 (4)
γ (°)	68.014 (3)
Volume ($Å^3$)	3076.24
Z/Z'	2/1
ρ_{calc} (g/cm3)	1.323
F (000)	1316.0
Temperature(K)	100
R_1	0.0662
wR_2	0.1713
R_{int}	0.1171
Goodness-of fit	1.031
Maximum and minimum residual electron density ($e/Å^3$)	0.945 and -0.752
CCDC No.	1949137

Table S3. 4. Intermolecular interaction energies estimated using B3LYP-D2/6-31G(d,p) dispersion-corrected DFT model. Both the total energy ($E_{(tot)}$) and electrostatic ($E_{(ele)}$), polarization ($E_{(pol)}$), dispersion ($E_{(dis)}$), and exchange-repulsion ($E_{(rep)}$) components are listed (kJ/mol). R indicated the distance between centers of mass of the pair of molecules (Å).

	Symop	R	E_{ele}	E_{pol}	E_{dis}	E_{rep}	E_{tot}
	-	8.52	-10.1	-1.6	-3.5	4.6	-12.1
	-	2.92	-18.9	-4.7	-3.0	18.8	-14.5
	-	5.40	2.4	-3.5	-5.0	1.9	-3.2
	-x, -y, -z	4.35	-3.7	-0.1	-0.4	0.0	-4.3
	-	2.77	-46.2	-9.3	-3.9	46.4	-30.4
	-	6.87	-9.9	-7.0	-6.3	5.0	-18.1
	-	7.51	-46.4	-18.3	-5.4	40.7	-42.2
	-	5.35	-16.4	-3.7	-7.1	3.0	-24.4
	-	8.09	-58.6	-21.1	-4.7	55.2	-47.6
	-	6.68	1.4	-0.8	-4.3	2.8	-1.2
	-	8.50	23.6	-3.7	-1.8	0.2	20.8
	-	8.17	-34.9	-5.7	-5.0	41.4	-19.9

	-	3.90	-2.7	-0.3	-1.0	0.2	-3.8
	-	11.76	2.0	-1.0	-2.2	0.7	-0.1
	-	6.81	-88.2	-31.0	-10.5	78.7	-76.8
	-	7.99	-2.0	-0.6	-1.2	0.1	-3.5
	-x, -y, -z	3.67	-6.8	-0.4	-1.1	0.3	-8.2
	-	6.53	-81.9	-25.1	-9.3	53.9	-80.0
	-	8.01	-25.9	-5.3	-6.3	33.6	-16.0
	-	8.69	2.8	-0.7	-1.8	0.6	1.2
	-	8.59	-8.5	-5.3	-1.9	0.8	-14.0
	-	7.42	23.5	-4.2	-3.1	0.6	19.4
	-	5.57	5.6	-2.9	-3.7	1.7	1.6
	x, y, z	14.28	96.9	-7.4	-9.3	5.0	92.0
	-	16.98	50.3	-0.6	-20.1	14.4	44.0
	-	15.48	-87.2	-8.5	-8.7	4.8	-103.1
	-x, -y, -z	6.71	86.7	-9.0	-49.7	33.0	62.1
	-	5.30	97.1	-17.8	-42.2	27.3	69.6
	-	9.12	94.8	-2.7	-12.0	3.6	90.1
	-	14.79	-109.1	-15.7	-9.4	5.2	-132.0

	-	5.20	-344.4	-77.2	-44.1	41.4	-434.1
	-	5.16	-145.5	-13.3	-32.2	15.9	-181.8
	-	8.59	-8.5	-5.3	-1.9	0.8	-14.0
	-	8.27	101.0	-4.2	-20.2	9.0	91.7
	-	6.33	180.8	-26.8	-25.3	15.0	158.6
	-	17.48	68.4	-7.6	-7.0	2.7	62.2
	-	8.13	-331.0	-68.5	-23.9	25.5	-405.7
	-	6.68	1.4	-0.8	-4.3	2.8	-1.2
	-	7.51	-46.4	-18.3	-5.4	40.7	-42.2
	-	8.09	-58.6	-21.1	-4.7	55.2	-47.6
	-	10.99	-163.8	-30.3	-8.1	11.0	-195.9
	-	11.86	-183.5	-22.3	-5.0	4.9	-211.8
	-x, -y, -z	6.30	82.9	-11.0	-25.0	8.0	62.7
	-x, -y, -z	14.46	53.7	-1.6	-18.4	6.2	43.4
	-	13.49	-357.0	-56.9	-13.2	19.1	-419.2
	-	9.11	-181.2	-44.2	-23.0	23.6	-229.7
	-	3.57	-158.8	-51.9	-51.5	35.6	-229.2
	-	13.01	-406.6	-79.6	-17.2	67.4	-462.1

	-	14.74	-81.0	-17.0	-13.4	8.4	-104.8
	-	11.76	2.0	-1.0	-2.2	0.7	-0.1
	-x, -y, -z	21.01	43.6	-0.3	-1.7	0.0	44.5
	-x, -y, -z	5.91	9.1	-22.4	-83.7	52.8	-47.2
	-x, -y, -z	10.34	149.8	-19.3	-12.6	3.2	135.1
	-	10.18	51.0	-5.8	-11.8	8.7	44.7
	-	9.98	235.4	-40.7	-19.3	7.2	206.4
	-	5.57	5.6	-2.9	-3.7	1.7	1.6
	-	8.52	-10.1	-1.6	-3.5	4.6	-12.1
	x, y, z	14.28	61.8	-9.4	-2.3	0.0	56.3
	-	3.79	236.5	-47.3	-101.6	56.6	161.5
	-	8.01	-25.9	-5.3	-6.3	33.6	-16.0
	-	6.87	-9.9	-7.0	-6.3	5.0	-18.1
	-	14.04	25.8	-26.1	-7.8	25.9	17.1
	-	6.53	-81.9	-25.1	-9.3	53.9	-80.0
	-	13.38	80.6	-22.3	-7.9	9.8	67.8
	-	8.83	246.7	-21.0	-9.8	2.7	238.5
	-	7.99	-2.0	-0.6	-1.2	0.1	-3.5

	-	5.40	2.4	-3.5	-5.0	1.9	-3.2
	-	8.50	23.6	-3.7	-1.8	0.2	20.8
	x, y, z	14.65	57.3	-8.6	-2.1	0.0	52.4
	-	7.42	23.5	-4.2	-3.1	0.6	19.4
	-x, -y, -z	10.19	73.9	-11.6	-12.3	3.3	60.8
	-	8.69	2.8	-0.7	-1.8	0.6	1.2
	-	5.35	-16.4	-3.7	-7.1	3.0	-24.4
	-	6.81	-88.2	-31.0	-10.5	78.7	-76.8
	-	8.17	-34.9	-5.7	-5.0	41.4	-19.9

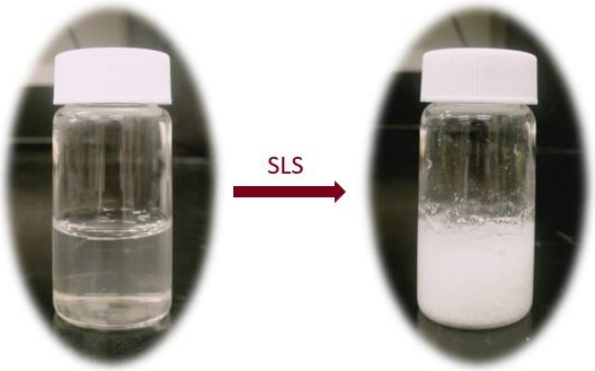

Figure S3. 1. Precipitation from a NOR solution at pH 1.2 induced by adding SLS

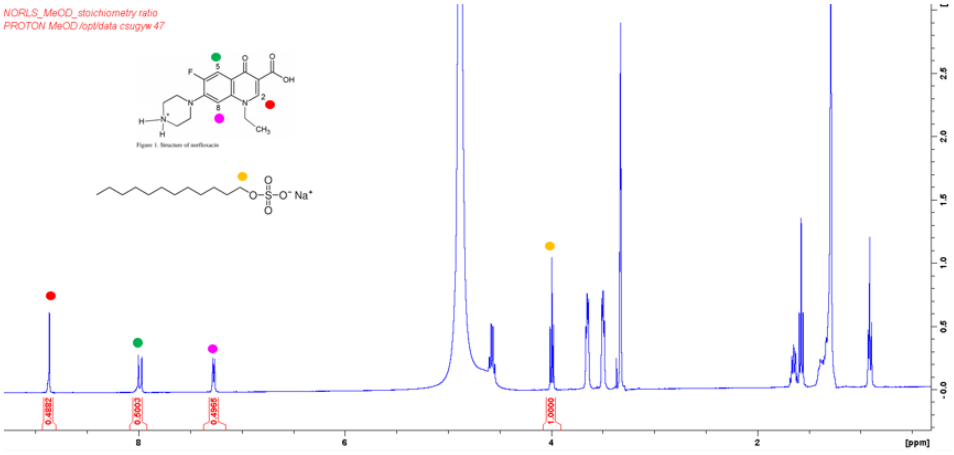

Figure S3. 2. Solution NMR data of the precipitate. Experiment was performed in CD_3OD on a Bruker Avance III HD nanobay AX-400 spectrometer at 400 MHz equipped with a 5 mm BBO SmartProbe.

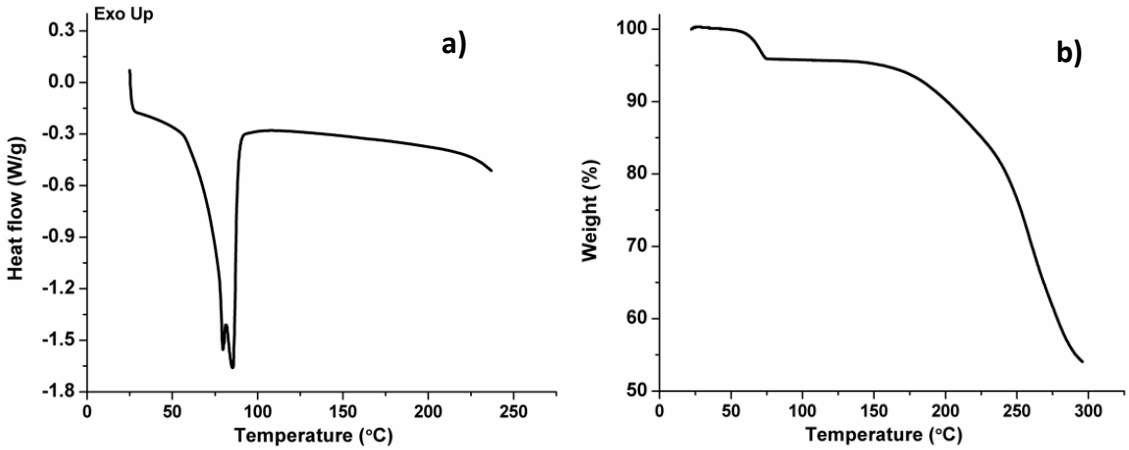

Figure S3. 3. Thermal behavior of the precipitate a) DSC by hermetically sealed pan with a pinhole, and b) TGA

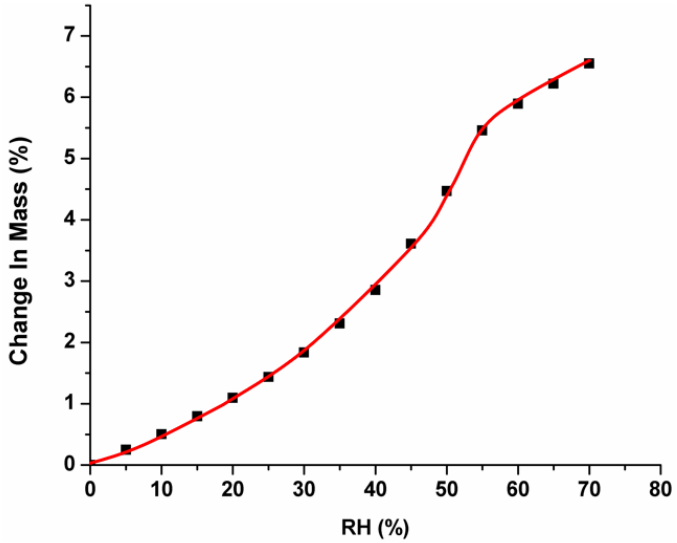

Figure S3. 4. DVS of amorphous [NORH$^+$] [LS$^-$] salt from 0 – 70% RH at 25 °C

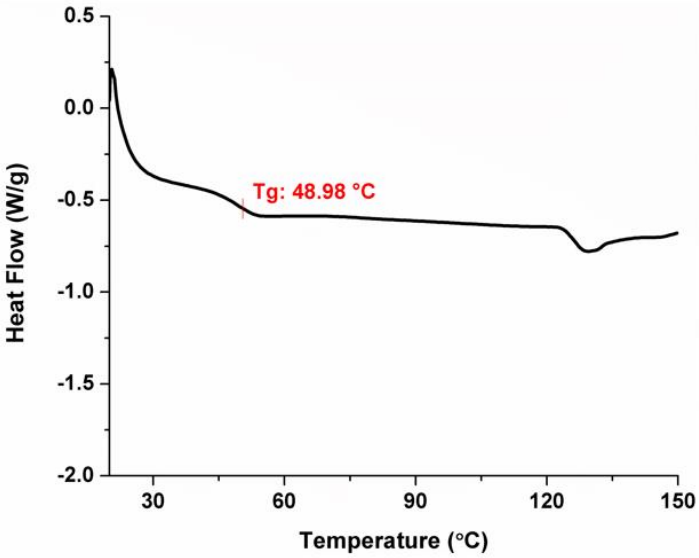

Figure S3. 5. DSC of dry amorphous [NORH$^+$] [LS$^-$] salt at a heating rate of 30 °C/min

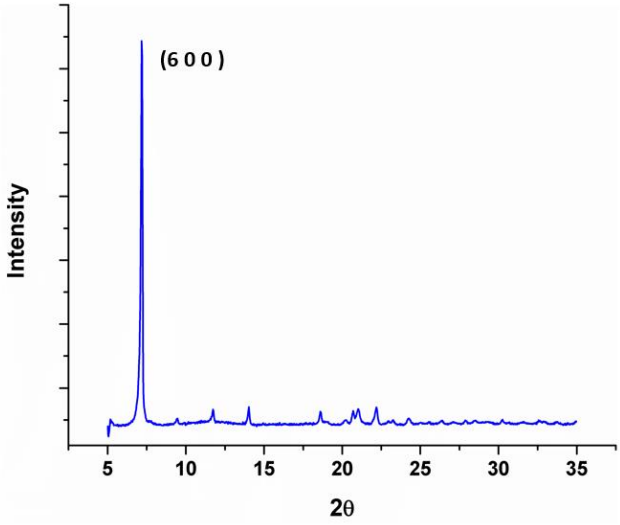

Figure S3. 6. PXRD of compressed SLS ribbon for contact angle test.

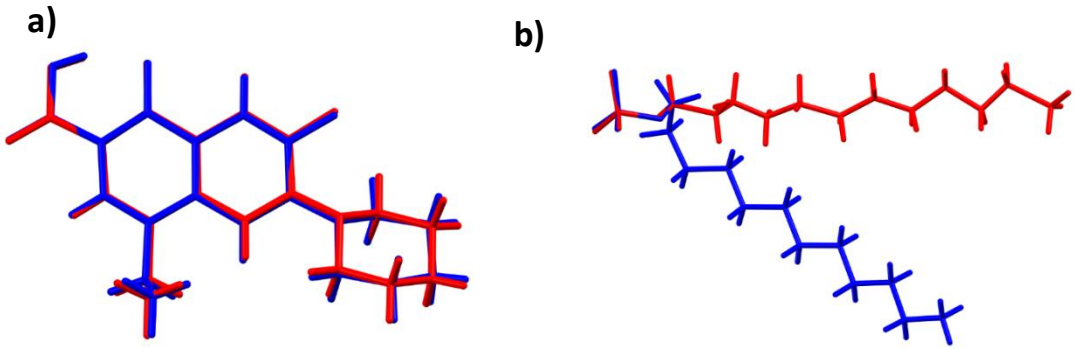

Figure S3. 7. Conformation of a) $NORH^+$ cations and b) LS^- anions in asymmetric unit of $[NORH^+][LS^-]\cdot 1.5\ H_2O$

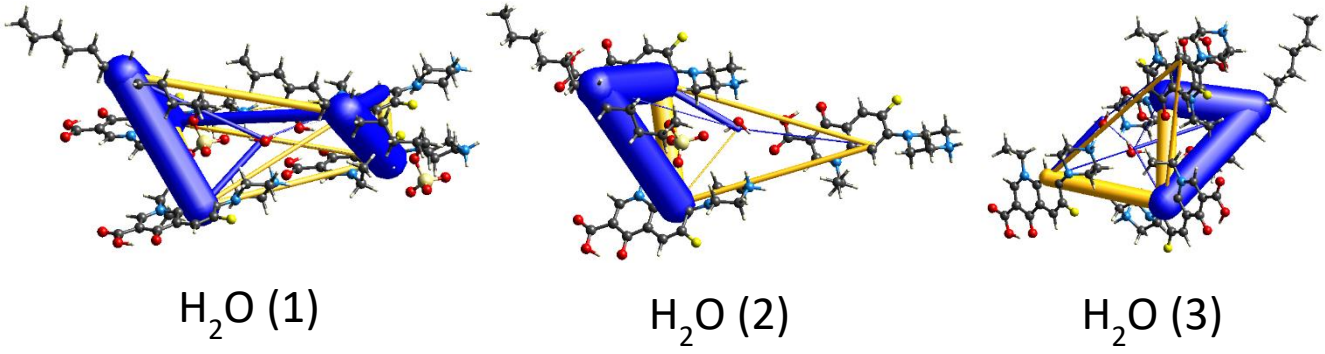

Figure S3. 8. Water - host molecules interaction.

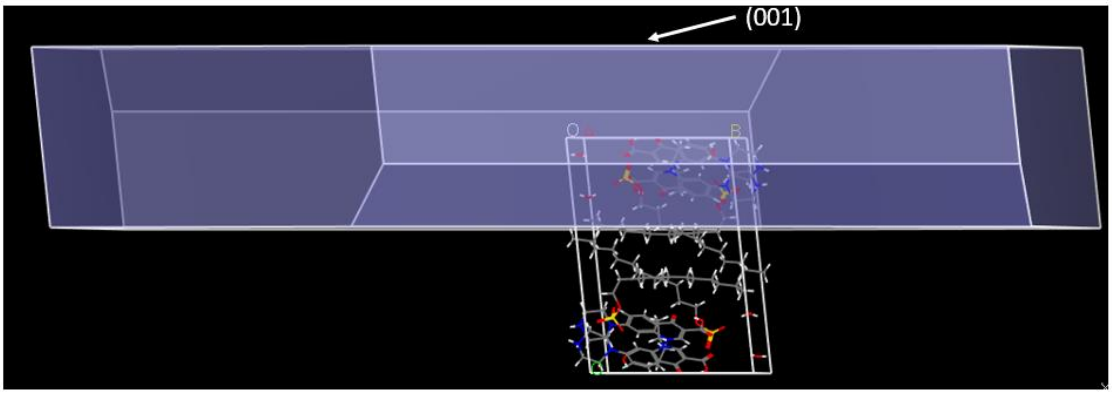

Figure S3. 9. Predict crystal morphology of [$NORH^+$][LS^-]·1.5 H_2O based on attachment energy calculation.

Chapter 4

Pharmaceutical lauryl sulfate salts – Prevalence, formation rules and formulation implications

4.1 Synopsis

The anionic surfactant sodium lauryl sulfate (SLS) is known to deteriorate the dissolution of some drugs by forming poor soluble lauryl sulfate (LS) salts. However, because of the perception of its infrequent occurrence, this phenomenon is usually not investigated in drug development until unexpected dissolution slowdown is encountered. This work demonstrates the prevalence of this phenomenon, where 14 out of 18 compounds with diverse chemical structures, including salt of basic drugs, a quaternary ammonium salt, organic bases, and zwitterionic molecules, precipitated as LS salts from a solution when mixed with SLS. Although no precipitation was observed for the other 4 compounds, their FTIR spectra suggested 3 of them had intermolecular interactions with SLS when dried from a solution. Along with the 5 other compounds reported in the literature, the prevalence of this phenomenon is demonstrated. The occurrence of precipitation is thermodynamically driven by the relative difference between the ion product in solution (Q) and the solubility product of the lauryl sulfate salt (K_{sp}). SLS, as a surfactant, also affects precipitation kinetics through influencing the interfacial tension of nuclei of the insoluble salt. When a potential issue associated with the LS salt is identified, effective mitigation strategies should be proactively designed and implemented to alleviate its possible negative impact on drug dissolution.

4.2 Introduction

Poor aqueous solubility of a drug is a major challenge facing the development of an oral solid dosage form because it causes slow release of drug and limits the bioavailability. Formulation approaches to address this problem include 1) use of more soluble solid forms, cocrystal, salts, and amorphous solid dispersions; 2) use of complexation agents, e.g., cyclodextrin; 3) enhancement of dissolution rate by reducing particle size or improving wetting. [4] The wettability enhancement of hydrophobic drug particles is commonly achieved by incorporating in the formulation a surfactant, which reduces interfacial tension between the drug solid and water. In addition to improving wetting, surfactants can also deliver other benefits, such as solubilization through micelle formation, stabilization of emulsions, and enhancement of absorption by facilitating drug permeability through the gut wall. [4, 112]

Sodium lauryl sulfate (SLS) is an anionic surfactant, consisting of a negatively charged lauryl sulfate group with a hydrophobic twelve carbon chain (LS^-) and sodium cation. SLS is a commonly used additive in many domestic cleaning products, processed foods, personal hygiene and cosmetics products, as well as in pharmaceuticals. [74, 137-138] Although the use of SLS in solid oral dosage form is intended to improve drug dissolution, the negatively charged LS^- can form insoluble salts with the positively charged drug molecules in an acidic environment. [5-10, 12, 95] The precipitation of the insoluble LS salt both reduces the surface active function of SLS and deteriorates the dissolution of drugs, [5-10, 95] which may lower the bioavailability and therapeutic effect of the drug. When *in vitro* dissolution experiments are performed in a SLS containing medium, the inadvertent formation of an insoluble LS salt causes slower dissolution of the drug, which may sound a false alarm and mislead formulators in their efforts to optimize formulation as human gastrointestinal tract (GI tract) is free of SLS. This potential pitfall, however, has not

attracted the attention of most formulators despite a few published examples of this phenomenon. [5, 9-10, 12, 28, 91, 95] One possible reason is the impression that such insoluble LS salts rarely form.

Given the straightforward acid-base reaction underlying the formation of insoluble LS salts, we expected that many basic drugs can form LS salt, provided they are protonated in an acidic environment, such as the stomach. Hence, we set out to examine the prevalence of such LS salts, along with the efforts to better understand their formation rules to inform effective mitigation strategies.

4.3 Materials and Methods

4.3.1 Materials

Sodium lauryl sulfate was purchased from Ward's Science (Rochester, NY). Hydrochloride acid aqueous solution (36.5%−38%, VWR international, Eagan, MN) was ACS reagent grade. A total of 18 compounds with diverse chemical structures used in this work include salt of bases (isoniazid HCl, diphenhydramine HCl, metformin HCl, caffeine HCl, nicotinamide HCl, ligustrazine HCl, leucine HCl), quaternary ammonium salt (berberine Cl^-), bases (4-Aminobenzoic, lamivudine, ritonavir, erlotinib, cytosine, fluorocytosine), and zwitterionic compounds (norfloxacin, levofloxacin, fleroxacin, ciprofloxacin). They were obtained from respective suppliers.

4.3.2 Methods

4.3.2.1 Precipitation of LS salt

The driving force for precipitation of any LS salt is the relative difference between the solubility product of the salt and the ion product (Q) in solution. For a given salt, a higher Q value leads to a greater driving force for precipitation. To maximize the chance of observing precipitation of LS salts, saturated solutions of all model compounds, except berberine chloride, in pH 1.2 HCl solution were prepared to maximize the concentrations

of respective cations. Berberine chloride was saturated in water since berberine carries a permanent positive charge and the dissociation of this quaternary ammonium salt is pH independent. Its solubility is depressed in HCl solution due to the common ion effect. To 2 mL of each of the saturated solution, 0.2 mL SLS aqueous solution (100 mM) was added. The mixed solution was placed on the bench top undisturbed for visual observation of possible precipitation. Water was used to prepare SLS solution to avoid its degradation in a low pH (< 2.5) solution. [139] However, the LS moiety is chemically stable in the phase separated LS salt precipitate.

4.3.2.2 Solubility determination for *p*-ABA lauryl sulfate salt

Precipitated *p*-ABA lauryl sulfate salt, [$PABAH^+$][LS^-], was recovered and suspended in deionized water for 72 hr at room temperature. After filtration with a 0.45 µm polypropylene membrane, the total concentration of PABA in the supernatant was determined by UV-Vis spectrometry (DU® 530 UV-Vis spectrophotometer; Beckman, Brea, CA) using a separately constructed calibration curve. The concentration of ionized PABA, [$PABAH^+$], was calculated using the Henderson-Hasselbalch equation from the total concentration and the measured solution pH with a pH meter (Orion Star A211 pH Meter, Thermo Scientific, Waltham, MA). The [LS^-] concentration cannot be directly measured by UV due to the absence of a chromophore. It is assumed to be the same as the measured total concentration of PABA.

4.3.2.3 ^{1}H NMR study for [$PABAH^+$][LS^-]

The [$PABAH^+$][LS^-] was recovered and suspended in D_2O along with sodium salt of deuterated trimethylsilylpropanoic acid (TMSP-d_4) as an internal standard at a concentration of 5.12 mM. After stirring for 72 hr at room temperature, the supernatant was passed through a 0.45 µm polypropylene syringe membrane and the concentration of PABA in the filtrate was determined using a NMR spectrometer (Varian 400 MHz, Varian

Inc., CA) at 25 °C. The spectrometer is equipped with a Varian NMR System console and a Varian 7600-AS automatic sample change system. Data was acquired with an acquisition time of 2.6 s and a relaxation delay of 1.0 s. The NMR spectra were analyzed by MestReNova software (version 14.2.1 – 27684, Varian Inc., CA).

4.3.2.4 Solutions with various ion products (Q) by varying either [LS^-] or [$PABAH^+$] at a constant pH

A stock solution of PABA was prepared by dissolving ~100 mg PABA powder in 15 mL pH 1.2 HCl solution, the solution pH was shifted to 1.75 after PABA was completely dissolved. This solution was diluted with pH 1.75 HCl solution to obtain various concentrations of PABA. A stock solution of SLS was prepared by dissolving ~575.4 mg SLS powder into 20 mL DI water to obtain a concentration of ~9.98 mM. This stock SLS solution was diluted with DI water to obtain SLS solutions with various concentrations. Then, either 1 mL PABA stock solution ([$PABAH^+$] ~ 35.87 mM) was mixed with 0.1 mL SLS solutions with various concentration, or 0.1 mL SLS stock solution ([LS^-] ~ 9.07 mM) was mixed with 1 mL PABA solutions of various concentrations. Additionally, two more [LS^-] stock solutions at 0.4 mM or 0.2 mM were prepared and mixed with various concentrations of PABA solutions using a similar process.

4.3.2.5 Solutions with varying Q values prepared by adjusting pH of a PABA solution

Blank media with different pHs (0.91-2.88) were prepared by diluting concentrated HCl with DI water. A PABA solution in DI water (29.17mM, pH = 3.56) was mixed with the various HCl solutions at 2:1 volume ratio (PABA solution:HCl solution). In this way, solutions having the same total concentration of PABA but different pHs (1.66 - 3.48) were obtained. In these solutions, [$PABAH^+$] differed because of the different extents of

ionization caused by pH variation. To 1 mL of each of these solutions, 0.1 mL SLS solution in DI water (11 mM) was added to attain different Q values.

4.3.2.6 Determination of CMC of SLS in pH 1.75 HCl solution

A SLS stock solution (20 mM) in pH 1.75 HCl solution was prepared. The stock solution was diluted consecutively with a blank pH 1.75 HCl medium to different concentrations. The surface tension of these SLS solutions was immediately measured with the Wilhelmy plate method using a force tensiometer (K100, KRÜSS GmbH, Germany). It was reported that for a 20 mM SLS solution, ~ 7% was hydrolyzed in 30 min when medium pH is 2.09 at 25 °C, [140] therefore, due to the inevitable acid-catalyzed hydrolysis of SLS, especially for the high SLS concentration (20 mM) and high acidity (pH 1.75) medium, the surface tension measurement in this study was conducted immediately after the SLS solution was prepared to minimize the degradation. The entire process was finished within 30 min. Furthermore, the trace impurities in the commercially available SLS affected the measurement of CMC such that the measured surface tension did not reach a plateau with increasing SLS concentration. In this study, CMC was taken as the minimum in the surface tension - SLS concentration profile. [141-142]

4.3.2.7 Nucleation induction time

Precipitation in a supersaturated solution was monitored using a fiber optic UV-Vis fiber-optic probe (Ocean Optics, Dunedin, FL) at 800 nm with 1 s sampling intervals, the wavelength was chosen to monitor the nucleation kinetics. At this wavelength, these model compounds do not have absorption in solution but particles scattered light to cause reduced light transmission. Induction time was taken as the intersection point between the linear regression line of the rising portion of the curve and the baseline.

4.3.2.8 Preparation of soluble lauryl sulfate salts

Some compounds, e.g., fluorocytosine, caffeine HCl, nicotinamide HCl, ligustrazine HCl, and leucine HCl, did not precipitate when mixed with SLS as described above, suggesting a high solubility of their LS salts, if any. To prove the existence of ion-ion interaction between the cations and LS^- anion in these cases, 5 mL of concentrated (0.5 mM) solutions containing each of the compounds and SLS were dissolved in DI water. Then, one to two drops of concentrated HCl solution were added to attain a pH at least 2 units below pK_a to ensure the complete protonation of the compound. Precipitation occurred immediately in the solution of fluorocytosine and SLS when the concentrated HCl was added. No precipitation occurred after adding the concentrated HCl solution for the other four compounds. These solutions were then allowed to evaporate quickly (in 20 min) in large open petri dishes on bench top. The fast evaporation minimized possible degradation of SLS at a low pH. [139] The dried solids were characterized using a Fourier-transform infrared (FT-IR) spectrometer (Nicolet iS50; Thermo Scientific, Waltham, MA) with a built-in diamond attenuated total reflection. The detector was DLaTGS. A total of 32 scans were collected and averaged for each sample. IR spectra in the range of 4000-400 cm^{-1} at a resolution of 2 cm^{-1} were processed using the software OMNIC 9.2.

4.4 Results and Discussion

4.4.1 Fast screening results of the pharmaceutical lauryl sulfate

Out of the 18 compounds tested in this work, precipitation occurred in 14 cases when mixed with SLS at pH 1.2 (Figure 4.1 and Table 4.1). These precipitants were positively identified as simple LS salts since their solution in MeOD contained both LS^- and corresponding drug cation based on solution NMR data. In the case of florocytosine, the solid was a florocytosine – florocytosine lauryl sulfate salt cocrystal, which was confirmed by its single crystal structure (unpublished data). Regardless of the nature of

the precipitate, these compounds risk the precipitation of less soluble LS salts in stomach, if their formulations contain SLS. This may negatively affect their dissolution performance.

The precipitation of these 14 compounds can be explained from the acid-base reaction in acidic solutions. The calculated pK_a of lauryl sulfuric acid is -3.29. Thus, for most drugs with a basic group having a pK_a 4 units above it, i.e., pK_a > 0.71, salt formation with LS^- can likely happen. If the LS salts are poorly soluble, precipitation occurs. [5-10, 109] The list of compounds studied in this work represent four distinct groups, i.e., salts of basic drugs, quaternary ammonium salt, bases, and zwitterionic drugs, with pK_a in the range of 1.8-11.27 (Figure 4.1 and Table 4.1).

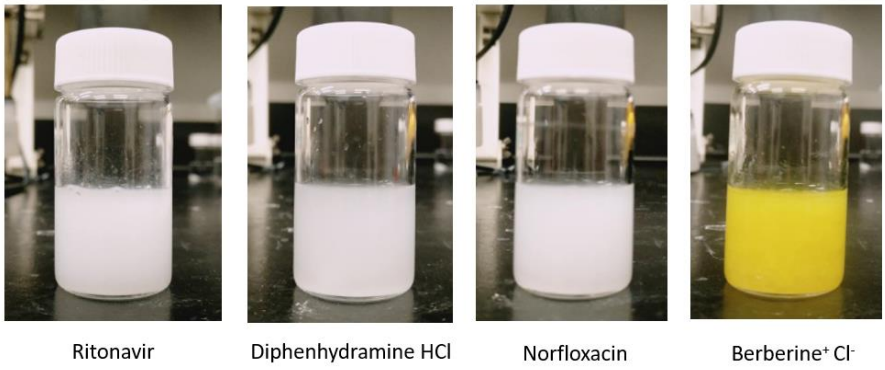

Figure 4. 1. Precipitation of representative model drug solutions upon mixing with a SLS solution, base (ritonavir), salt of a basic drug (diphenhydramine HCl), zwitterionic drug (norfloxacin) and quaternary ammonium salt ($berberine^+ Cl^-$).

Table 4. 1. A list of 18 model drugs and their precipitation tendency with SLS in this study.

No.	Compounds	p*K*a	Precipitation visually observed	Interaction by FTIR
1	isoniazid	3.79 and 11.27	Y	
2	diphenhydramine	8.87	Y	
3	metformin [6]	2.8 and 11.5	Y	
4	caffeine HCl	0.7 and 14.0	N	Y
5	nicotinamide HCl	3.63	N	N
6	ligustrazine HCl	2.19	N	Y
7	leucine HCl	9.60	N	Y
8	berberine Cl^-	NA	Y	
9	4-aminobenzoic acid	2.38	Y	
10	lamivudine	4.3	Y	
11	ritonavir [8]	1.8 and 2.6	Y	
12	erlotinib	4.62	Y	
13	cytosine	4.45	Y	
14	fluorocytosine	3.26	Y	
15	norfloxacin [7]	8.68	Y	
16	levofloxacin	6.02	Y	
17	fleroxacin	6.06	Y	
18	ciprofloxacin	8.74	Y	

The choice of pH 1.2 HCl solution as a medium for examining the tendency to form an LS salt is to simulate the acidity of the gastric fluid. Upon mixing SLS with the saturated

solution at pH 1.2, precipitation occurred immediately in 14 compounds (Figure 4.1 and Table 4.1), which is ~76.4% of the 18 compounds. Along with the 5 more cases reported in the literature, [5, 9-10, 95] the prevalence of this phenomenon calls for more attention when using SLS in an oral solid formulation. To that end, a clear understanding of rules underlying LS salt formation is helpful to effectively addressing potential problems that may be caused by unexpected precipitation of an insoluble LS salt during dissolution. This is addressed in the following sections.

4.4.2 Thermodynamic driving force - ion product (Q) vs solubility product (K_{sp})

The nature of the observed precipitation is the formation of an insoluble salt between LS^- anions and drug cations. For this reaction, the driving force for precipitation is the degree of supersaturation defined by the ion product (Q) relative to solubility product (K_{sp}), where precipitation tends to occur only when $Q > K_{sp}$. The critical degree of supersaturation required for the precipitation, i.e., the width of the metastable zone, is system dependent. [143-145]

The model compound, *p*-aminobenzoic acid (PABA), used in this work is a zwitterionic compound with pK_a of 2.38 (-NH_2 group) and 4.85 (-COOH group). In an acidic environment, the -NH_2 group is protonated to form -NH_3^+, which reacts with LS^- to form the [$PABAH^+$][LS^-] salt. The 1:1 stoichiometry is expected based on charge balance and was verified by solution NMR data (Figure 4.2).

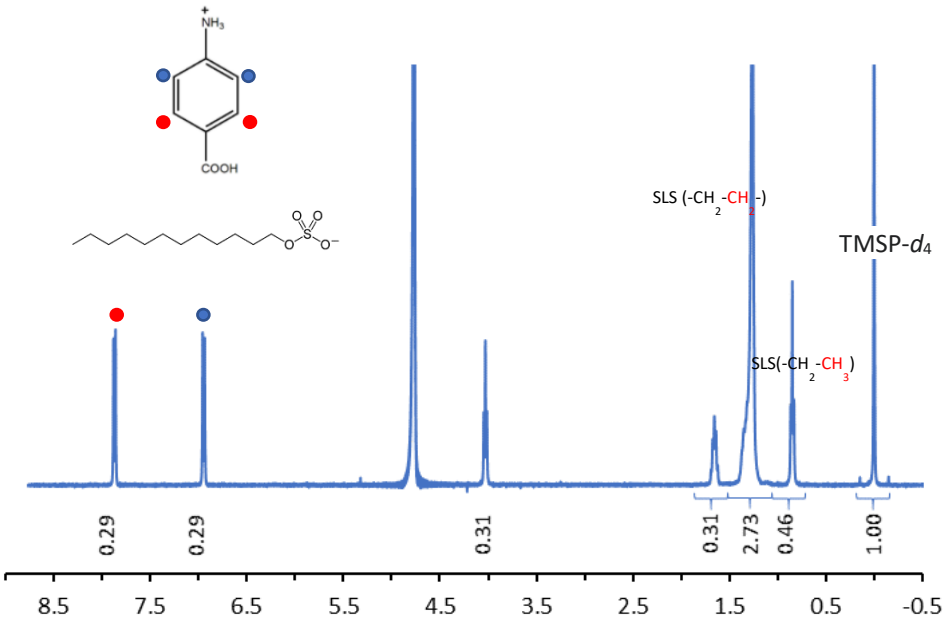

Figure 4. 2. ^{1}H NMR spectrum of [PABAH^{+}][LS^{-}] salt with TMSP-d$_4$ as an internal standard.

Based on the ^{1}H NMR spectrum (Figure 4.2), the 1:1 stoichiometry of [PABAH^{+}][LS^{-}] was confirmed using equation (1). The concentration of the internal standard of TMSP-*d*$_4$ (5.12 mM number of H = 9) was used to determine the concentration of both [PABAH^{+}] and [LS^{-}].

$$\frac{C_{[PABAH^+]}}{C_{[LS^-]}} = \frac{I_{[PABAH^+]} * H_{[LS^-]}}{I_{[LS^-]} * H_{[PABAH^+]}} \quad (1)$$

where I is signal intensity (integral), H is the number of protons in a functional group, C is concentration.

For the mono-salt, K_{sp} is [PABAH^{+}]*[LS^{-}], which was 42.05 ± 4.22 mM^2 in D_2O. This value is much higher than that determined in H_2O (2.44 ± 0.21 mM^2) by a UV method using equation (2). The large difference is attributed to the different solvents. As K_{sp} determined in H_2O is more relevant to this work, the 2.44 ± 0.21 mM^2 is used to predict the solubility

curve (Figure 4.3). Any point above the curve represents a state of supersaturation, i.e., $Q > K_{sp}$. The observations of precipitation behaviors of various combinations of [$PABAH^+$] and [LS^-] qualitatively validate the solubility curve predicted from K_{sp} in the sense that precipitation occurred only when the points lie above the predicted solubility line not below it.

$$K_{sp} = [PABAH^+][LS^-] = [PABAH^+][PABA]_{total} = ([PABA]_{total})^2\left(\frac{1}{1+10^{pH-pK_a}}\right) \quad (2)$$

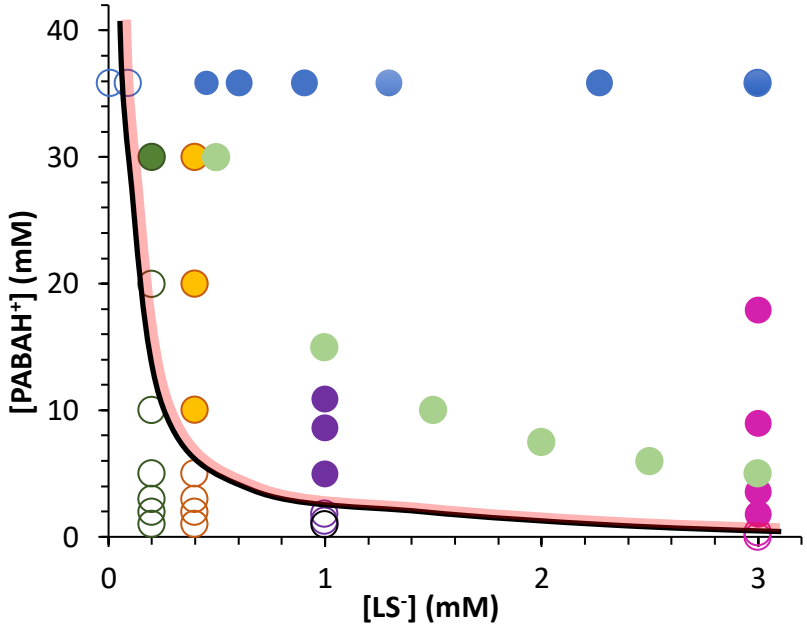

Figure 4. 3. Solubility curve of [$PABAH^+$][LS^-] in water predicted from K_{sp} (black line). Solid symbols indicate the occurrence of precipitation, and open symbols indicate absence of precipitation. The different approaches for preparing solutions with various Q is distinguished with color. The red shaded area above the solubility line represents the estimated metastable zone.

To ensure the robustness of the test, solutions with different Q values were prepared using different approaches. The first approach involved keeping [$PABAH^+$] constant at 37.87 mM and pH constant at 1.75, but varying the concentration of [LS^-] from 0.009 to 9.070 mM (Table 4.2, blue symbols in Figure 3). At pH 1.75, the CMC of SLS is 3 mM based on surface tension measured by the tensiometer (Figure S4.1). Since only the LS^- monomers, not micelles, contribute to the salt formation, the Q values are the same when total SLS concentration is above the CMC. In this set of samples, precipitation occurred only in those with Q > K_{sp} where a lower Q resulted in longer induction time consistent with the lower driving force for precipitation. The absence of precipitation in 48 hrs for solution with Q of 3.25 mM^2, which is greater than K_{sp} = 2.44 mM^2, suggests the width of the metastable zone is >0.81 mM^2 in this system.

Table 4. 2. Precipitation behaviors of solutions with varying Q values prepared by keeping [$PABAH^+$] constant (35.87 mM) at pH 1.75 but allowing [LS^-] to change (blue symbols in Figure 4.3). The K_{sp} of [$PABAH^+$][LS^-] is 2.44 ± 0.21 mM^2.

SLS Conc. (mM)	Q (mM^2)	Precipitation induction time
9.070	107.62	2 s
6.800	107.62	2 s
4.535	107.62	2 s
2.267	81.34	2 s
1.296	46.48	4 s
0.907	32.54	8 s
0.605	21.69	15 s
0.453	16.27	25 s
0.091	3.25	> 48 hr
0.009	0.33	> 48 hr

The second approach involved keeping [LS^-] constant but varying [$PABAH^+$] to prepare solutions with different Q values. Here, three sets of such solutions were prepared using [LS^-] at 9.07 mM (Table 4.3, pink symbols in Figure 4.3), 0.4 mM (Table S4.1, yellow symbols in Figure 4.3) and 0.2 mM (Table S4.2, dark green symbols in Figure 4.3). Since the solution pH was 1.75 in all these cases, the effective [LS^-] in the 9.07 mM [LS^-] set was 3 mM corresponding to the CMC of SLS at pH 1.75. Again, in these samples, precipitation occurred only when $Q > K_{sp}$ not when $Q < K_{sp}$ and the precipitation induction time increased as Q value approached K_{sp}. Interestingly, precipitation occurred when [LS^-] is 0.4 mM, but not when [LS^-] is 0.2 mM when Q was 4 mM^2. Thus, the same apparent driving force (Q/K_{sp}) does not guarantee same precipitation kinetics. This may be

attributed to the different interfacial surface tension induced by different SLS concentrations, which affects precipitation kinetics. [146] This is discussed further in the next section.

Table 4. 3. Precipitation behaviors of solutions with varying Q values prepared by keeping a constant [LS^-] (9.07 mM) at pH 1.75 but allowing [$PABAH^+$] to change (pink symbols in Figure 4.3). The K_{sp} of [$PABAH^+$][LS^-] is 2.44 ± 0.21 mM^2.

[$PABAH^+$] (mM)	Q (mM^2)	Precipitation induction time
35.87	107.62	2 s
17.94	53.81	16 s
8.97	26.90	23 s
3.59	10.76	125 s
1.79	5.38	20 hr
0.36	1.08	None in 48 hr
0.04	0.11	None in 48 hr

The third approach for preparing solutions with different Q values is to keep the total PABA concentration constant but allowing the medium pH to vary, which leads to various [$PABAH^+$] and, therefore, different Q values (Table 4.4, purple symbols in Figure 4.3). In this study, solution pH was in the range of 1.66-3.48 and the [SLS] was 1 mM. Since the concentration of SLS is above the CMC (1 mM) in this pH range, the SLS monomer concentration was taken as 1 mM for calculating Q. Once again, precipitation occurred when $Q > K_{sp}$, but not when $Q < K_{sp}$. The precipitation was slower when the Q value was lower (Table 4.4). The absence of precipitation in the sample with Q of 2.5 mM^2, which is slightly greater than K_{sp} = 2.44 mM^2, may be attributed to the existence of a metastable zone associated with crystallization or precipitation.

Table 4. 4. Precipitation behaviors of solutions with varying Q values prepared from a constant [PABA] (17.59 mM) but different [$PABAH^+$] due to different pHs (purple symbols in Figure 4.3). The $[LS^-]_{monomer}$ was 1 mM and the K_{sp} of [$PABAH^+$][LS^-] is 2.44 ± 0.21 mM^2.

pH	[$PABAH^+$] (mM)	Q (mM^2)	Precipitation induction time
1.66	14.78	14.78	25 s
2.08	11.72	11.72	35 s
2.58	6.81	6.81	1 min 29 s
3.16	2.50	2.50	None in 48 hr
3.35	1.70	1.70	None in 48 hr
3.48	1.29	1.29	None in 48 hr

4.4.3 Kinetic factor- surface tension

Unlike precipitation of other salts, one unique feature of the precipitation of LS salts is that SLS is also a surfactant. Thus, a change in SLS concentration not only affect thermodynamic driving force but also the kinetic barrier of nucleation due to its surface active property, as suggested by the classical nucleation equation 3.

$$J = A \exp\left[-\frac{16\pi\gamma^3 v^2}{3k^3T^3(\ln S)^2}\right] \quad (3)$$

where J is the nucleation rate, k is the Boltzmann constant and v is the molecular volume, T is temperature, S is the degree of supersaturation (= Q/K_{sp} in this study), and γ is interfacial tension, which is lower at higher SLS concentration. As the nucleation rate is inversely proportional to the induction time, a higher SLS monomer concentration is expected to promote nucleation and lower induction time.

To investigate the effect of SLS on precipitation kinetics, a series of solutions with the same Q value were prepared at pH 1.75 by varying both [$PABAH^+$] (3 – 60 mM) and [LS^-] (0.25 - 5 mM) so that the degree of supersaturation is the same in all these samples but their interfacial tension of nuclei varied (Table S4.3, light green symbols in Figure 4.3). The induction time was approximately constant, ~16 s, when SLS was above 2 mM. However, below 2 mM SLS concentration, the induction time increased gradually when [SLS] decreased to 0.5 mM but sharply increased when [SLS] was below 0.5 mM (from ~23 s at 0.5 mM to ~70 s at 0.25 mM). This behavior is consistent with that predicted from equation 3, reflecting the higher interfacial tension at lower SLS concentrations.

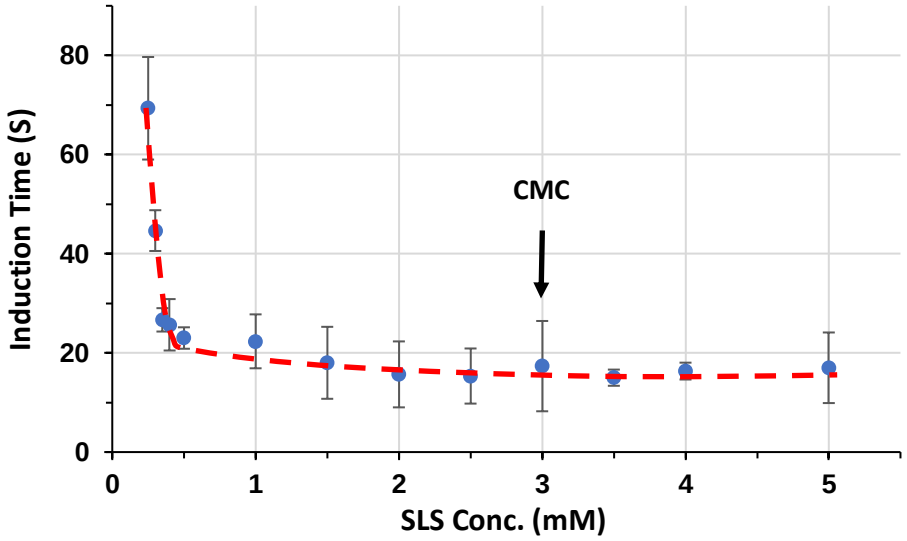

Figure 4. 4. Induction time vs. SLS concentration when ion product, Q, is constant at 15 mM^2.

4.4.4 Soluble pharmaceutical lauryl sulfate salt

The precipitation necessarily indicates that the newly formed LS salts are less soluble in water. An absence of precipitation can be a result of either an LS salt does not exist, or the salt is actually soluble. In fact, all 4 compounds (caffeine HCl, nicotinamide

HCl, ligustrazine HCl, leucine HCl) that did not precipitate in this study are highly soluble in water. This point finds support from the ΔpK_a rule, [109] which states that a salt is very likely formed in solid state when ΔpK_a between the conjugate acid of the base and the acid is more than 4. In the case of LS^- salts, the calculated pK_a of LS-H is -3.29 while the pK_a of the 4 compounds ranged 2.19 - 9.60, giving ΔpK_as much larger than 4. Thus, rather than suggesting their LS salts does not exist, we hypothesize that their LS salts are highly soluble in water, i.e., their K_{sp} values are high. To test this hypothesis, powder mixtures of each of the 4 compounds and SLS (1:1 mole ratio) were dissolved in a medium with pH at least two units below their pK_a to form high concentration solutions, which were quickly evaporated in a large petri dish on a bench. The recovered solids after drying were analyzed by FT-IR spectroscopy (Figure 4.5).

When the cations of these compounds interact with SLS sulfate head group, shifting of the characteristic peaks of SO_2 asymmetric v_{as} (SO_2) at 1216 and 1247 cm^{-1} and symmetric v_{sym} (SO_2) at 1080 cm^{-1} vibrations is expected. [147] For the leucine-SLS sample, the $v_{as}(SO_2)$ red shifted to 1167 and 1214 cm^{-1}, and the $v_{sym}(SO_2)$ red shifted to 1052 cm^{-1} (Figure 4.5a), this clearly indicates the leucine LS salt was formed. In caffeine-SLS (Figure 4.5b) and ligustrazine-SLS (Figure 4.5c), the $v_{as}(SO_2)$ and v_{sym} (SO_2) bands underwent complex changes in width, intensity, and wavenumbers, suggesting the SO_2 group engaged in new kinds of intermolecular interactions. The characteristic $v_{as}(SO_2)$ bands of SLS are not visible in the caffeine-SLS sample, further substantiating a significant change in the intermolecular interactions involving the lauryl sulfate anion. However, the nature of these interactions requires further investigation. The spectrum of nicotinamide-SLS appears to be a simple addition of the spectra of nicotinamide HCl and SLS, with no observable changes in the vibrational bands (Figure 4.5d), suggesting it is a physical mixture between nicotinamide HCl and SLS.

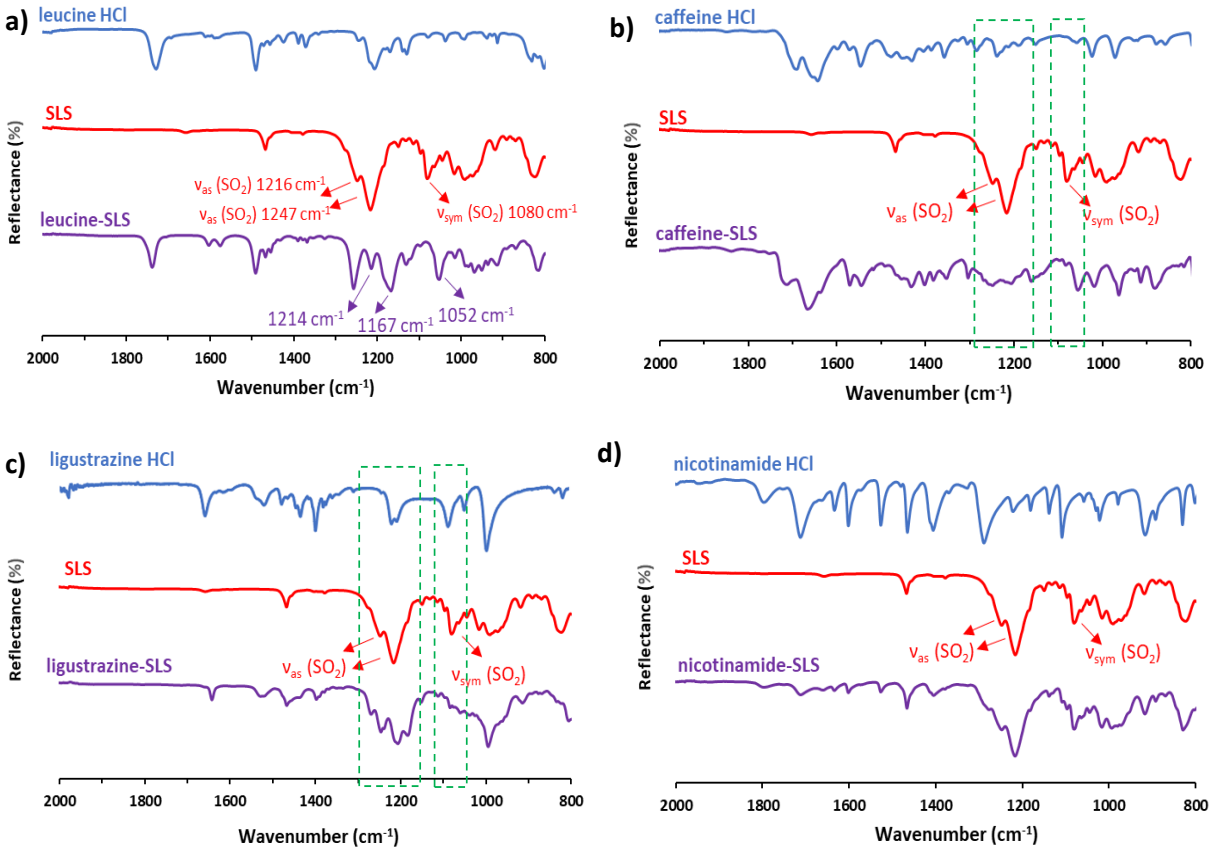

Figure 4. 5. FTIR of solids obtained from drying SLS solutions and four compounds, a) leucine, b) caffeine, c) ligustrazine, d) nicotinamide

4.4.5 Formulation implications

A clear understanding of the nature of precipitation of pharmaceutical LS salts and factors that affect their precipitation kinetics leads to several formulation strategies that can be applied to mitigate the negative impact of SLS.

1) Since the precipitation is mostly between protonated bases (berberine is an exception) and the lauryl sulfate anions, the acid-base reaction can be eliminated if the dosage form is protected from the acidic environment in the stomach, which is necessary

for protonation of the base. A common formulation strategy to attain this effect is enteric coating.

2) When a poorly soluble LS salt is anticipated or suspected but SLS must be used for whatever reasons, an appropriate polymer may be added to inhibit or slow down the nucleation of the possible LS salt during dissolution.

3) Because the driving force for such precipitation reaction is the high Q, any strategies that reduce the Q values may mitigate this problem. For example, since Q is determined by the monomer concentration of SLS, strategies that reduce CMC of SLS by introducing electrolyte may be considered. [65] This strategy can also lead to the generation of more micelles, which can potentially solubilize the drug. Other strategies that reduce cations concentration, such as using a pH modifier to adjust the microenvironmental pH in diffusion layer or a salt with a common ion to suppress the dissolution of drug cation from a soluble salt, [47, 59] can lower the propensity to forming a LS salt so that the nucleation induction time is long enough to ensure the drug safely diffuse into the bulk medium before precipitation takes place.

4.5 Conclusion

We have shown that almost all drugs with cations or protonatable in an acidic environment have the potential to form LS salts. Among the compounds studied in this work, ~77.8% (14 out of 18) model compounds resulted in precipitation, which likely deteriorates drug dissolution. Although only 5 cases of SLS induced precipitation were reported in the published literature so far, the phenomenon is actually rampant. Therefore, a preliminary assessment of precipitation propensity in the presence of SLS should be carried out for such compounds before SLS is used to improve their dissolution. If

precipitation occurs in the presence of SLS, other surfactants are recommended. If SLS must be used, appropriate formulation strategies should be implemented to mitigate any negative impact on the dissolution of the drug.

4.6 support information

Table S4. 1. A series of Q values prepared by 0.4 mM [LS^-] and various [$PABAH^+$] at pH 1.75 (yellow symbols in Figure 4.2)

[LS^-] (mM)	0.4 mM		
[$PABAH^+$] (mM)	Q	K_{sp}	precipitation
30.00	12.01	2.44 ± 0.21	✓
20.00	8.01		✓
10.00	4.00		✓
5.00	2.00		×
3.00	1.20		×
2.00	0.80		×
1.00	0.40		×

Table S4. 2. A series of Q values prepared by 0.2 mM [LS^-] and various [$PABAH^+$] at pH 1.75 (dark green symbols in Figure 4.2)

[LS^-] (mM)	0.2 mM		
[$PABAH^+$] (mM)	Q	K_{sp}	precipitation
30.00	6.01	2.44 ± 0.21	✓
20.00	4.00		×
10.00	2.00		×
5.00	1.00		×
3.00	0.60		×
2.00	0.40		×
1.00	0.20		×

Table S4. 3. Induction time vs SLS conc. when ion product is constant at 15 mM^2 (light green symbols in Figure 4.2)

	Induction time (S)												
SLS Conc. (mM)	0.25	0.3	0.35	0.4	0.5	1	1.5	2	2.5	3	3.5	4	5
1	83	44	30	22	22	19	28	25	13	13	17	18	27
2	67	40	25	22	21	18	15	10	23	30	15	14	13
3	58	50	25	33	26	30	11	12	10	9	13	17	11
AVE	69.33	44.67	26.67	25.67	23.00	22.33	18.00	15.67	15.33	17.33	15.00	16.33	17.00
SD	10.34	4.11	2.36	5.19	2.16	5.44	7.26	6.65	5.56	9.10	1.63	1.70	7.12

Figure S4. 1. CMC determination by surface tension measurement in pH 1.75 HCl solution

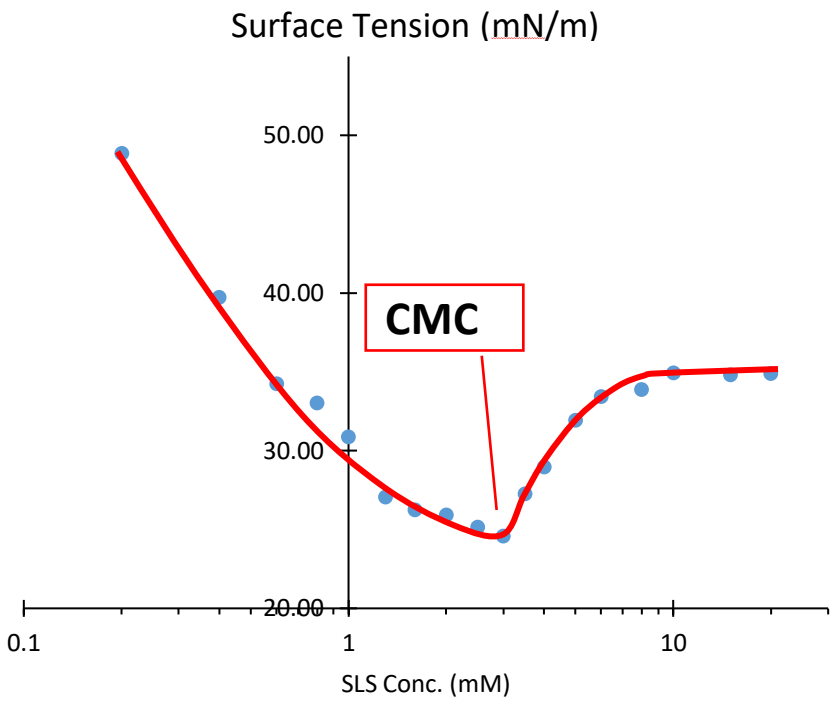

Chapter 5

Formulation strategies for mitigating dissolution reduction of PABA by sodium lauryl sulfate through diffusion layer modulation

5.1 Synopsis

The use of the surfactant, sodium lauryl sulfate (SLS), instead of enhancing drug dissolution, deteriorates the dissolution of some alkaline drugs through forming poorly soluble lauryl sulfate salts. The thermodynamic driving force for precipitation of such salts is the ratio of ion product in solution (Q) to the solubility product of the salt (K_{sp}). In this work, we have examined two formulation strategies for mitigating the negative effect of SLS on the dissolution of *p*-aminobenzoic acid (PABA) by reducing the Q value of its LS salt in the diffusion layer: 1) introducing alkalizing excipient, Na_3PO_4, to reduce the concentration of $PABAH^+$ by elevating the microenvironment pH, and 2) introducing NaCl to reduce the LS^- monomer concentration by depressing the critical micelle concentration (CMC) of SLS.

5.2 Introduction

Sodium lauryl sulfate (SLS) may deteriorate the dissolution of drugs with functional groups that can be protonated in an acidic medium, through the precipitation of an insoluble lauryl sulfate (LS) salt.[5-10, 95] To form a salt, the pH of the medium must be sufficiently low to protonate drug molecules.[8-10] Salt formation was confirmed by analyzing the single crystal structure of an LS salt of norfloxacin, in which strong ion pairs between protonated norfloxacin molecules and LS anions exhibit low solubility in water.[7] Our further investigations have shown that LS salts broadly form through the conventional acid - base reaction.[148] Hence, this raises a concern given the frequent use of SLS in formulation with the intention to improve wetting of hydrophobic drugs. If not proactively addressed, the formation of such insoluble LS salts may deteriorate dissolution performance and leads to poor decisions in formulation design.

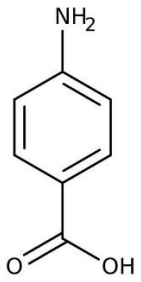

Figure 5. 1. Molecular structure of *p*-aminobenzoic acid.

To effectively mitigate the negative impact of LS salts on drug dissolution, we have investigated key factors that determine the precipitation of a LS salt of *p*-aminobenzoic acid (PABA, Figure 5.1), $[PABAH^+][LS^-]$.[148] Results show that the precipitation of $[PABAH^+][LS^-]$ is driven by a high ratio of ion product (Q), defined in Eq. (1), to solubility product (K_{sp}),

$$Q = [\mathrm{PABAH}^+] * [LS^-]_{\mathrm{mono}} \quad (1)$$

In Eq. (1), $[PABAH^+]$ is the concentration of protonated PABA and $[LS^-]_{mono}$ is the concentration of SLS monomer. Here, $[LS^-]_{mono}$ is equal or below the critical micelle concentration (CMC). Precipitation can occur only when the Q value sufficiently exceeds the K_{sp} of $[PABAH^+][LS^-]$, and a higher Q/K_{sp} corresponds to faster precipitation. Furthermore, at the same Q/K_{sp} value, the precipitation kinetics is affected by $[LS^-]_{mono}$, because a higher concentration of the surface-active SLS monomer more effectively lowers the interfacial tension between nuclei and medium, resulting in a faster nucleation rate.

Built upon this understanding of precipitation kinetics, here we investigate possible formulation strategies to mitigate the negative impact LS salt formation on dissolution of drugs. The classical thin-film diffusion layer model teaches that an indefinitely thin layer

of saturated solution is formed at the surface of the solid during dissolution. [34, 149-150] According to this model, the precipitation of LS salt should initiate in the diffusion layer where the Q value is the highest. As K_{sp} is usually a constant for a given salt in a given solvent at a fixed temperature, we focused on reducing the thermodynamic driving force, Q/K_{sp}, by decreasing Q value in the diffusion layer through formulation strategies.

The Q value in the diffusion layer can be lowered by lowering either [$PABAH^+$] through maintaining a high pH in the diffusion layer or [LS^-] by depressing the CMC of SLS. The effectiveness of these possible mitigation strategies was assessed using both intrinsic dissolution rate (IDR) and tablet dissolution in this work.

5.3 Materials and Methods

5.3.1 Materials

p-aminobenzoic acid was purchased from Sigma-Aldrich (St. Louis, MO). Microcrystalline cellulose (Pharmacel 102; DFE Pharma, Goch, Germany), magnesium stearate (MgSt, Covidien, Dublin, Ireland), croscarmellose sodium (Ac-Di-Sol; FMC Biopolymer, Philadelphia, PA), and SLS (Ward's Science, Rochester, NY), NaCl (Maillinckrodt Baker, Inc., Phillipsburg, NJ), and $Na_3PO_4 \cdot 12\ H_2O$ (Acros Organics, *Fair Lawn*, NJ) were purchased from respective suppliers. Hydrochloride acid aqueous solution (36.5%−38%, ACS reagent grade, VWR international, Eagan, MN) and deionized water were used to prepare the dissolution medium, i.e., pH 1.2 HCl solution.

5.3.2 Methods

5.3.2.1 Intrinsic dissolution rate (IDR)

The IDRs of PABA and its physical mixtures with different additives were measured using the rotating disc method. [151-153] The individual ingredients were mixed using a mixer (Turbula; Glen Mills Inc., Clifton, NJ), running at a speed of 49 rpm for 20 min. NaCl and

$Na_3PO_4 \cdot 12\ H_2O$ were grinded and passed through a 230 mesh sieve with 63 μm opening before mixing. The relative humidity (RH) in the laboratory during the entire process was approximately 35%. A powder was compressed at a force of 2000 lb on a hydraulic press using a custom-made stainless-steel die against a flat stainless-steel disc for 2 min. The pellet (6.39 mm in diameter) had a visually smooth surface that was coplanar with the surface of the die. While rotating at 50 rpm, the die was immersed in 300 mL pH 1.2 HCl solution at 37°C in a water-jacketed beaker. A UV−Vis fiber optic probe (TI300-UV-VIS, Ocean Optics, Dunedin, FL) was used to monitor the UV absorbance, from which the concentration of PABA was calculated using a pre-constructed calibration curve. Results from at least triplicated measurements were used to calculate means and standard deviations at prescribed time points.

5.3.2.2 Tablet preparation

Tablets of physical mixtures of PABA, SLS, and NaCl or $Na_3PO_4 \cdot 12\ H_2O$ (Table 5.1) were prepared by compression. To achieve good uniformity, NaCl and $Na_3PO_4 \cdot 12\ H_2O$ were grinded and passed through a 230 mesh size sieve (63 μm opening) before mixing with a Turbula mixer (Glen Mills Inc., Clifton, NJ) at 49 rpm for 20 min. The mixtures were compressed at a force of 2000 lbs for 5 s to prepare ribbons (16.8 × 9.5 mm, 300 mg) using a laboratory hydraulic press (model C, Carver Inc., Wabash, IN, USA). The ribbons were grinded gently in a mortar with a pestle and then passed through a sieve with 90 μm opening. The sieved granules were mixed with all other components except the lubricant, MgSt, in the mixer at 49 rpm for 20 min. When used in a formulation, MgSt was mixed with the mixture of all other ingredients for 2 min. Batch size was 1.2 g in all cases.

Table 5. 1. Tablet formulations of PABA

Ingredient	Control 1 (MgSt)	Control 2 (SLS)	NaCl tablet	Na_3PO_4 tablet
PABA	10%	10%	10%	10%
MCC	84%	75%	25%	70%
CCNa	5%	5%	5%	5%
MgSt	1%			
SLS		10%	10%	10%
NaCl			50%	
$Na_3PO_4 \cdot 12\ H_2O$				10%
Total		100%		

5.3.2.3 Karl Fischer Titration (KFT)

The water content of the grinded and sieved $Na_3PO_4 \cdot 12H_2O$ powder was determined with a Karl Fischer Titrator (Metrohm 831 KF coulometer) equipped with a Metrohm 703 Ti Stand mixer. Titrations were carried out in HYDRANAL Coulomat AG (methanol-based anolyte, Sigma Aldrich, St. Louis, MO) under constant stirring. An accurately weighed sample (approximately 50 mg) was introduced into the titration vessel, which was immediately capped to minimize interference by moisture from the environment. The water content was recorded at the end of the run.

5.3.2.4 Tablet dissolution

The release of PABA from tablets was evaluated in 300 mL pH 1.2 HCl solution. The medium was maintained at 37 °C and stirred with an overhead stirrer at 50 rpm. Drug

release was monitored using the same fiber optic UV dip probe used in the IDR measurement.

5.3.2.5 pH dependent solubility of PABA

To determine the solubility of PABA at different pHs, an excess amount of the PABA was suspended in ~5 mL desired media, including pH 1.2 HCl solution, pH 2 HCl solution, DI water, and pH 6.8 phosphate buffer (0.1 M) for at least 48 hr under stirring at 37 °C. The pH of these media shifted to 2.24, 3.07, 3.59, 4.66, respectively after equilibration, and the solid phase of PABA remained unchanged according to their PXRD patterns. After passing through a 0.45 µm polypropylene filter membrane, the concentration of PABA was determined by UV-Vis spectrometry (DU® 530 UV-Vis spectrophotometer; Beckman, Brea, CA), using a separately constructed calibration curve with appropriate dilution if needed.

The solubility values at four pHs were fitted by the Henderson–Hasselbalch equation using p$K_{a,1}$ = 2.38 for -NH_3^+ [154] and p$K_{a,2}$ = 4.85 for -COOH [155] to generate a pH-solubility profile of PABA. The Non-linear regression was performed using SciPy's orthogonal distance regression (ODR) package (SciPy v1.6.2, Python v3.8.2). Ordinary least squares (job=2) was used, and y standard deviations were included for fitting. We did not use the solubility values at three pHs to obtain a pH – solubility profile of PABA because of a very poor fitting, suggesting errors in the literature values. [156]

5.3.2.6 Moisture Sorption Isotherm

The moisture sorption isotherm of Na_3PO_4 was collected using an automated dynamic vapor sorption analyzer (Intrinsic DVS, Surface Measurement Systems Ltd., Allentown, PA) at 25 °C. The sample was purged with nitrogen at a flow rate of 50 mL/min. Initially, RH was maintained at 95% until a constant sample weight was obtained to ensure complete phase conversion to the highest hydrate at 25 °C. Then, the sample was

exposed to a series of decreasing RHs from 95 to 0% with a step size of 5%. The sorption isotherm was obtained by exposing the dried sample to a series of RHs from 0 to 90% with a step size of 10% RH. At each specific RH, the equilibration criterion of either dm/dt ≤ 0.002% with a minimum equilibration time of 20 min or a maximum equilibration time of 6 h was applied. The RH moved to the next target value once one of the criteria was met.

5.4 Results and discussion

5.4.1 Q reduction by lowering $[LS^-]_{mono}$

The SLS monomer concentration, $[LS^-]_{mono}$, directly drives possible precipitation of the $[PABAH^+][LS^-]$ salt by contributing to Q (Eq. 1). In the diffusion layer, $[LS^-]_{mono}$ is equal to the CMC of SLS because the medium at the surface is saturated by the dissolving SLS solid. [34] Therefore, reducing the CMC of SLS lowers $[LS^-]_{mono}$, which subsequently lowers the thermodynamic driving force for precipitation.

The CMC of SLS in DI water is 8.2 mM at 25 °C, [64] the value is strongly affected by several factors, such as temperature, [64] pH, [66] species and concentration of electrolyte present in the solution. [65, 157] The cationic electrolyte binds to the negatively charged micelle surface, which decreases the electronic repulsion between micelles, and leads to a reduced CMC of SLS. [158-159] Therefore, the maximal concentration of the LS^- monomer in solution is expected to be lower in the presence of an inorganic salt. [65] Correspondingly, we hypothesized that the incorporation of NaCl in tablet formulation of PABA can reduce Q by depressing the CMC of SLS in the diffusion layer. This hypothesis was tested by determining IDR and tablet dissolution of formulations containing NaCl, PABA, and SLS at different weight ratios.

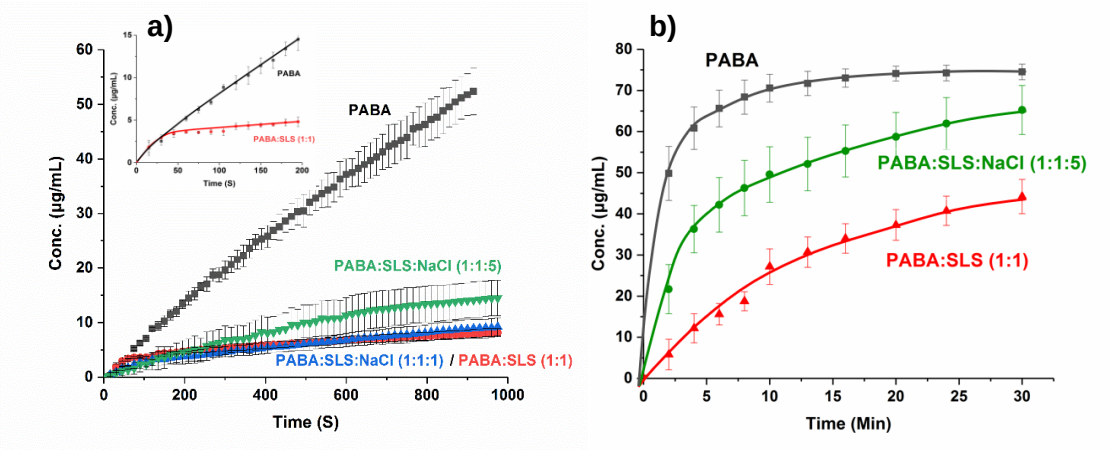

Figure 5. 2. Effects of NaCl and SLS on the dissolution of PABA in a pH 1.2 medium, a) intrinsic dissolution, b) tablet dissolution.

In the pH 1.2 solution, SLS reduced the IDR of PABA significantly (Figure 5.2a). Although its initial rate is comparable to that of PABA alone (66.85 ± 7.65 $\mu gcm^{-2}s^{-1}$), the IDR of PABA: SLS (1:1 w/w) pellet decreased significantly after ~50 s to be 3.52 ± 0.29 $\mu gcm^{-2}s^{-1}$. This is attributed to the gradual coverage of the surface of the PABA:SLS (1:1 w/w) pellet by the $[PABAH^+][LS^-]$ that precipitated out with time. Thus, the terminal IDR is essentially that of the $[PABAH^+][LS^-]$. Correspondingly, the IDR ratio of PABA to $[PABAH^+][LS^-]$ is 18.99 (Figure 1a). The deleterious effect of SLS on the dissolution of PABA is also clear when comparing the dissolution from a tablet containing 1% MgSt and 10% SLS (Figure 5.2b). At 30 min, the amount of released PABA from the SLS-containing formulation (control formulation 1) is only slightly more than 50% of that from the PABA tablet free from SLS (control formulation 2).

The incorporation of NaCl into the mixture had little impact on IDR when the weight ratio was PABA: SLS: NaCl 1:1:1 (Figure 5.2a). However, a higher IDR was obtained at a higher NaCl amount (1:1:5 w/w/w), despite the smaller effective surface area of PABA for dissolution due to the dilution by the larger amount of NaCl in the formulation.

The mitigation effect of NaCl during tablet dissolution is expected to be more significant than that indicated by IDR, since the total area of PABA exposed to the medium is less negatively affected by NaCl upon tablet disintegration (Figure 5.2b). Indeed, significant recovery of the dissolution of PABA from the tablet was observed when NaCl was used at 5 times the weight of PABA (Figure 5.2b). However, the lost dissolution performance by forming the poorly soluble $[PABAH^+][LS^-]$ was still not fully recovered (Figure 5.2b). Nevertheless, the results support the hypothesis that the incorporation of NaCl in formulation can mitigate dissolution slowdown caused by the formation of a less soluble LS salt of PABA during dissolution.

5.4.2 Q reduction by lowering $[PABAH^+]$

Eq. (1) also suggests that Q can be reduced by lowering $[PABAH^+]$. The $[PABAH^+]$ in diffusion layer can be reduced by maintaining a higher local pH using an alkalizer, which shifts the ionic equilibrium of PABA in solution from $[PABAH^+]$ to [PABA]. In fact, pH-modification is a commonly used strategy to enhance the dissolution and oral bioavailability of drugs. [59, 160-161]

A suitable alkalizer should have a relatively high aqueous solubility and a higher pK_a than that of PABA. Such an alkalizer dissolves and creates a local pH sufficiently high to minimize protonation of dissolved PABA molecules, which is a necessary condition for forming the less soluble LS salt. Based on this consideration, Na_3PO_4 was chosen as the alkalizer in this work. The physical stability of Na_3PO_4 was assessed by DVS because it is known to form hydrates. [162] The DVS data revealed four hydrates based on weight change, where the $Na_3PO_4 \cdot 15H_2O$, $Na_3PO_4 \cdot 12H_2O$, $Na_3PO_4 \cdot 8H_2O$, $Na_3PO_4 \cdot 6H_2O$, and the anhydrate are stable at RH ranges of 95%, 65-90%, 35-60%, 20-30%, and below 15%, respectively (Figure 5.3). Thus, under normal manufacturing conditions with RH in the range of 30% - 50%, either the $Na_3PO_4 \cdot 6H_2O$ or $Na_3PO_4 \cdot 8H_2O$

is the stable form. In fact, the water content of Na_3PO_4 powder used in the formulation was 50%, which is between the theoretical water contents of $Na_3PO_4 \cdot 8H_2O$ (46.8%) and $Na_3PO_4 \cdot 12H_2O$ (56.8%). It is worth mentioning that the main goal here is to investigate the feasibility of Na_3PO_4 as an alkalizer to reduce the thermodynamic driving force of the $[PABAH^+][LS^-]$ precipitation by elevating the pH in the diffusion layer. Therefore, the relative physical stability of the Na_3PO_4 hydrate forms is not a major concern in this study. Should this strategy be adopted in any commercial formulations, alternative alkalizers that do not have the complication of various hydration states should be pursued.

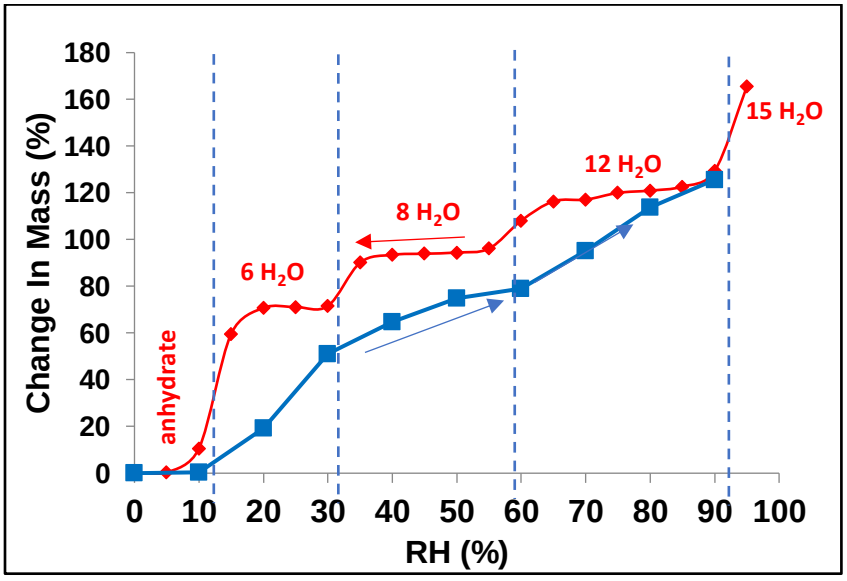

Figure 5. 3. Dynamic vapor sorption (squares) and desorption (diamonds) of Na_3PO_4 at 25 ^oC.

The effectiveness of Na_3PO_4 in mitigating the negative effect by SLS was also assessed by both IDR and tablet dissolution. The incorporation of Na_3PO_4 significantly increased both the IDR and tablet dissolution at the 1:1:1 weight ratio of

PABA:SLS:Na_3PO_4 (Figure 5.4), suggesting Na_3PO_4 is an effective alkalizer to counter the negative impact of SLS on the dissolution of PABA. The IDR of PABA:SLS:Na_3PO_4 (1:1:1, w/w/w) pellet is even higher than that of PABA alone (control 1 tablet) despite the reduced effective surface area of PABA by SLS and Na_3PO_4. The higher IDR is attributed to both the higher solubility of PABA at an elevated pH than that at pH 1.2 (Figure 5.4), due to ionization of –COOH, and the elimination of the precipitation of $[PABAH^+][LS^-]$. The ionization of -COOH is demonstrated by the significantly higher IDR of PABA: Na_3PO_4 (1:1 w/w) than PABA. The plateau observed in the profiles of both Na_3PO_4-containing pellets corresponded to complete dissolution. The higher plateau value of the PABA: Na_3PO_4 profile reflects the larger amount of PABA in the pellet. Importantly, the higher IDR achieved by Na_3PO_4 could be successfully translated to higher tablet dissolution, leading to a nearly fully recovered release of PABA from tablet (Figure 5.4b).

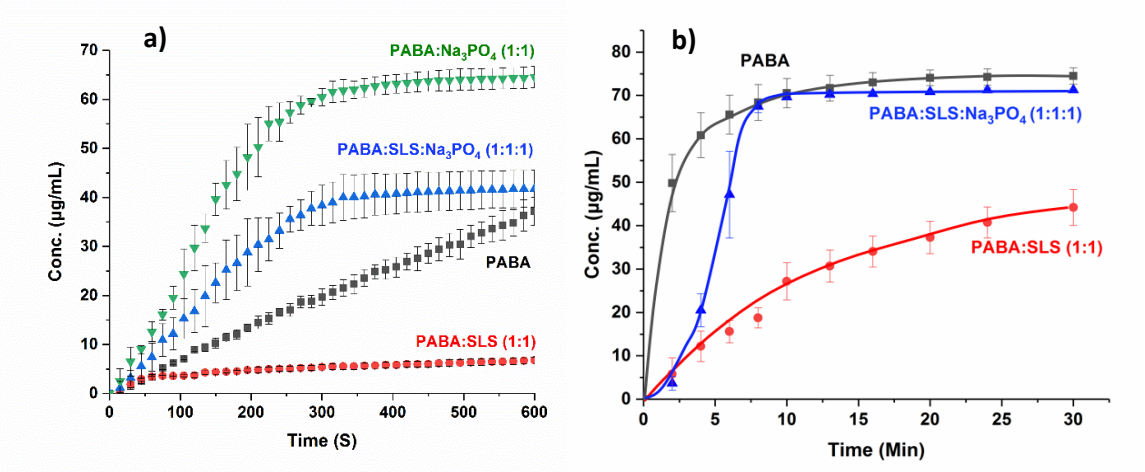

Figure 5. 4. Effect of Na_3PO_4 on mitigating dissolution reduction by SLS, a) intrinsic dissolution, b) tablet dissolution.

The micro-environment pH of the PABA:SLS:Na_3PO_4 (1:1:1, w/w/w) pellet can be estimated from the pH - solubility profile of PABA (Figure 5.5), assuming IDR is

proportional to the equilibrium solubility under identical hydrodynamic conditions. [149] In the pH 1.2 medium, the pH in the diffusion layer of PABA pellet is 2.19 instead of 1.2 because of the self-buffering effect due to the ionic equilibrium of dissolved PABA molecules. [163-164] The pH in the diffusion layer was inferred from the pH of a saturated solution of PABA in the pH 1.2 medium.

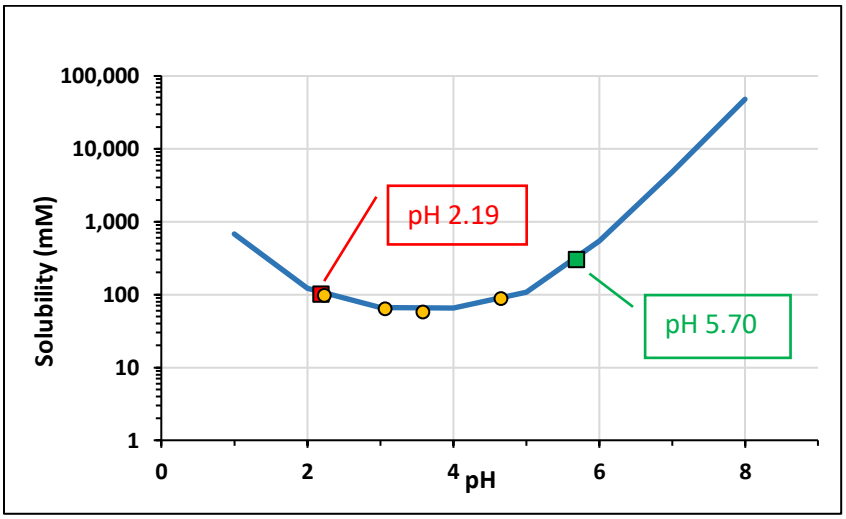

Figure 5. 5. pH - solubility profile of PABA in water at 37 °C. The profile is obtained by nonlinear regression for the four solubility values (yellow symbol) using the Henderson–Hasselbalch equation.

From figure 5.4a, the true IDR of PABA from PABA:SLS:Na_3PO_4 (1:1:1 w/w/w) is at least 3 times that of PABA if the surface area is corrected. Thus, as the solubility of PABA is 100.24 mM at pH of 2.19, this corresponds to a local pH of ~5.70 surrounding PABA according to the pH-solubility profile (Figure 5.5). Since this pH is more than 3 pH units above the pK_a of $-NH_3^+$ (2.38), almost all the $-NH_2$ groups are in their neutral state. Additionally, the CMC of SLS, which is 8.2 mM in water, is lower at a lower pH. [157] Therefore, at pH ~5.70, the Q value would be lower than 0.10 mM^2 ($[LS^-]$ = 8.2 mM and

[$PABAH^+$] = 0.012 mM at pH 5.70), which is much lower than the K_{sp} (2.44 ± 0.21 mM^2) of [$PABAH^+$][LS^-]. Thus, the elimination of the precipitation of [$PABAH^+$][LS^-] is justified by an absence of thermodynamic drive force for it to occur.

Since PABA is a zwitterionic compound, a higher pH reduces [$PABAH^+$] but not necessarily the solubility of PABA because of the ionization of –COOH at high pHs. Therefore, maintaining a high local pH can both reduce the propensity to form a less soluble complex with LS^- and maintain a fast dissolution of PABA. For non-zwitterionic bases, dissolution rate may be reduced at a high pH. Hence, judicious choice of the type and amount of pH modifiers in formulations requires systematic examination of their impact on dissolution.

5.5 Conclusion

Using PABA as a model drug, we have demonstrated that dissolution deterioration by SLS can be mitigated through formulation strategies, i.e., 1) pH elevation using an alkalizer, Na_3PO_4, and 2) depression of the CMC of SLS using NaCl. These strategies modulate the environment in the diffusion layer to reduce the thermodynamic driving force for forming a poorly soluble lauryl sulfate salt.

Chapter 6

Research summary and future work

Research summary

The story starts from a peculiar observation, in which the dissolution enhancer of SLS surprisingly deteriorated the dissolution of ritonavir (RTV) in its tablet formulation. With a series characterization techniques, such dissolution reduction was confirmed to be due to the formation of a poorly soluble amorphous lauryl sulfate salt between SLS and RTV, i.e., $[RTV^{2+}][LS^-]_2$, at a low pH.

With the solved single crystal structure of norfloxacin (NOR) lauryl sulfate salt, i.e. $[NORH^+][LS^-]\cdot 1.5\ H_2O$, the columbic interaction between protonated drug cation and LS^- was confirmed. From the single crystal structure, stacked layer with a sandwiched structure for each layer was observed, in which polar moieties with strong interactions, like strong ionic interaction, hydrogen bonds, and π−π stacking, are buried inside each layer, while nonpolar moieties with only weak dispersive forces are energetically favored outside each layer. This gives the salt a high hydrophobicity and disfavors the dissolution.

Due to the straightforward acid – base reaction, SLS is observed to form lauryl sulfate salt with many other compounds. Among the 18 model compounds, 14 of them (77.8%) formed poor soluble lauryl sulfate salt with precipitation observed. 4 other compounds, although no precipitation observed, 3 of them also exhibited interactions with SLS suggested by FT-IR spectra. With the additional 5 compounds that are reported in literature, LS salt is shown to be a rather general phenomenon.

The formation rules was investigated by *p*-aminobenzoic acid (PABA), which forms $[PABAH^+][LS^-]$ with SLS. It was found that the occurrence of precipitation is thermodynamically driven by the relative difference between the ion product in solution (Q) and the solubility product of the lauryl sulfate salt (K_{sp}), i.e., Q/K_{sp}. On the other hand, as a surfactant, SLS also affects precipitation kinetics by influencing the interfacial tension during nucleation.

To mitigate the negative effect of SLS, two mitigation strategies were proposed to reduce the thermodynamically driving force Q/K_{sp} in the thin diffusion layer of the dissolving solid, they are 1) lowering LS^- monomer concentration by introducing NaCl, and 2) lowering $PABAH^+$ concentration by introducing Na_3PO_4, which is an alkalizing excipient that can elevate the microenvironment pH. Importantly, with the application of Na_3PO_4, the dissolution of PABA in presence of SLS was nearly fully recovered.

Future work

1. Exploring other surfactants

SLS was initially proposed as a surrogate for MgSt, due to its dual functionalities as both a lubricant and a wetting agent. The negative impact on drug dissolution limits its universal use in tablet formulations. Therefore, exploring the feasibility of other alternative lubricants that are free from this mechanism of forming poorly soluble salts is needed. For example, Poloxamer P188 and P407 have been shown to exhibit good lubrication property while also facilitate *in vitro* drug release. [165] Other solid surfactants, such as PEG 2000, can also be explored.

2. Using other model compounds

In this study, PABA was chosen as the model compound to investigate the formation rules of lauryl sulfate salt and mitigation strategies. The effectiveness of using a pH modifier, Na_3PO_4, on recovering the release of PABA in a SLS contained tablet resulted, in part, from the increased ionization of –COOH, which leads to a high solubility. For non-zwitterionic compounds, the use of Na_3PO_4 risks overly depressing the solubility so that the dissolution is not much improved, even if precipitation of the LS salt is prevented. In such system, judicious use of the amount and type of alkalizer needs to be systematically investigated to ensure robust dissolution performance of tablet formulations.

3. *In vivo* study

For a tablet formulation, adequate *in vivo* bioavailability is critical. Therefore, it is important to know how these *in vitro* dissolution phenomena affects the *in vivo* performance. For example, does SLS reduced dissolution lead to a reduced bioavailability? Are the mitigation strategies also effective in terms of bioavailability? These will require further testing of engineered formulations in animals and, if successful, in humans.

Bibliography

1. Bircumshaw, L.; Riddiford, A., Transport control in heterogeneous reactions. *Quarterly Reviews, Chemical Society* **1952,** *6* (2), 157-185.
2. Wen, C., Noncatalytic heterogeneous solid-fluid reaction models. *Industrial & Engineering Chemistry* **1968,** *60* (9), 34-54.
3. Siepmann, J.; Siepmann, F., Mathematical modeling of drug dissolution. *Int J Pharm* **2013,** *453* (1), 12-24.
4. Williams, H. D.; Trevaskis, N. L.; Charman, S. A.; Shanker, R. M.; Charman, W. N.; Pouton, C. W.; Porter, C. J., Strategies to address low drug solubility in discovery and development. *Pharmacological reviews* **2013,** *65* (1), 315-499.
5. Bhattachar, S. N.; Risley, D. S.; Werawatganone, P.; Aburub, A., Weak bases and formation of a less soluble lauryl sulfate salt/complex in sodium lauryl sulfate (SLS) containing media. *Int J Pharm* **2011,** *412* (1-2), 95-8.
6. Desai, D.; Wong, B.; Huang, Y.; Ye, Q.; Tang, D.; Guo, H.; Huang, M.; Timmins, P., Surfactant-mediated dissolution of metformin hydrochloride tablets: wetting effects versus ion pairs diffusivity. *J Pharm Sci* **2014,** *103* (3), 920-6.
7. Guo, Y.; Mishra, M. K.; Wang, C.; Sun, C. C., Crystallographic and Energetic Insights into Reduced Dissolution and Physical Stability of a Drug–Surfactant Salt: The Case of Norfloxacin Lauryl Sulfate. *Molecular Pharmaceutics* **2020,** *17* (2), 579-587.
8. Guo, Y.; Wang, C.; Dun, J.; Du, L.; Hawley, M.; Sun, C. C., Mechanism for the Reduced Dissolution of Ritonavir Tablets by Sodium Lauryl Sulfate. *Journal of Pharmaceutical Sciences* **2019,** *108* (1), 516-524.
9. Huang, Z.; Parikh, S.; Fish, W. P., Interactions between a poorly soluble cationic drug and sodium dodecyl sulfate in dissolution medium and their impact on in vitro dissolution behavior. *Int J Pharm* **2018,** *535* (1-2), 350-359.
10. Jain, A.; Ran, Y.; Yalkowsky, S. H., Effect of pH-sodium lauryl sulfate combination on solubilization of PG-300995 (an anti-HIV agent): a technical note. *AAPS PharmSciTech* **2004,** *5* (3), e45.
11. Nokhodchi, A.; Norouzi-Sani, S.; Siahi-Shadbad, M. R.; Lotfipoor, F.; Saeedi, M., The effect of various surfactants on the release rate of propranolol hydrochloride from hydroxypropylmethylcellulose (HPMC)-Eudragit matrices. *European journal of pharmaceutics and biopharmaceutics : official journal of Arbeitsgemeinschaft fur Pharmazeutische Verfahrenstechnik e.V* **2002,** *54* (3), 349-56.
12. Jon, D. I.; Chang, D. L., Interactions between an amine functional polymer and an anionic surfactant. *J Soc Cosmet Chem* **1990,** *41*, 213-225.
13. Jivraj, M.; Martini, L. G.; Thomson, C. M., An overview of the different excipients useful for the direct compression of tablets. *Pharmaceutical Science & Technology Today* **2000,** *3* (2), 58-63.
14. Sun, C. C., Microstructure of Tablet-Pharmaceutical Significance, Assessment, and Engineering. *Pharmaceutical research* **2017,** *34* (5), 918-928.
15. Burgess, D. J.; Hussain, A. S.; Ingallinera, T. S.; Chen, M.-L., Assuring quality and performance of sustained and controlled release parenterals: workshop report. *Aaps Pharmsci* **2002,** *4* (2), 13-23.
16. Ubhe, T. S.; Gedam, P., A Brief Overview on Tablet and It's Types. *Journal of Advancement in Pharmacology 1* (1).
17. Hogan, J. E., Hydroxypropylmethylcellulose sustained release technology. *Drug Development and Industrial Pharmacy* **1989,** *15* (6-7), 975-999.

18. Boussery, K.; Belpaire, F. M.; Van de Voorde, J., Chapter 23 - Physiological Aspects Determining the Pharmacokinetic Properties of Drugs. In *The Practice of Medicinal Chemistry (Fourth Edition)*, Wermuth, C. G.; Aldous, D.; Raboisson, P.; Rognan, D., Eds. Academic Press: San Diego, 2008; pp 539-559.
19. Amidon, G. L.; Lennernäs, H.; Shah, V. P.; Crison, J. R., A theoretical basis for a biopharmaceutic drug classification: the correlation of in vitro drug product dissolution and in vivo bioavailability. *Pharmaceutical research* **1995,** *12* (3), 413-20.
20. Alexander, T. A., Lubricants for use in tabletting. Google Patents: 1998.
21. Hauss, D. J., *Oral lipid-based formulations: enhancing the bioavailability of poorly water-soluble drugs*. CRC Press: 2007; Vol. 170.
22. Wurster, D. E.; Taylor, P. W., Dissolution rates. *J. Pharm. Sci* **1965,** *54* (2), 169-175.
23. Thomas Dürig, K. K., *Handbook of Pharmaceutical Wet Granulation*. 2019.
24. Lee, D.-K.; Choi, S. Y.; Park, M. S.; Cho, Y. H., Wetting properties of hybrid structure with hydrophilic ridges and hydrophobic channels. *Applied Physics A* **2018,** *124* (2), 192.
25. Briggner, L.-E.; Hendrickx, R.; Kloo, L.; Rosdahl, J.; Svensson, P. H., Solid-State Perturbation for Solubility Improvement: A Proof of Concept. *ChemMedChem* **2011,** *6* (1), 60-62.
26. Briggner, L.-E.; Kloo, L.; Rosdahl, J.; Svensson, P. H., In Silico Solid State Perturbation for Solubility Improvement. *ChemMedChem* **2014,** *9* (4), 724-726.
27. Bergström, C. A. S.; Larsson, P., Computational prediction of drug solubility in water-based systems: Qualitative and quantitative approaches used in the current drug discovery and development setting. *Int J Pharm* **2018,** *540* (1-2), 185-193.
28. Koehl, N. J.; Holm, R.; Kuentz, M.; Griffin, B. T., New Insights into Using Lipid Based Suspensions for 'Brick Dust' Molecules: Case Study of Nilotinib. *Pharmaceutical research* **2019,** *36* (4), 56.
29. Bergström, C. A.; Charman, W. N.; Porter, C. J., Computational prediction of formulation strategies for beyond-rule-of-5 compounds. *Advanced drug delivery reviews* **2016,** *101*, 6-21.
30. Taylor, L. S.; Zhang, G. G. Z., Physical chemistry of supersaturated solutions and implications for oral absorption. *Advanced Drug Delivery Reviews* **2016,** *101*, 122-142.
31. Bergström, C. A. S.; Wassvik, C. M.; Johansson, K.; Hubatsch, I., Poorly Soluble Marketed Drugs Display Solvation Limited Solubility. *Journal of Medicinal Chemistry* **2007,** *50* (23), 5858-5862.
32. Liang, C.; Qiao, J.-q.; Lian, H.-z., Determination of reversed-phase high performance liquid chromatography based octanol-water partition coefficients for neutral and ionizable compounds: Methodology evaluation. *Journal of Chromatography a* **2017,** *1528*, 25-34.
33. Dokoumetzidis, A.; Macheras, P., A century of dissolution research: from Noyes and Whitney to the biopharmaceutics classification system. *Int J Pharm* **2006,** *321* (1-2), 1-11.
34. Noyes, A. A.; Whitney, W. R., The rate of solution of solid substances in their own solutions *Journal of the American Chemical Society* **1897,** *19* (12), 930-934.
35. Bruner, L.; Tolloczko, S., Über die Auflösungsgeschwindigkeit fester Körper. In *Zeitschrift für Physikalische Chemie*, 1900; Vol. 35U, p 283.
36. Levich, V. G., Physicochemical hydrodynamics. **1962**.
37. Sheng, J. J.; Sirois, P. J.; Dressman, J. B.; Amidon, G. L., Particle diffusional layer thickness in a USP dissolution apparatus II: a combined function of particle size and paddle speed. *J Pharm Sci* **2008,** *97* (11), 4815-29.
38. Roller, P. S., The Physical and Chemical Relatics in Fluid Phase Hetergeneous Reaction. *J Phys Chem.* **1934,** *39* (2), 221-238.
39. Danckwerts, P., Significance of liquid-film coefficients in gas absorption. *Industrial & Engineering Chemistry* **1951,** *43* (6), 1460-1467.

40. Wurster, D. E.; Taylor Jr, P. W., Dissolution kinetics of certain crystalline forms of prednisolone. *Journal of pharmaceutical sciences* **1965,** *54* (5), 670-676.
41. LaMer, V. K., The Kinetics of Reactions in Solution (Moelwyn-Hughes, E. A.). *J Chem Educ.* **1934,** *11* (8), 483.
42. Fage, A.; Townend, H. C., An examination of turbulent flow with an ultramicroscope. *Proceedings of the Royal Society of London. Series A, Containing Papers of a Mathematical and Physical Character* **1932,** *135* (828), 656-677.
43. Brunner, E., Reaktionsgeschwindigkeit in heterogenen Systemen. In *Zeitschrift für Physikalische Chemie*, 1904; Vol. 47U, p 56.
44. Babu, N. J.; Nangia, A., Solubility Advantage of Amorphous Drugs and Pharmaceutical Cocrystals. *Cryst Growth Des.* **2011,** *11* (7), 2662-2679.
45. Bilgili, E.; Rahman, M.; Palacios, D.; Arevalo, F., Impact of polymers on the aggregation of wet-milled itraconazole particles and their dissolution from spray-dried nanocomposites. *Advanced Powder Technology* **2018,** *29* (12), 2941-2956.
46. D, S.; Muthudoss, P.; Khullar, P.; A, R. V., Micronization and Agglomeration: Understanding the Impact of API Particle Properties on Dissolution and Permeability Using Solid State and Biopharmaceutical "Toolbox". *Journal of Pharmaceutical Innovation* **2021,** *16* (1), 136-151.
47. Hawley, M.; Morozowich, W., Modifying the Diffusion Layer of Soluble Salts of Poorly Soluble Basic Drugs To Improve Dissolution Performance. *Molecular Pharmaceutics* **2010,** *7* (5), 1441-1449.
48. Mullin, J. W., *Crystallization*. Elsevier: 2001.
49. Kanaujia, P.; Poovizhi, P.; Ng, W. K.; Tan, R. B. H., Amorphous formulations for dissolution and bioavailability enhancement of poorly soluble APIs. *Powder Technology* **2015,** *285*, 2-15.
50. Carino, S. R.; Sperry, D. C.; Hawley, M., Relative bioavailability estimation of carbamazepine crystal forms using an artificial stomach–duodenum model. *J. Pharm. Sci* **2006,** *95* (1), 116-125.
51. Bavishi, D. D.; Borkhataria, C. H., Spring and parachute: How cocrystals enhance solubility. *Progress in Crystal Growth and Characterization of Materials* **2016,** *62* (3), 1-8.
52. Guzmán, H. R.; Tawa, M.; Zhang, Z.; Ratanabanangkoon, P.; Shaw, P.; Gardner, C. R.; Chen, H.; Moreau, J. P.; Almarsson, Ö.; Remenar, J. F., Combined Use of Crystalline Salt Forms and Precipitation Inhibitors to Improve Oral Absorption of Celecoxib from Solid Oral Formulations. *Journal of Pharmaceutical Sciences* **2007,** *96* (10), 2686-2702.
53. Chavan, R. B.; Thipparaboina, R.; Kumar, D.; Shastri, N. R., Evaluation of the inhibitory potential of HPMC, PVP and HPC polymers on nucleation and crystal growth. *RSC advances* **2016,** *6* (81), 77569-77576.
54. Trasi, N. S.; Taylor, L. S., Effect of polymers on nucleation and crystal growth of amorphous acetaminophen. *CrystEngComm* **2012,** *14* (16), 5188-5197.
55. Trasi, N. S.; Oucherif, K. A.; Litster, J. D.; Taylor, L. S., Evaluating the influence of polymers on nucleation and growth in supersaturated solutions of acetaminophen. *CrystEngComm* **2015,** *17* (6), 1242-1248.
56. Yamashita, H.; Sun, C. C., Expedited Tablet Formulation Development of a Highly Soluble Carbamazepine Cocrystal Enabled by Precipitation Inhibition in Diffusion Layer. *Pharmaceutical research* **2019,** *36* (6), 90.
57. Yamashita, H.; Sun, C. C., Harvesting potential dissolution advantages of soluble cocrystals by depressing precipitation using the common coformer effect. *Crystal Growth & Design* **2016,** *16* (12), 6719-6721.

58. Hawley, M.; Morozowich, W., Modifying the diffusion layer of soluble salts of poorly soluble basic drugs to improve dissolution performance. *Mol Pharm* **2010,** *7* (5), 1441-9.
59. Badawy, S. I. F.; Hussain, M. A., Microenvironmental pH modulation in solid dosage forms. *Journal of pharmaceutical sciences* **2007,** *96* (5), 948-959.
60. Doherty, C.; York, P., Microenvironmental pH control of drug dissolution. *Int J Pharm* **1989,** *50* (3), 223-232.
61. Santos, F. K. G.; Neto, E. L. B.; Moura, M. C. P. A.; Dantas, T. N. C.; Neto, A. A. D., Molecular behavior of ionic and nonionic surfactants in saline medium. *Colloids and Surfaces A: Physicochemical and Engineering Aspects* **2009,** *333* (1), 156-162.
62. Fluksman, A.; Benny, O., A robust method for critical micelle concentration determination using coumarin-6 as a fluorescent probe. *Analytical Methods* **2019,** *11* (30), 3810-3818.
63. Torchilin, V. P., Micellar Nanocarriers: Pharmaceutical Perspectives. *Pharmaceutical research* **2006,** *24* (1), 1.
64. Mukerjee, P.; Mysels, K. J. *Critical micelle concentrations of aqueous surfactant systems*; National Standard reference data system: 1971.
65. Dutkiewicz, E.; Jakubowska, A., Effect of electrolytes on the physicochemical behaviour of sodium dodecyl sulphate micelles. *Colloid and Polymer Science* **2002,** *280* (11), 1009-1014.
66. Rahman, A.; Brown, C. W., Effect of pH on the critical micelle concentration of sodium dodecyl sulphate. *Journal of Applied Polymer Science* **1983,** *28* (4), 1331-1334.
67. Ugelstad, J.; El-Aasser, M. S.; Vanderhoff, J. W., Emulsion polymerization: Initiation of polymerization in monomer droplets. *Journal of Polymer Science: Polymer Letters Edition* **1973,** *11* (8), 503-513.
68. Aungst, B. J.; Rogers, N. J.; Shefter, E., Enhancement of naloxone penetration through human skin in vitro using fatty acids, fatty alcohols, surfactants, sulfoxides and amides. *Int J Pharm* **1986,** *33* (1-3), 225-234.
69. Dun, J.; Osei-Yeboah, F.; Boulas, P.; Lin, Y.; Sun, C. C., A systematic evaluation of dual functionality of sodium lauryl sulfate as a tablet lubricant and wetting enhancer. *Int J Pharm* **2018,** *552* (1), 139-147.
70. Vaithianathan, S.; Haidar, S. H.; Zhang, X.; Jiang, W.; Avon, C.; Dowling, T. C.; Shao, C.; Kane, M.; Hoag, S. W.; Flasar, M. H.; Ting, T. Y.; Polli, J. E., Effect of Common Excipients on the Oral Drug Absorption of Biopharmaceutics Classification System Class 3 Drugs Cimetidine and Acyclovir. *J Pharm Sci* **2016,** *105* (2), 996-1005.
71. Anderberg, E. K.; Artursson, P., Epithelial transport of drugs in cell culture. VIII: Effects of sodium dodecyl sulfate on cell membrane and tight junction permeability in human intestinal epithelial (Caco-2) cells. *J Pharm Sci* **1993,** *82* (4), 392-8.
72. van Hoogdalem, E. J.; de Boer, A. G.; Breimer, D. D., Intestinal drug absorption enhancement: an overview. *Pharmacology & therapeutics* **1989,** *44* (3), 407-43.
73. Moore, A., Final Report on the Safety Assessment of Sodium Lauryl Sulfate and Ammonium Lauryl Sulfate. *International Journal of Toxicology* **1983,** *2* (7), 127-181.
74. U.S. Food and Drug Administration (FDA), 21 C.F.R. Part 172—Food additives permitted for direct addition to food for human consumption. In *Subpart I—Multipurpose Additives*, 2021.
75. Billany, M.; Richards, J., Batch variation of magnesium stearate and its effect on the dissolution rate of salicylic acid from solid dosage forms. *Drug Development and Industrial Pharmacy* **1982,** *8* (4), 497-511.
76. Chowhan, Z.; Chi, L. H., Drug-excipient interactions resulting from powder mixing IV: Role of lubricants and their effect on in vitro dissolution. *Journal of pharmaceutical sciences* **1986,** *75* (6), 542-545.

77. Cruz-Cabeza, A. J., Acid–base crystalline complexes and the p K a rule. *CrystEngComm* **2012,** *14* (20), 6362-6365.
78. Allam, A. N.; El Gamal, S.; Naggar, V., Bioavailability: A pharmaceutical review. *Int J Novel Drug Deliv Tech* **2011,** *1* (1), 77-93.
79. Khedulkar, A.; Tajne, M., Bio-availability enhancement of poorly water soluble drugs. *Metabolism* **2018,** *11*, 13-14.
80. Aljaberi, A.; Chatterji, A.; Dong, Z.; Shah, N. H.; Malick, W.; Singhal, D.; Sandhu, H. K., Understanding and optimizing the dual excipient functionality of sodium lauryl sulfate in tablet formulation of poorly water soluble drug: wetting and lubrication. *Pharm Dev Technol* **2013,** *18* (2), 490-503.
81. Chakraborty, S.; Shukla, D.; Jain, A.; Mishra, B.; Singh, S., Assessment of solubilization characteristics of different surfactants for carvedilol phosphate as a function of pH. *J Colloid Interface Sci* **2009,** *335* (2), 242-9.
82. Vadlamudi, M. K.; Dhanaraj, S. In *Significance of excipients to enhance the bioavailability of poorly water-soluble drugs in oral solid dosage forms: A Review*, IOP Conference Series: Materials Science and Engineering, IOP Publishing: 2017; p 022023.
83. Aburub, A.; Risley, D. S.; Mishra, D., A critical evaluation of fasted state simulating gastric fluid (FaSSGF) that contains sodium lauryl sulfate and proposal of a modified recipe. *Int J Pharm* **2008,** *347* (1), 16-22.
84. Rowe, R. C.; Sheskey, P. J.; Owen, S. C., *Handbook of pharmaceutical excipients*. Pharmaceutical press London: 2006; Vol. 6.
85. Zhao, J.; Koo, O.; Pan, D.; Wu, Y.; Morkhade, D.; Rana, S.; Saha, P.; Marin, A., The Impact of Disintegrant Type, Surfactant, and API Properties on the Processability and Performance of Roller Compacted Formulations of Acetaminophen and Aspirin. *AAPS J.* **2017,** *19* (5), 1387-1395.
86. Dun, J.; Osei-Yeboah, F.; Boulas, P.; Lin, Y.; Sun, C. C., A systematic evaluation of dual functionality of sodium lauryl sulfate as a tablet lubricant and wetting enhancer. *Int. J. Pharm.* **2018**, accepted.
87. Croy, S. R.; Kwon, G. S., Polysorbate 80 and Cremophor EL micelles deaggregate and solubilize nystatin at the core-corona interface. *J Pharm Sci* **2005,** *94* (11), 2345-54.
88. Florence, T. A., Drug Solubilization In Surfactant Systems. In *Techniques of Solubilization of Drugs*, Yalkowsky, H. S., Ed. Marcel Dekker Inc.: New York and Basel, 1981; Vol. 12, pp 15-89.
89. Polster, C. S.; Atassi, F.; Wu, S.-J.; Sperry, D. C., Use of Artificial Stomach− Duodenum Model for Investigation of Dosing Fluid Effect on Clinical Trial Variability. *Mol Pharm* **2010,** *7* (5), 1533-1538.
90. Bhattachar, S. N.; Risley, D. S.; Werawatganone, P.; Aburub, A., Weak bases and formation of a less soluble lauryl sulfate salt/complex in sodium lauryl sulfate (SLS) containing media. *Int J Pharm* **2011,** *412* (1), 95-98.
91. Desai, D.; Wong, B.; Huang, Y.; Ye, Q.; Tang, D.; Guo, H.; Huang, M.; Timmins, P., Surfactant-mediated dissolution of metformin hydrochloride tablets: wetting effects versus ion pairs diffusivity. *Journal of pharmaceutical sciences* **2014,** *103* (3), 920-926.
92. Huang, Z.; Parikh, S.; Fish, W. P., Interactions between a poorly soluble cationic drug and sodium dodecyl sulfate in dissolution medium and their impact on in vitro dissolution behavior. *Int J Pharm* **2018,** *535* (1), 350-359.
93. Jain, A.; Ran, Y.; Yalkowsky, S. H., Effect of pH-sodium lauryl sulfate combination on solubilization of PG-300995 (an anti-HIV agent): a technical note. *AAPS PharmSciTech* **2004,** *5* (3), 65-67.
94. Jon, D. I.; Chang, D. L., Interactions between an amine functional polymer and an anionic surfactant. *JSoc Cosmet Chem* **1990,** *41*, 213-225.

95. Nokhodchi, A.; Norouzi-Sani, S.; Siahi-Shadbad, M.-R.; Lotfipoor, F.; Saeedi, M., The effect of various surfactants on the release rate of propranolol hydrochloride from hydroxypropylmethylcellulose (HPMC)-Eudragit matrices. *European journal of pharmaceutics and biopharmaceutics* **2002,** *54* (3), 349-356.
96. Polster, C. S.; Wu, S.-J.; Gueorguieva, I.; Sperry, D. C., Mechanism for enhanced absorption of a solid dispersion formulation of LY2300559 using the artificial stomach duodenum model. *Mol Pharm* **2015,** *12* (4), 1131-1140.
97. Wang, C.; Chopade, S. A.; Guo, Y.; Early, J. T.; Tang, B.; Wang, E.; Hillmyer, M. A.; Lodge, T. P.; Sun, C. C., Preparation, Characterization, and Formulation Development of Drug–Drug Protic Ionic Liquids of Diphenhydramine with Ibuprofen and Naproxen. *Mol Pharm* **2018**.
98. Zhang, Y.; Huo, M.; Zhou, J.; Xie, S., PKSolver: An add-in program for pharmacokinetic and pharmacodynamic data analysis in Microsoft Excel. *Comput Meth Prog Bio* **2010,** *99* (3), 306-14.
99. Chow, S. F.; Shi, L.; Ng, W. W.; Leung, K. H. Y.; Nagapudi, K.; Sun, C. C.; Chow, A. H. L., Kinetic Entrapment of a Hidden Curcumin Cocrystal with Phloroglucinol. *Crystal Growth & Design* **2014,** *14* (10), 5079-5089.
100. Wang, C.; Perumalla, S. R.; Lu, R.; Fang, J.; Sun, C. C., Sweet Berberine. *Crystal Growth & Design* **2016,** *16* (2), 933-939.
101. Levy, G.; Gumtow, R. H., Effect of certain tablet formulation factors on dissolution rate of the active ingredient III. Tablet lubricants. *J. Pharm. Sci.* **1963,** *52* (12), 1139-1144.
102. Wang, J.; Wen, H.; Desai, D., Lubrication in tablet formulations. *European Journal of Pharmaceutics and Biopharmaceutics* **2010,** *75* (1), 1-15.
103. Law, D.; Krill, S. L.; Schmitt, E. A.; Fort, J. J.; Qiu, Y.; Wang, W.; Porter, W. R., Physicochemical considerations in the preparation of amorphous ritonavir-poly(ethylene glycol) 8000 solid dispersions. *J Pharm Sci* **2001,** *90* (8), 1015-25.
104. Kulkarni, V. S.; Shaw, C., Chapter 7 - Preparation and Stability Testing. In *Essential Chemistry for Formulators of Semisolid and Liquid Dosages*, Kulkarni, V. S.; Shaw, C., Eds. Academic Press: Boston, 2016; pp 99-135.
105. Lava, K.; Evrard, Y.; Van Hecke, K.; Van Meervelt, L.; Binnemans, K., Quinolinium and isoquinolinium ionic liquid crystals. *RSC Advances* **2012,** *2* (21), 8061-8070.
106. Sikorski, A.; Trzybiński, D., Structural insight into the interactions between a cationic dye and an anionic surfactant in crystals of 9-aminoacridinium dodecyl sulfate. *Journal of Molecular Structure* **2014,** *1076*, 490-495.
107. Tarafdar, P. K.; Reddy, S. T.; Swamy, M. J., A Base-Triggerable Catanionic Mixed Lipid System: Isothermal Titration Calorimetric and Single-Crystal X-ray Diffraction Studies. *The Journal of Physical Chemistry B* **2010,** *114* (43), 13710-13717.
108. Stahl, P. H.; Wermuth, C. G., Handbook of pharmaceutical salts: properties, selection and use. *Chem. Int* **2002,** *24*, 21.
109. Cruz-Cabeza, A. J., Acid–base crystalline complexes and the pKa rule. *CrystEngComm* **2012,** *14* (20), 6362-6365.
110. Vehovec, T.; Obreza, A., Review of operating principle and applications of the charged aerosol detector. *J Chromatogr A* **2010,** *1217* (10), 1549-1556.
111. Fuguet, E.; Ràfols, C.; Rosés, M.; Bosch, E., Critical micelle concentration of surfactants in aqueous buffered and unbuffered systems. *Analytica Chimica Acta* **2005,** *548* (1), 95-100.
112. Sekhon, B. S., Surfactants: pharmaceutical and medicinal aspects. **2014**.
113. Sekhon, B. S., Surfactants: pharmaceutical and medicinal aspects. *Management* **2013,** *1*, 11-36.
114. Tadros, T. F., *Applied surfactants: principles and applications*. John Wiley & Sons: 2006.

115. Rowe, R. C.; Sheskey, P.; Quinn, M., *Handbook of pharmaceutical excipients*. Libros Digitales-Pharmaceutical Press: 2009.
116. Jinno, J.; Oh, D. m.; Crison, J. R.; Amidon, G. L., Dissolution of ionizable water-insoluble drugs: The combined effect of pH and surfactant. *J. Pharm. Sci* **2000,** *89* (2), 268-274.
117. Soulie, M.; Carayon, C.; Saffon, N.; Blanc, S.; Fery-Forgues, S., A comparative study of nine berberine salts in the solid state: optimization of the photoluminescence and self-association properties through the choice of the anion. *Physical chemistry chemical physics : PCCP* **2016,** *18* (43), 29999-30008.
118. Sun, C. C., Materials Science Tetrahedron-A Useful Tool for Pharmaceutical Research and Development. *J. Pharm. Sci* **2009,** *98* (5), 1671-1687.
119. Hubschle, C. B.; Sheldrick, G. M.; Dittrich, B., ShelXle: a Qt graphical user interface for SHELXL. *Journal of Applied Crystallography* **2011,** *44* (6), 1281-1284.
120. Turner, M. J., McKinnon, J. J., Wolff, S. K., Grimwood, D. J., Spackman, P. R., Jayatilaka, D. & Spackman, M. A. CrystalExplorer17. http://hirshfeldsurface.net.
121. Frisch, M. J. E. A., G. W. Trucks, Hs B. Schlegel, G. E. Scuseria, M. A. Robb, J. R. Cheeseman, G. Scalmani et al. , Gaussian 09. Wallingford, CT 200.: 2009.
122. Wang, C.; Sun, C. C., Computational Techniques for Predicting Mechanical Properties of Organic Crystals: A Systematic Evaluation. *Mol Pharm* **2019,** *16* (4), 1732-1741.
123. Turner, M. J.; Thomas, S. P.; Shi, M. W.; Jayatilaka, D.; Spackman, M. A., Energy frameworks: insights into interaction anisotropy and the mechanical properties of molecular crystals. *Chemical communications (Cambridge, England)* **2015,** *51* (18), 3735-8.
124. Turner, M. J.; Grabowsky, S.; Jayatilaka, D.; Spackman, M. A., Accurate and Efficient Model Energies for Exploring Intermolecular Interactions in Molecular Crystals. *The Journal of Physical Chemistry Letters* **2014,** *5* (24), 4249-4255.
125. Buckingham, D.; Clark, C.; Nangia, A., The acidity of norfloxacin. *Australian Journal of Chemistry* **1990,** *43* (2), 301-309.
126. Stein, G. E., Review of the bioavailability and pharmacokinetics of oral norfloxacin. *The American Journal of Medicine* **1987,** *82* (6, Supplement 2), 18-21.
127. Wang, C.; Hu, S.; Sun, C. C., Expedited development of a high dose orally disintegrating metformin tablet enabled by sweet salt formation with acesulfame. *Int J Pharm* **2017,** *532* (1), 435-443.
128. Arora, K. K.; Bhardwaj, S. P.; Mistry, P.; Suryanarayanan, R., Modulating the dehydration conditions of adefovir dipivoxil dihydrate to obtain different physical forms of anhydrate. *J Pharm Sci* **2015,** *104* (3), 1056-64.
129. Kaushal, A. M.; Vangala, V. R.; Suryanarayanan, R., Unusual effect of water vapor pressure on dehydration of dibasic calcium phosphate dihydrate. *J Pharm Sci* **2011,** *100* (4), 1456-66.
130. Surov, A. O.; Voronin, A. P.; Drozd, K. V.; Churakov, A. V.; Roussel, P.; Perlovich, G. L., Diversity of crystal structures and physicochemical properties of ciprofloxacin and norfloxacin salts with fumaric acid. *CrystEngComm* **2018,** *20* (6), 755-767.
131. Lou, B.; Bostrom, D.; Velaga, S. P., Monohydrous dihydrogen phosphate salts of norfloxacin and ciprofloxacin. *Acta Crystallographica Section C* **2007,** *63* (12), o731-o733.
132. Modi, S. R.; Dantuluri, A. K. R.; Perumalla, S. R.; Sun, C. C.; Bansal, A. K., Effect of Crystal Habit on Intrinsic Dissolution Behavior of Celecoxib Due to Differential Wettability. *Cryst Growth Des.* **2014,** *14* (10), 5283-5292.
133. Paul, S.; Wang, C.; Wang, K.; Sun, C. C., Reduced Punch Sticking Propensity of Acesulfame by Salt Formation: Role of Crystal Mechanical Property and Surface Chemistry. *Mol Pharm* **2019,** *16* (6), 2700-2707.

134. Westergren, J.; Lindfors, L.; Höglund, T.; Lüder, K.; Nordholm, S.; Kjellander, R., In Silico Prediction of Drug Solubility: 1. Free Energy of Hydration. *The Journal of Physical Chemistry B* **2007,** *111* (7), 1872-1882.
135. Briggner, L. E.; Kloo, L.; Rosdahl, J.; Svensson, P. H., In silico solid state perturbation for solubility improvement. *ChemMedChem* **2014,** *9* (4), 724-6.
136. Chang, S.-Y.; Wang, C.; Sun, C. C., Relationship between hydrate stability and accuracy of true density measured by helium pycnometry. *Int J Pharm* **2019,** *567*, 118444.
137. Lee, C. H.; Maibach, H. I., The sodium lauryl sulfate model: an overview. *Contact Dermatitis* **1995,** *33* (1), 1-7.
138. Singer, M. M.; Tjeerdema, R. S., Fate and effects of the surfactant sodium dodecyl sulfate. *Reviews of environmental contamination and toxicology* **1993**, 95-149.
139. Raymond C Rowe; Paul J Sheskey; Marian E Quinn, *Handbook of pharmaceutical excipients*. 6 th ed.; Pharmaceutical Press: IL, USA, 2009.
140. Nakagaki, M.; Yokoyama, S., Acid-catalyzed hydrolysis of sodium dodecyl sulfate. *Journal of pharmaceutical sciences* **1985,** *74* (10), 1047-1052.
141. Miles, G. D.; Shedlovsky, L., Minima in Surface Tension–Concentration Curves of Solutions of Sodium Alcohol Sulfates. *The Journal of Physical Chemistry* **1944,** *48* (1), 57-62.
142. Miles, G. D., Minima in Surface-tension and Interfacial-tension Curves. *The Journal of Physical Chemistry* **1945,** *49* (2), 71-76.
143. Kim, K.-J.; Mersmann, A., Estimation of metastable zone width in different nucleation processes. *Chemical Engineering Science* **2001,** *56* (7), 2315-2324.
144. O'Grady, D.; Barrett, M.; Casey, E.; Glennon, B., The Effect of Mixing on the Metastable Zone Width and Nucleation Kinetics in the Anti-Solvent Crystallization of Benzoic Acid. *Chemical Engineering Research and Design* **2007,** *85* (7), 945-952.
145. Srinivasan, K.; Meera, K.; Ramasamy, P., A novel method to enhance metastable zone width for crystal growth from solution. *Crystal Research and Technology: Journal of Experimental and Industrial Crystallography* **2000,** *35* (3), 291-297.
146. Mullin, J. W., *Crystallization* 4th ed.; Reed Educational and Professional Publishing Ltd: 2001.
147. Viana, R. B.; da Silva, A. B.; Pimentel, A. S., Infrared spectroscopy of anionic, cationic, and zwitterionic surfactants. *Advances in physical chemistry* **2012,** *2012*.
148. Guo, Y.; Sun, C. C., Pharmaceutical lauryl sulfate salts – Prevalence, formation rules and formulation implications. Unpublished manuscript. **2021**.
149. Dokoumetzidis, A.; Macheras, P., A century of dissolution research: From Noyes and Whitney to the Biopharmaceutics Classification System. *International journal of pharmaceutics* **2006,** *321* (1), 1-11.
150. Shekunov, B.; Montgomery, E. R., Theoretical Analysis of Drug Dissolution: I. Solubility and Intrinsic Dissolution Rate. *Journal of Pharmaceutical Sciences* **2016,** *105* (9), 2685-2697.
151. Wen, H.; Wang, C.; Sun, C. C., Fast Determination of Phase Stability of Hydrates Using Intrinsic Dissolution Rate Measurements. *Crystal Growth & Design* **2019,** *19* (10), 5471-5476.
152. Yu, L. X.; Carlin, A. S.; Amidon, G. L.; Hussain, A. S., Feasibility studies of utilizing disk intrinsic dissolution rate to classify drugs. *International journal of pharmaceutics* **2004,** *270* (1), 221-227.
153. Wadke, D. A.; Reier, G. E., Use of intrinsic dissolution rates to determine thermodynamic parameters associated with phase transitions. *Journal of pharmaceutical sciences* **1972,** *61* (6), 868-871.
154. Kortüm, G.; Vogel, W.; Andrussow, Disssociation constants of organic acids in aqueous solution. *Pure and Applied Chemistry* **1960,** *1* (2-3), 187-536.

155. Serjeant EP, D. B., *Ionization constants of organic acids in aqueous solution*. IUPAC Chem Data Ser No.23: New York, NY: Pergamon, 1979.
156. Shayanfar, A.; Jouyban, A., Physicochemical characterization of a new cocrystal of ketoconazole. *Powder Technology* **2014,** *262*, 242-248.
157. Thongngam, M.; McClements, D. J., Influence of pH, Ionic Strength, and Temperature on Self-Association and Interactions of Sodium Dodecyl Sulfate in the Absence and Presence of Chitosan. *Langmuir* **2005,** *21* (1), 79-86.
158. Woolfrey, S. G.; Banzon, G. M.; Groves, M. J., The effect of sodium chloride on the dynamic surface tension of sodium dodecyl sulfate solutions. *Journal of Colloid and Interface Science* **1986,** *112* (2), 583-587.
159. Chattopadhyay, A.; Harikumar, K., Dependence of critical micelle concentration of a zwitterionic detergent on ionic strength: implications in receptor solubilization. *FEBS letters* **1996,** *391* (1-2), 199-202.
160. Siepe, S.; Herrmann, W.; Borchert, H.-H.; Lueckel, B.; Kramer, A.; Ries, A.; Gurny, R., Microenvironmental pH and microviscosity inside pH-controlled matrix tablets: An EPR imaging study. *Journal of Controlled Release* **2006,** *112* (1), 72-78.
161. Taniguchi, C.; Kawabata, Y.; Wada, K.; Yamada, S.; Onoue, S., Microenvironmental pH-modification to improve dissolution behavior and oral absorption for drugs with pH-dependent solubility. *Expert opinion on drug delivery* **2014,** *11* (4), 505-516.
162. National Center for Biotechnology Information PubChem Compound Summary for CID 24243, Trisodium phosphate. https://pubchem.ncbi.nlm.nih.gov/compound/Trisodium-phosphate.
163. Serajuddin, A. T. M.; Jarowski, C. I., Effect of Diffusion Layer pH and Solubility on the Dissolution Rate of Pharmaceutical Bases and their Hydrochloride Salts I: Phenazopyridine. *Journal of Pharmaceutical Sciences* **1985,** *74* (2), 142-147.
164. Serajuddin, A. T. M.; Jarowski, C. I., Effect of Diffusion Layer pH and Solubility on the Dissolution Rate of Pharmaceutical Acids and Their Sodium Salts II: Salicylic Acid, Theophylline, and Benzoic Acid. *Journal of Pharmaceutical Sciences* **1985,** *74* (2), 148-154.
165. Dun, J.; Osei-Yeboah, F.; Boulas, P.; Lin, Y.; Sun, C. C., A systematic evaluation of poloxamers as tablet lubricants. *Int J Pharm* **2020,** *576*, 118994.

Appendix

This appendix contains copies of copyright permissions granted by the journal publishers where the work is published.

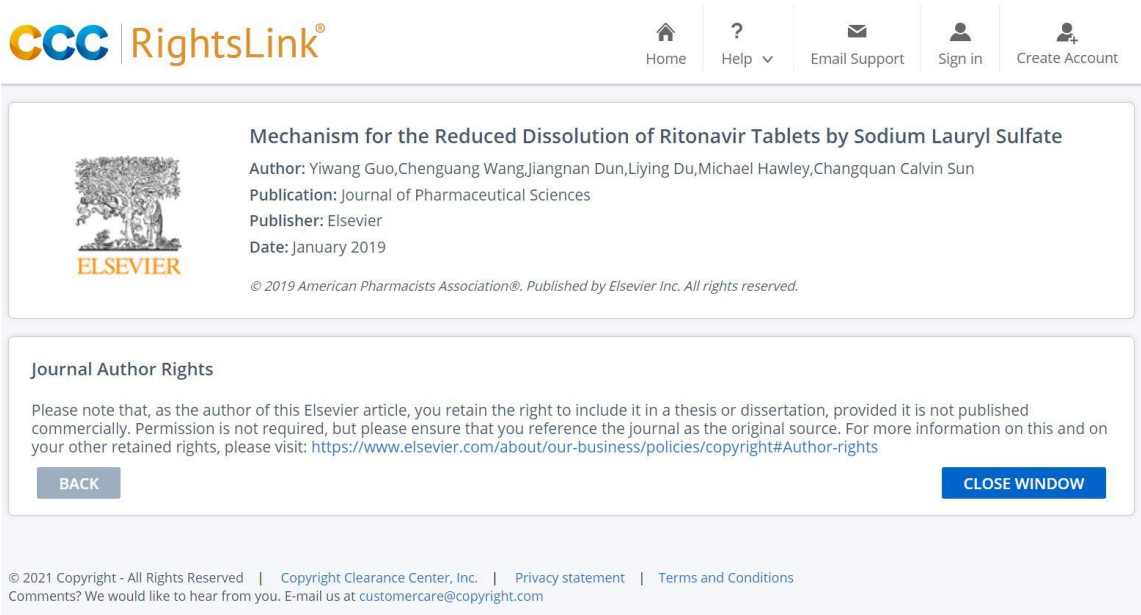

Chapter 2 - Mechanism for the reduced dissolution of ritonavir tablets by sodium lauryl sulfate of this thesis is adapted from the published original research article by Yiwang Guo at Journal of Pharmaceutical Sciences:

https://www.sciencedirect.com/science/article/pii/S0022354918306798

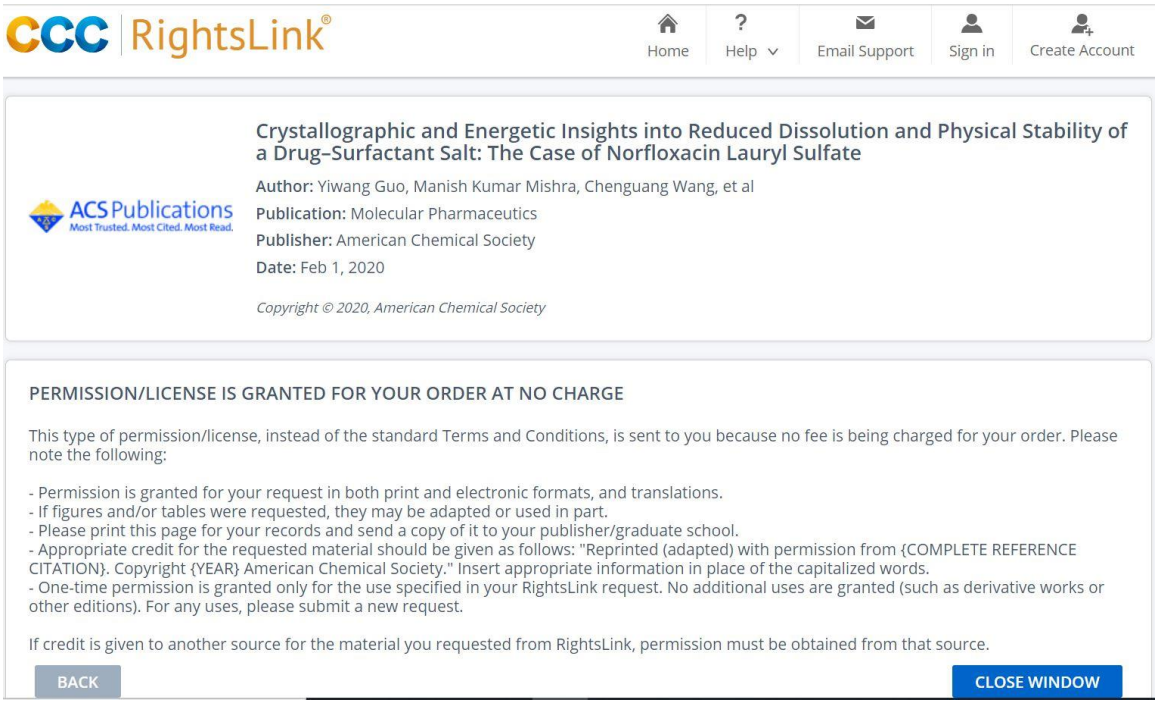

Chapter 3 – Crystallographic and Energetic Insights into Reduced Dissolution and Physical Stability of a Drug-Surfactant Salt – The Case of Norfloxacin Lauryl Sulfate is an original research article by Yiwang Guo published on Molecular Pharmaceutics. It is adapted with permission from Guo, Y.; Mishra, M. K.; Wang, C.; Sun, C. C., Crystallographic and Energetic Insights into Reduced Dissolution and Physical Stability of a Drug–Surfactant Salt: The Case of Norfloxacin Lauryl Sulfate. Molecular Pharmaceutics 2020, 17 (2), 579-587.Copyright (2021) American Chemical Society.